Aalborg Universitet

AALBORG UNIVERSITY

Technical Background Material for the Wave Generation Software AwaSys 5

Frigaard, Peter; Andersen, Thomas Lykke

Publication date:
2010

Document Version
Publisher's PDF, also known as Version of record

Link to publication from Aalborg University

Citation for published version (APA):
Frigaard, P., & Andersen, T. L. (2010). *Technical Background Material for the Wave Generation Software AwaSys 5*. Department of Civil Engineering, Aalborg University. DCE Technical reports No. 64

Technical Background Material for the

Wave Generation Software AwaSys 5

Peter Frigaard & Thomas Lykke Andersen

AALBORG UNIVERSITY
Department of Civil Engineering

Aalborg University
Department of Civil Engineering
Water and Soil

DCE Technical Reports No. 64

Technical Background Material for the Wave Generation Software AwaSys 5

by

Peter Frigaard & Thomas Lykke Andersen

January 2010

Scientific Publications at the Department of Civil Engineering

Technical Reports are published for timely dissemination of research results and scientific work carried out at the Department of Civil Engineering (DCE) at Aalborg University. This medium allows publication of more detailed explanations and results than typically allowed in scientific journals.

Technical Memoranda are produced to enable the preliminary dissemination of scientific work by the personnel of the DCE where such release is deemed to be appropriate. Documents of this kind may be incomplete or temporary versions of papers—or part of continuing work. This should be kept in mind when references are given to publications of this kind.

Contract Reports are produced to report scientific work carried out under contract. Publications of this kind contain confidential matter and are reserved for the sponsors and the DCE. Therefore, Contract Reports are generally not available for public circulation.

Lecture Notes contain material produced by the lecturers at the DCE for educational purposes. This may be scientific notes, lecture books, example problems or manuals for laboratory work, or computer programs developed at the DCE.

Theses are monograms or collections of papers published to report the scientific work carried out at the DCE to obtain a degree as either PhD or Doctor of Technology. The thesis is publicly available after the defence of the degree.

Latest News is published to enable rapid communication of information about scientific work carried out at the DCE. This includes the status of research projects, developments in the laboratories, information about collaborative work and recent research results.

Contents

Chapter 1

Biésel Transfer Functions

"Les Appareils Generateurs de Houle en Laboratorie" presented by Biésel and Suquet in 1951 discussed and solved the analytical problems concerning a number of different wave generator types. For each wave maker type the paper presented the transfer function between wave maker displacement and wave amplitude in those cases where the analytical problem could be solved. The article therefore represented a giant step in wave generation techniques and found the basis for today's wave generation in hydraulics laboratories.

In this chapter the main results from Biésel and Suquet will be discussed, and the transfer function between wave amplitude and paddle displacement, The Biésel Transfer Function, for a piston-type and a flap-type wave maker will be presented.

In Figure 1.1 the definitions used in the following calculations are presented for a piston-type wave maker.

In Figure 1.2 the fundamental hydrodynamic problem is shown in mathematical terms. The flow is assumed irrotational. Therefore a velocity potential, φ, exists and the velocity field can be found from

$$\vec{v} = \mathrm{grad}\varphi$$

If the fluid is assumed incompressible, the continuity equation yields that the potential must satisfy the Laplace equation.
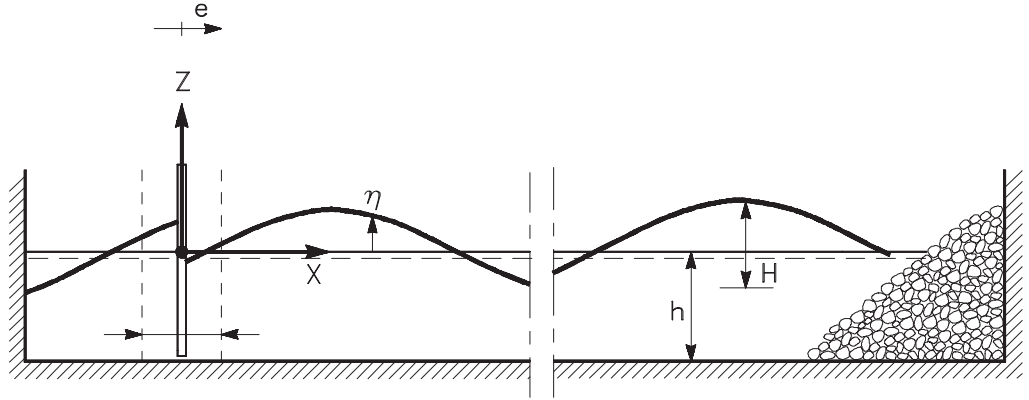
Figure 1.1: Definition sketch of flume with piston-type wave maker. e = e(z,t) = displacement of wave paddle. S = S(z) = stroke of wave paddle. $\eta = \eta$(x,t) = surface elevation. H = wave heigth far away from the wave maker. h = water depth, (assumed to be constant).

In Figure 1.2 the equations express:

0. Laplace equation. Basic equation for potential flow.

1. All water particles at the free surface remain at the free surface (kinematic B.C.). Free surface is at constant pressure (dynamic B.C.).

2. The water accompanies the wave paddle, which is displaced as a sine: $e(z,t) = \frac{S(z)}{2} \sin(\omega t)$, where $\omega = 2\pi/T$.

3. The bottom is impermeable.

4. The propagating wave is of constant form.

$$\text{①} \quad \frac{\partial^2 \varphi(x,z,t)}{\partial t^2} + g \; \frac{\partial \varphi(x,z,t)}{\partial z} = 0$$

$$\text{②} \quad \frac{\partial \varphi(x,z,t)}{\partial x} = \omega \times e(z) \times \cos(\omega t)$$

$$\text{⓪} \quad \frac{\partial^2 \varphi(x,z,t)}{\partial x^2} + \frac{\partial^2 \varphi(x,z,t)}{\partial z^2} = 0$$

$$\text{④} \quad \frac{d\varphi(x,z,t)}{dt} = 0$$

$$\text{③} \quad \frac{\partial \varphi(x,z,t)}{\partial z} = 0$$

Figure 1.2: Partial differential equation (PDE), and boundary conditions (BC).

Solution, with respect to φ, of the boundary value problem presented in Figure 1.2 can be divided into 3 steps:

A. Solving the homogeneous problem. That is PDE with BC 1,2 and 3. BC 2 with right side equal to zero.

B. Finding a particular solution satisfying PDE and BC 1, 2 and 3.

C. Determining the final solution as a linear combination of the homogeneous solution and the particular solution that satisfies BC 4.

The main results from each step (linearised BC) are listed below:

A. The homogeneous solution is any linear combination of functions of the form:

$$\varphi_H(x, z, t) \quad = \quad A_H \cdot \cos(k_i x) \cdot \cosh(k_i (z + h)) \cdot \cos(\omega_i t - \psi_0)$$

where A_H and ψ_0 are arbitrary constants and k is the solution to the dispersion relation:

$$\omega^2{}_i \quad = \quad k_i \cdot g \cdot \tanh(k_i h)$$

B. Particular solution.

$$\varphi_P(x, z, t) \;=\; \left(\sum_{n=0}^{\infty} c_n \varphi_n\right) \cos(\omega\, t)$$

where

$$\varphi_0 \;=\; \frac{\omega}{k_0}\,\cosh\,(k_0(z+h))\cdot\sin\,(k_0 x)$$

$$c_0 \;=\; 2\cdot k_0\,\frac{\int_{-h}^{0} e(z)\cdot\cosh\,(k_0\,(z+h))\cdot dz}{\sinh\,(k_0 h)\cdot\cosh\,(k_0 h)+k_0 h}$$

$$\varphi_n \;=\; -\frac{\omega}{k_n}\,\cos\,(k_n\,(z+h))\cdot e^{-k_n x} \qquad,\qquad n>0$$

$$c_n \;=\; 2\cdot k_n\,\frac{\int_{-h}^{0} e(z)\cdot\cos\,(k_n\,(z+h))\cdot dz}{\sin\,(k_n h)\cdot\cos\,(k_n h)+k_n h} \qquad,\qquad n>0$$

where k_0 is the solution to the dispersion relation:

$$\omega^2 \;=\; k_0 \cdot g \cdot \tanh\,(k_0 h)$$

and k_1 is the first positive solution (n=1) to

$$\omega^2 \;=\; -k_n\, g\, tan\,(k_n h)$$

k_2 the second and so forth.

C. Determining the final solution.
Now, requiring BC 4 to be satisfied far away from the wavemaker the only velocity potential $\varphi = \varphi_H + \varphi_P$ that satisfy the PDE and BC 1 to 4 is found to be, omitting index 0 :

$$\varphi(x, z, t) \;=\; -\frac{\omega}{k}\cdot c_0\cdot\cosh\,(k\,(z+h))\cdot\sin(\omega t - kx) -$$
$$\sum_{n=1}^{\infty} c_n\cdot\frac{\omega}{k_n}\cdot\cos\,(k_n\,(z+h))\cdot e^{-k_n x}\cdot\cos(\omega t)$$

The surface elevation $\eta(x, t)$ in the generated wave field is calculated by:

$$\eta(x, t) \;=\; -\frac{1}{g}\,\frac{\partial\varphi(x, 0, t)}{\partial t}$$

that yields

$$\eta(x, t) =$$
$$c_0\cdot\sinh(kh)\,\cos(\omega t - kx) + \sum_{n=1}^{\infty} c_n\,\sin\,(k_n h)\,e^{-k_n\cdot x}\,\sin(\omega t)$$

8
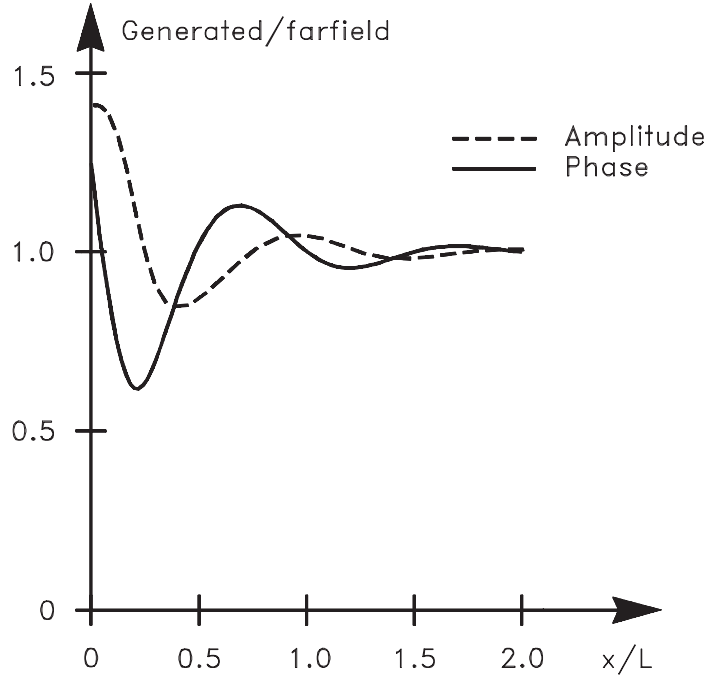
Figure 1.3: Wave amplitude and phase of the generated wave field relative to the far-field solution, h = 0.7 m, T = 0.7 sec ⇒ L=0.77 m

The first term in the function expresses the velocity potential at infinity, by Biésel called the far-field solution, while the second term is the near-field solution. The first term describes the generated progressive wave, while the second describes the standing waves which decreases with the distance from the wavemaker.

In general only the far-field solution is considered. As the displacement, e, of the wave generator is defined by

$$e(z,t) \quad = \quad \frac{S(z)}{2} \sin(\omega t)$$

The far-field surface elevation is seen to be phase shifted $\frac{\pi}{2}$ relative to the displacement of the wave generator. The "disturbance" from the near-field solution will at a distance of 1-2 wave lengths from the wavemaker be less than 1% of the far-field solution. See Figure 1.3

It is now straight forward to calculate the Biésel Transfer Function for any wave maker as long as the stroke, $S(z)$, of the paddle can be described. As stated by Biésel, it is necessary to require that $S(z)$ and its first two(three) derivatives are limited for $-h < z < 0$.
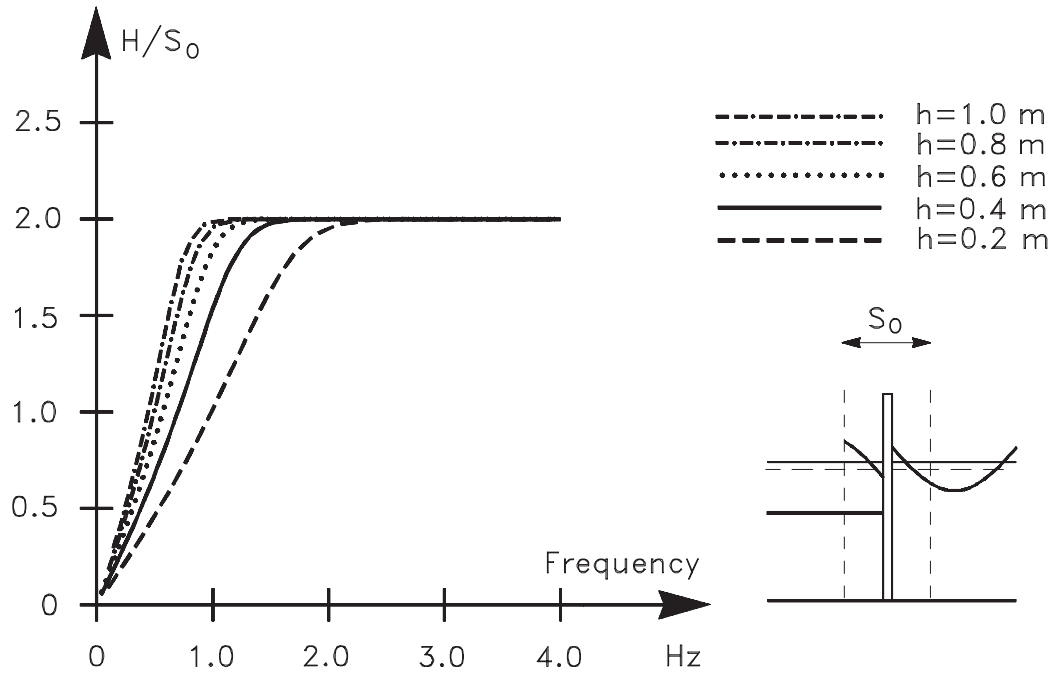
$$S(z) = S_0.$$

$$\frac{H}{S_0} = \frac{2\sinh^2(kh)}{\sinh(kh)\cosh(kh) + kh}$$

Figure 1.4: Far field Biésel Transfer Function for piston-type wave maker.

In Figures 1.4 to 1.7 are listed some solutions for the piston-type and the hinged-type wave maker. The reader can with little effort add any wave maker to this list. The Biésel Transfer Function is in these figures defined as the ratio between the far-field wave height, H and the stroke of the paddle for $z = 0$, denoted S_0.
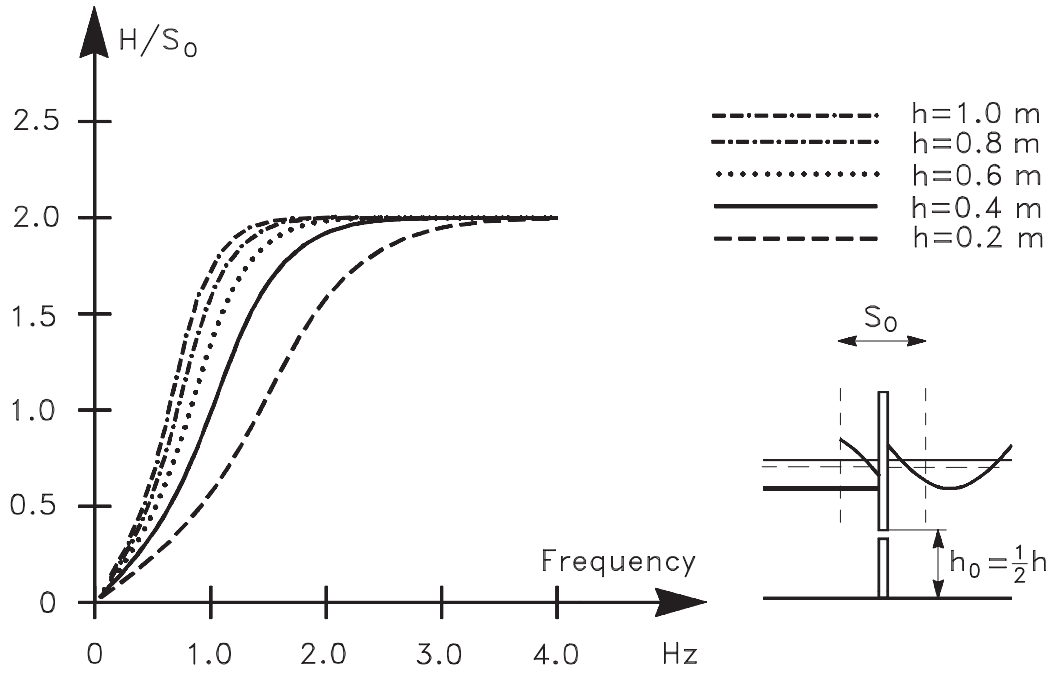
$$S(z) = S_0 \quad, \quad (z+h) > h_0$$
$$S(z) = 0 \quad, \quad (z+h) < h_0$$
$$\frac{H}{S_0} = \frac{2\,\sinh^2(kh) - 2\,\sinh(kh_0)\,\sinh(kh)}{\sinh(kh)\,\cosh(kh) + kh}$$

Figure 1.5: Far field Biésel Transfer Function for elevated piston-type wave maker.

$$S(z) \ = \ \frac{S_0}{h} \cdot (h + z)$$

$$\frac{H}{S_0} \ = \ \frac{2 \, \sinh(kh) \, (1 - \cosh(kh) + kh \, \sinh(kh))}{kh \, (\sinh(kh) \, \cosh(kh) + kh)}$$
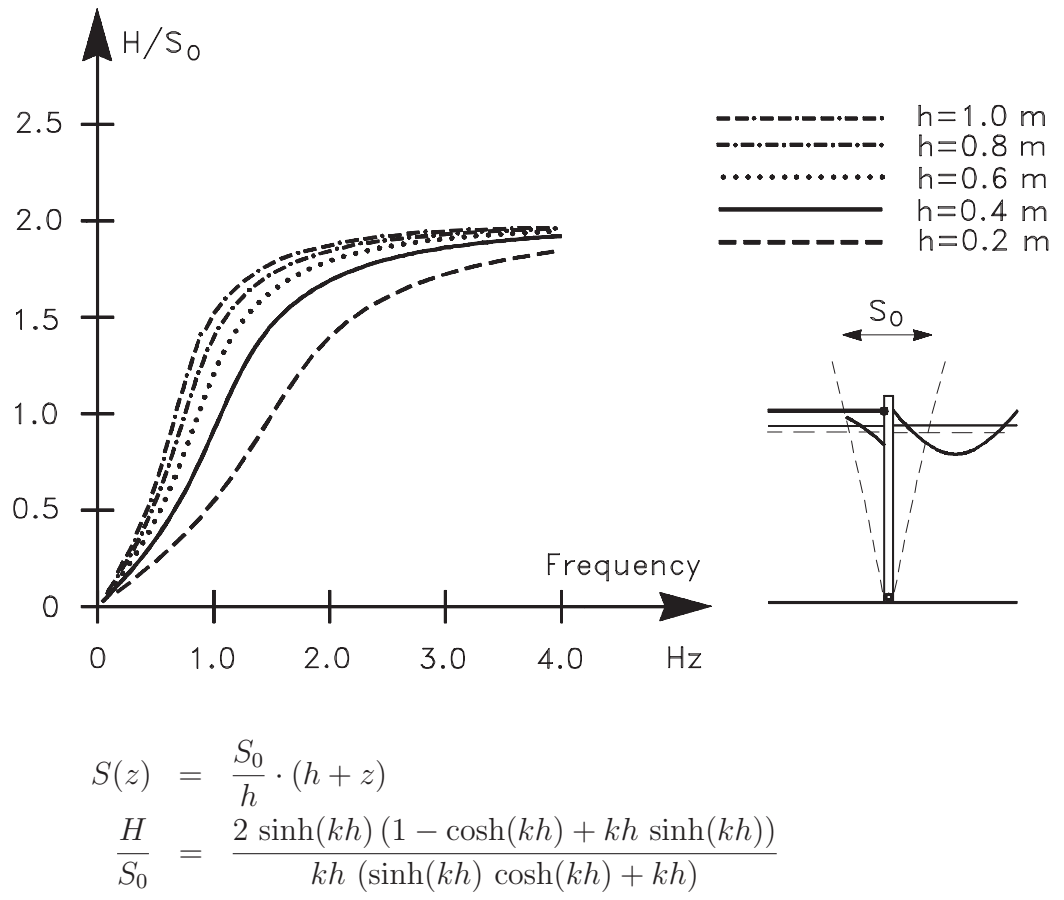
Figure 1.6: Far field Biésel Transfer Function for hinged-type wave maker.
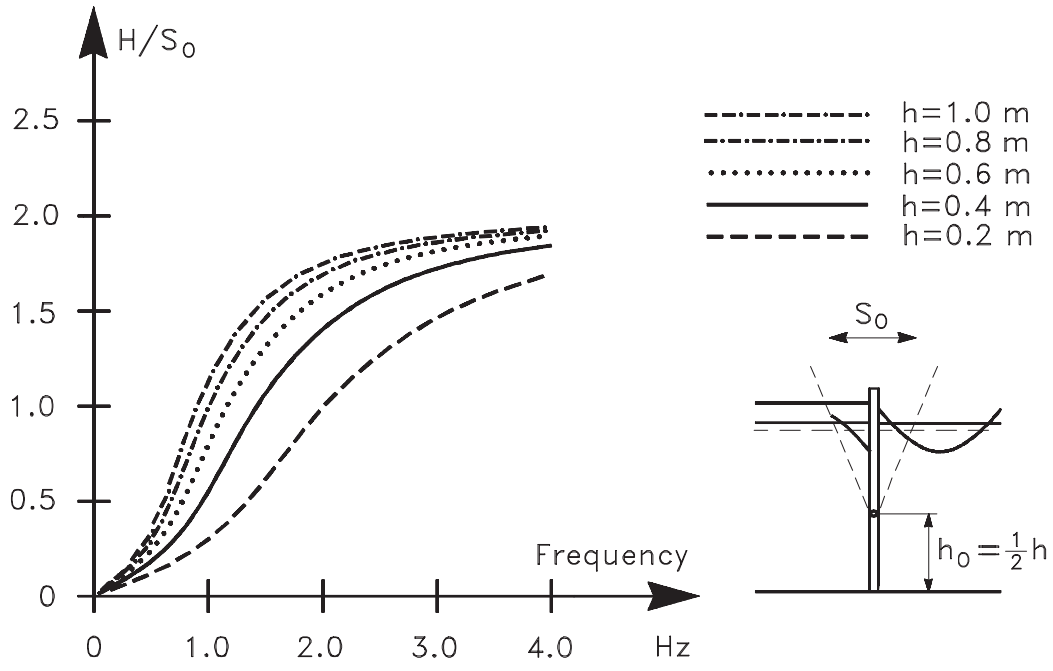
$$S(z) = S_0 \cdot \frac{h + z - h_0}{h - h_0} \quad , \quad (z + h) > h_0$$

$$S(z) = 0 \quad , \quad (z + h) < h_0$$

$$\frac{H}{S_0} = \frac{2}{k\,(h - h_0)} \left[\frac{\sinh(kh)\,((h - h_0)\,k\,\sinh(kh) - \cosh(kh) + \cosh(kh_0))}{\sinh(kh)\,\cosh(kh) + kh} \right]$$

Figure 1.7: Far field Biésel Transfer Function for elevated hinged-type wave maker.

13

Chapter 2

Generation of Long crested Waves

This chapter introduces three mathematical techniques for generating 2 dimensional waves in a laboratory environment. The techniques are: the Random Phase Method, the Random Complex Spectrum Method and the White Noise Filtering Method. The pros and cons of the outlined techniques are discussed in detail in each section.

First a mathematical description of ocean waves and the general hydrodynamic considerations are listed.

2.1 Charachteristics of waves

Wind generated ocean waves are random in nature. Normally they are described mathematically as the summation of a large number of sinusoids. The amplitudes and phases of these sinusoids are determined by means of Fourier transformation of the surface elevation time series. The Fourier transform yields the frequency charachteristics of a given sea state. It is common practice to describe a wave train by means of its energy (variance) spectrum.

A mathematical formula is often used to describe the spectrum of a wave train. These mathematical formulas have been derived by fitting actual recorded wave data under various conditions. Spectral densities are given as a function of conditions (wind speed and fetch length) or statistics describing the sea state (significant wave height H_s and peak frequency f_p). Different forms of the spectrum at its various generation stages have been obtained. Two such empirical spectra, the Pierson-Moskowitz and JONSWAP spectra, are given below. The former represents fully-developed sea states

whereas the latter represents conditions at which the fetch length of the wind is a limiting factor.

Pierson-Moskowitz type:

$$S_\eta(f) \quad = \quad \frac{\alpha g^2}{(2\pi)^4} \, f^{-5} \, exp\left(-0.74\left(\frac{f_0}{f}\right)^4\right)$$

where

$$\alpha \quad = \quad 0.0081$$
$$f_0 \quad = \quad g\left(2\pi U_{19.5}\right)^{-1}$$

and $U_{19.5}$ denotes the wind speed 19.5 m above mean water level.

Pierson-Moskowitz type, parametrized:

$$S_\eta(f) \quad = \quad \frac{5}{16} \, H_{m0}^2 \, f_p^4 \, f^{-5} \, exp\left(-\frac{5}{4}\left(\frac{f_p}{f}\right)^4\right)$$

Jonswap type:

$$S_\eta(f) \quad = \quad \frac{\alpha g^2}{(2\pi)^4} \, f^{-5} \, exp\left(-\frac{5}{4}\left(\frac{f}{f_m}\right)^{-4}\right) \, \gamma^{exp\left(-\frac{1}{2\sigma^2}\left(\frac{f}{f_m}-1\right)^2\right)}$$

where

$$\alpha \quad = \quad 0.076 \, x^{-0.22}$$
$$x \quad = \quad g \, F \, U_{10}^{-2}$$
$$f_m \quad = \quad \frac{3.5 \, g \, x^{-0.33}}{U_{10}}$$

$$
\begin{aligned}
\sigma_f &= 0.07 & f &\leq f_p \\
\sigma_f &= 0.09 & f &> f_p \\
\gamma &= 3.3 \text{ in average in the North Sea}
\end{aligned}
$$

and U_{10} denotes the wind speed 10 m above mean water level.

Jonswap type, parametrized:

$$
\begin{aligned}
S_\eta(f) &= \alpha\, H_{m0}^2\, f_p^4\, f^{-5}\, \gamma^\beta\, exp\left(-\frac{5}{4}\left(\frac{f_p}{f}\right)^4\right) \\
\alpha &= \frac{0.0624}{0.230 + 0.0336\,\gamma - \frac{0.185}{1.9+\gamma}} \\
\beta &= exp\left(-\frac{(f - f_p)^2}{2\sigma_f^2 f_p^2}\right)
\end{aligned}
$$

where

$$
\begin{aligned}
\sigma_f &= 0.07 & f &\leq f_p \\
\sigma_f &= 0.09 & f &> f_p \\
\gamma &= 3.3 \text{ in average in the North Sea}
\end{aligned}
$$

Generation of irregular waves in laboratory environments combines the mathematical description of irregular waves presented above with the transfer function describing the relation between wave generator displacements and surface elevations for sinusoidal motions of the generator.

2.2   Wave Generation Techniques

A number of techniques for reproducing irregular sea states with specified characteristics have been developed. In general, these wave generation techniques fall into two categories: deterministic and non-deterministic techniques.

Deterministic wave generation techniques produce wave trains of finite duration which match the specified charachteristics (the target wave spectrum)

exactly – at least that is the goal.

Non-deterministic (probabilistic) techniques produce wave trains which only match the specified charachteristics within the bounds of probability. Thus, a single generated wave train will not match the target wave energy spectrum. However, the average energy spectrum will approach the target energy spectrum as the number of generated wave trains increases.

In the following, three wave generation techniques will be presented.

The Random Phase Method and the Random Complex Spectrum Method simulate random waves in the frequency domain with subsequent use of the FFT-algorithm in order to obtain the time domain representation of the wave train. The Random Phase Method is a deterministic wave generation technique whereas the Random Complex Spectrum Method is non-deterministic. Both techniques were developed by Rice (1944) and their application to random wave generation (linear and non-linear) was described by Tuah and Hudspeth (1982).

The White Noise Filtering Method simulates random waves in the time domain by means of digital filtering. This method is non-deterministic. It was described by Nunes (1981).

In nature, non-linear interaction between individual wave components in irregular wave trains give rise to so-called group bounded long waves (Ottesen-Hansen, 1978). In physical model tests, correct reproduction of these waves is often essential. Nevertheless, this chapter will focus on linear waves. Methods for correct reproduction of group bounded long waves will be given in chapters 6 and 7.

2.3   Random Phase Method

In the Random Phase Method, wave trains are generated by combining the discrete amplitude wave spectrum corresponding to the target wave energy spectrum with a random phase spectrum synthesized from a random number generator. This yields the Fourier Transform of a time series with the desired discrete power spectrum. The corresponding time series is obtained by Inverse Fourier Transformation.

The steps of calculating a time series using the Random Phase Method are:

1. Define a target wave energy density spectrum. This might be from measurements in nature or from calculations using deterministic expressions like the Pierson-Moskowitz formulation of the spectral density S_η:

$$S_\eta(f) = \frac{5}{16} \, H_s^2 \, f_p^4 \, f^{-5} \, exp\left(-\frac{5}{4}\left(\frac{f_p}{f}\right)^4\right)$$

    where
    $$\begin{aligned} H_s &= \text{significant wave height}\\ f_p &= \text{peak frequency}\\ f &= \text{frequency} \end{aligned}$$

2. Choose the sample frequency, f_s and the resolution of the spectrum (half the number of Fourier components) N. This yields a frequency domain resolution of $\Delta f = \frac{f_s}{N}$. Calculate the discrete wave energy spectrum $\sigma_\eta^2(f_i)$:

$$\sigma_\eta^2(f_i) = S_\eta(i \cdot \Delta f) \cdot \Delta f$$

3. Determine the discrete paddle-displacement energy spectrum.
    The far field transfer function for small amplitude regular waves was given by Biésel (1951) in the following form for piston wave paddles:

$$\frac{H}{S_0} = \frac{2\,\sinh^2(kh)}{\sinh(kh)\,\cosh(kh) + kh}$$

    where
    $$\begin{aligned} H &= \text{wave height}\\ k &= \text{wave number } \left(\tfrac{2\pi}{L}\right)\\ h &= \text{water depth}\\ S_0 &= \text{stroke of the piston} \end{aligned}$$

When the water depth is known it is possible to calculate the Biésel transfer function.

It is now possible to determine the discrete paddle-displacement energy spectrum, $\sigma_x^2(f_i)$:

$$\sigma_x^2(f_i) = \frac{\sigma_\eta^2(f)}{\left(\frac{2\,\sinh^2(kh)}{\sinh(kh)\,\cosh(kh)+kh}\right)^2}$$

note that k is a function of frequency.

4. Calculate the N complex Fourier coefficients $C = A + i \cdot B$ by picking a random phase, $\varphi(f)$, between 0 and 2π for all frequencies smaller than the Nyquist frequency, $f_n = f_s/2$:

$$A_i = \cos\left(\varphi(f_i)\right) \cdot \sqrt{\sigma_x^2(f_i)}/\sqrt{2}$$
$$B_i = \sin\left(\varphi(f_i)\right) \cdot \sqrt{\sigma_x^2(f_i)}/\sqrt{2}$$

Mirror the N Fourier components into the Nyquist frequency f_n in order to obtain a hermitian Fourier Transform, i.e.:

$$C_{N+i} = C_{N-i+1}^* , \quad i = 1..N$$

where * denotes complex conjugate.

5. Apply the inverse Fourier Transform (InvFFT) and calculate the time series of the control signal for the wave paddle (the real parts of the inverse Fourier Transform is the time series, the imaginary parts are zero due to the fact that the Fourier Transform is hermitian).

6. Use oversampling in order to get a better discretization of the control signal.

Figures 2.1-2.5 illustrate the procedure described above applied to a specific example.

The Random Phase Method is a deterministic wave generation method, i.e. the power spectrum of the generated wave train is identical to that of the target wave power spectrum over the length of the time series. This means that two different realizations with different spectral properties can be directly compared.

The length of the time series is only limited by the capacity of the computer performing the Fourier transform. Often a number of relatively short time series, say 5-10 minutes in length, calculated by means of the Random Phase
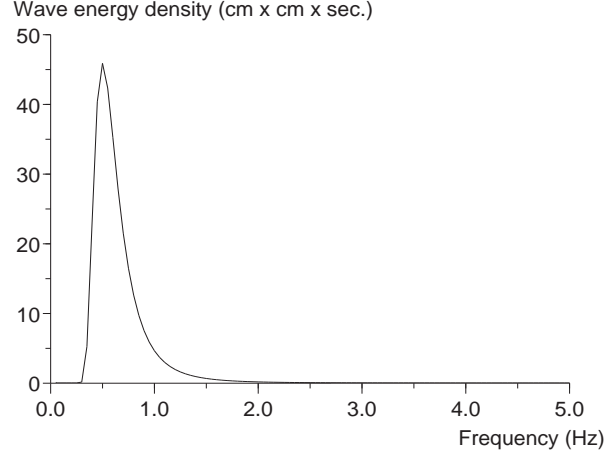
Figure 2.1: Example of calculated model wave energy density spectra $S_f(f)$ using the PM-spectra with $H_s = 0.16 \ m, f_p = 0.5 \ Hz$.

Method are connected substituting a long realization in order to save computing time. This method is very efficient for pilot testings, calibration of wave generators, measurements of reflections etc.

However, for long simulations, where the right variations in the spectral distribution are required, one long time series must be used in order to get the right variability of the spectra for short samples. Alternatively another wave generation technique i.e. the Filtered White Noise technique should be used.

2.4   Random Complex Spectrum Method

The Random Complex Spectrum Method is a non-deterministic wave generation technique which produces time series with Gaussian distributed amplitude spectra.

The technique is rather similar to the Random Phase Method. However, When the Random Complex Spectrum Method is applied, the real and imaginary components of the complex Fourier coefficients (compare with page 6, item 4) are determined as:

$$A_i \ = \ G_j \cdot \sqrt{\sigma_x^2(f_i)}/\sqrt{2}$$

$$B_i \quad = \quad G_{j+1} \cdot \sqrt{\sigma_x^2(f_i)}/\sqrt{2}$$

where G is a normally distributed random variable with zero mean and a standard deviation of $\sigma = 1$.

This method has the same limitations as the Random Phase Method: the length of the time series is limited by the capacity of the computer performing the Fourier transformation. An equivalent method which is not subject to this limitation will be described in the following section.

2.5   White Noise Filtering Method

The technique is based on the use of digital filters. Socalled FIR-filters (Finite Impulse Response filters) are applied (Karl, p. 165).
In essence, a digital filter is designed by computing the time domain terms h_i called filter coefficients (or the filter operator), for use in convolving with the input data in order to achieve a specific frequency response.

The surface elevation time series $\eta(t)$ is obtained by generating a white noise signal $W(t)$ (samples from a unit normal random variable) which is convolved with a filter operator determined by Inverse Fourier Transformation of a discrete frequency response function corresponding to the discrete target wave energy spectrum (the surface elevation filter). The input/output relation of this filter is given by the discrete convolution integral:

$$\eta_j = \sum_{i=0}^{2 \cdot N - 1} h_i \cdot W_{j-i}$$

where $2 \cdot N$ denotes the number of filter coefficients.

To determine the corresponding wave paddle displacement time series, the surface elevation time series is convolved with another filter operator obtained by Inverse Fourier Transformation of a frequency response function corresponding to the inverse of the far field Biesel transfer function (the Biesel filter).

Designing the surface elevation filter can be divided into 6 steps:

1. The desired wave power spectrum is defined.

2. The wave power spectrum is discretized in N components.

3. For each component, a phase Φ_i is chosen as

$$\Phi_i = \begin{cases} 0 & \text{if i is even} \\ \pi & \text{if i is odd} \end{cases}$$

This phase removes the phase shift introduced by the filter delay. For wave generation removing the phase shift is unnessecary. However, it is of importance in other applications.

4. Determine the value of the frequency response function H corresponding to each component i (frequency sampling)

$$H(f_i).re = cos(\Phi_i)\sqrt{\sigma_\eta^2(f_i)}/\sqrt{2}$$
$$H(f_i).im = sin(\Phi_i)\sqrt{\sigma_\eta^2(f_i)}/\sqrt{2}$$

H specifies the desired frequency response of the surface elevation filter.

5. Mirror the discrete frequency responce function into the nyquist frequency to obtain a Hermitian discrete frequency response function , i.e.

$$H(f_n + f_i) = H^*(f_n - f_i)$$

6. Compute the Inverse Fourier Transform of the frequency response function to produce the filter operator (the real parts of the InvFFT are the filter coefficients, the imaginary parts are zero due to the fact that H is hermitian).

The Biesel filter is designed by proceeding from step 3 and determining the discrete values of the frequency response function as

$$H(f_i).re = cos(\Phi_i)\frac{1}{K_f(f_i)}$$
$$H(f_i).im = sin(\Phi_i)\frac{1}{K_f(f_i)}$$

where K_f denotes the far field Biesel transfer function.
The phase Φ_i is chosen as $-\pi/2$ in order to eliminate the phase shift between flap displacements and surface elevations.

Figures 2.6-2.10 illustrate the White Noise Filtering Method applied to a specific example.
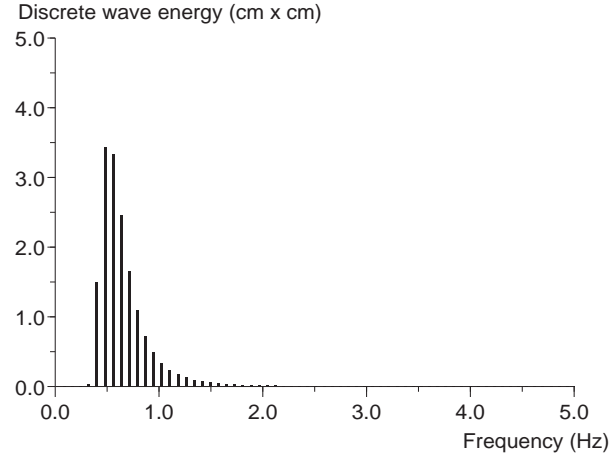
Figure 2.2: Example of discrete wave energy spectrum σ_η^2. PM-spectrum. $H_s = 0.16\ m, f_p = 0.5\ Hz, f_s = 5\ Hz, N = 64$. For practical use N must be much larger.
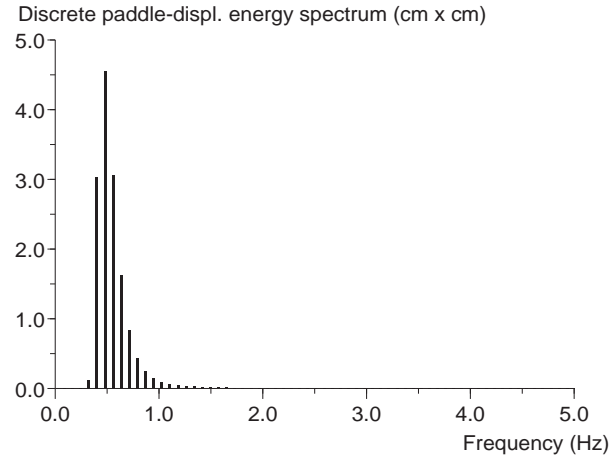
Figure 2.3: Discrete paddle displacement energy spectrum σ_x^2. Example using PM-spectrum with $H_s = 0.16\ m$, $f_p = 0.5\ Hz$, $f_s = 5\ Hz$, $N = 64$, $h = 0.70\ m$ and piston wave generator.
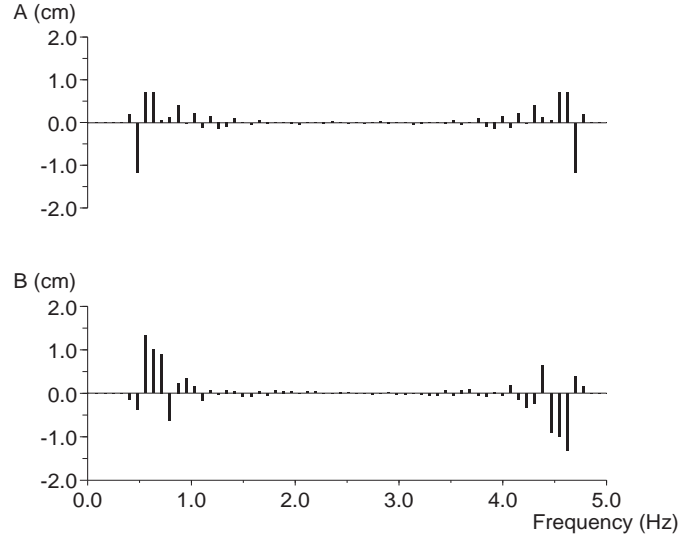
Figure 2.4: Real and imaginary parts of hermitian Fourier Transform. Example using PM-spectrum with $H_s = 0.16\ m$, $f_p = 0.5\ Hz$, $f_s = 5\ Hz$, $N = 64$, $h = 0.70\ m$ and piston wave generator.
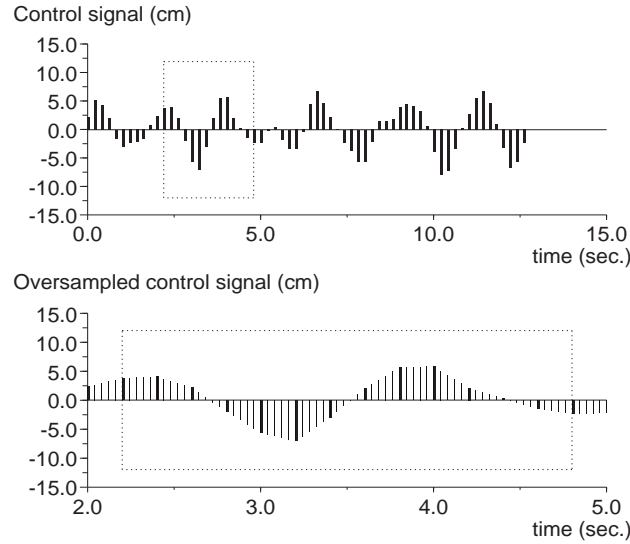
Figure 2.5: Paddle displacement time series. Example using PM-spectrum with $H_s = 0.16\ m$, $f_p = 0.5\ Hz$, $f_s = 5\ Hz$, $N = 64$, $h = 0.70\ m$ and piston wave generator.
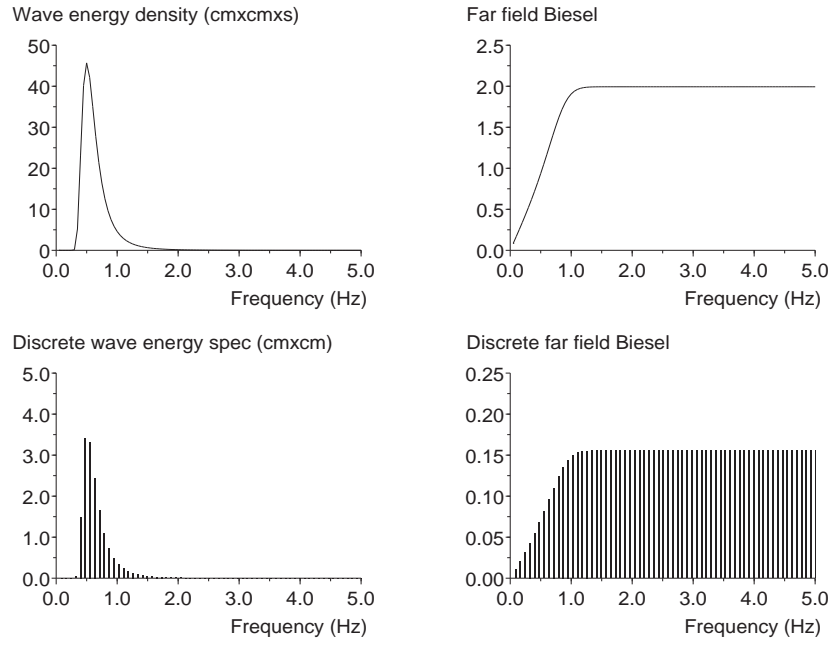
Figure 2.6: Discretization of wave energy spectrum (left) and Biesel far field transfer function (right). Example using the PM-spectra with $H_s = 0.16\ m, f_p = 0.5\ Hz,\ f_s = 5Hz,\ N = 64\ h = 0.70\ m$ and piston wave generator.
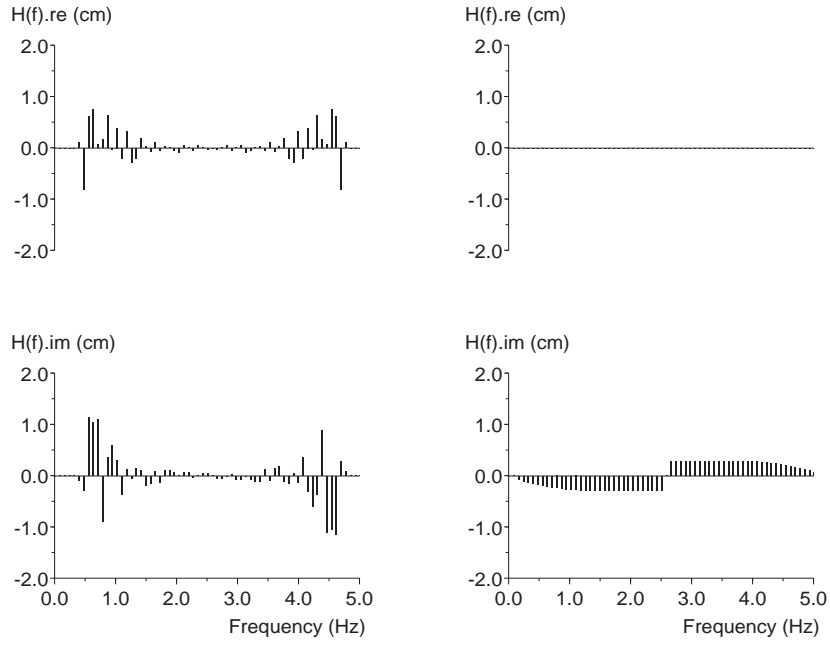
Figure 2.7: Discrete complex frequency response functions corresponding to surface elevation filter operator (left) and Biesel filter operator (right). Example using the PM-spectra with $H_s = 0.16 \ m$, $f_p = 0.5 \ Hz$, $f_s = 5Hz$, $N = 64 \ h = 0.70 \ m$ and piston wave generator.
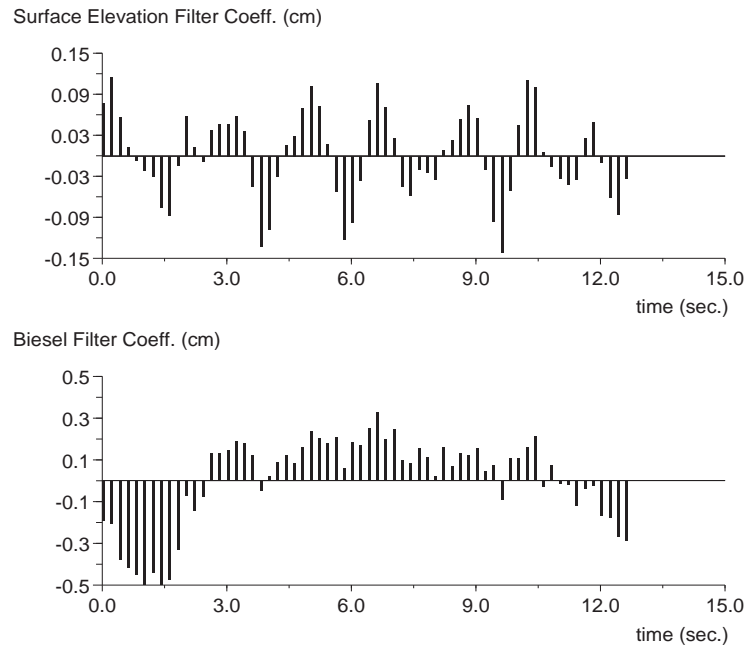
Figure 2.8: Surface elevation filter operator (upper) and Biesel filter operator (lower) obtained by means of InvFFT of complex frequency response functions. Example using the PM-spectra with $H_s = 0.16\ m, f_p = 0.5\ Hz$, $f_s = 5Hz$, $N = 64\ h = 0.70\ m$ and piston wave generator.
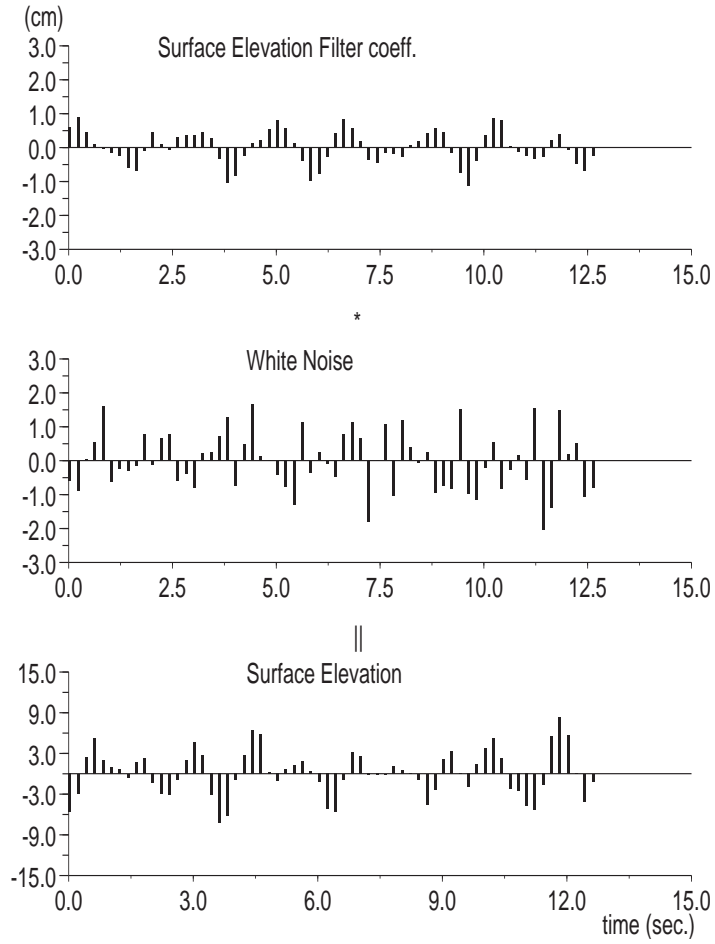
Figure 2.9: Surface elevation time series obtained by convolving the surface elevation filter operator with white noise time series. Convolution denoted by *. Example using the PM-spectra with $H_s = 0.16\ m$, $f_p = 0.5\ Hz$, $f_s = 5Hz$, $N = 64$ $h = 0.70\ m$ and piston wave generator.
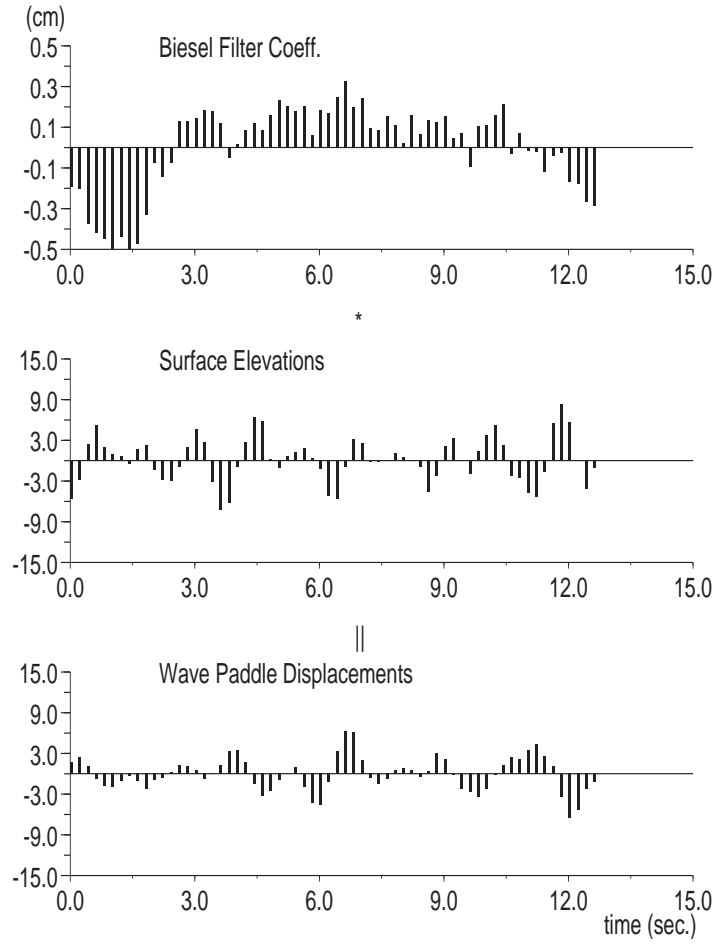
Figure 2.10: Wave paddle displacement time series obtained by convolving the Biesel filter operator with the surface elevation time series. Convolution denoted by *. Example using the PM-spectra with $H_s = 0.16\,m$, $f_p = 0.5\,Hz$, $f_s = 5Hz$, $N = 64$, $h = 0.70\,m$ and piston wave generator.

Chapter 3

# Seperation of Incident and Reflected Long-Crested Waves Using Digital Filters

In the hydraulic laboratory environment a separation of an irregular wave field into incident waves propagating towards a structure, and reflected waves propagating away from the structure is often wanted. This is due to the fact that the response of the structure to the incident waves is the target of the model test.

Goda and Suzuki (1976) presented a frequency domain method for estimation of irregular incident and reflected waves in random waves. Mansard and Funke (1980) improved this method using a least squares technique.

In the following a time-domain method for Separating the Incident waves and the Reflected Waves (SIRW-method) is presented. The method is based on the use of digital filters and can separate the wave fields in *real time*.

3.1   Principle

To illustrate the principle of the SIRW-method the set-up shown in Fig. 3.1 will be considered. The surface elevation $\eta(x, t)$ at a distance x from the wave generator may be written as the sum of the incident and reflected waves: the incident wave propagating away from the wave generator, and the reflected wave propagating towards the wave generator. Even though the method works for irregular waves it will be demonstrated in the following pages for
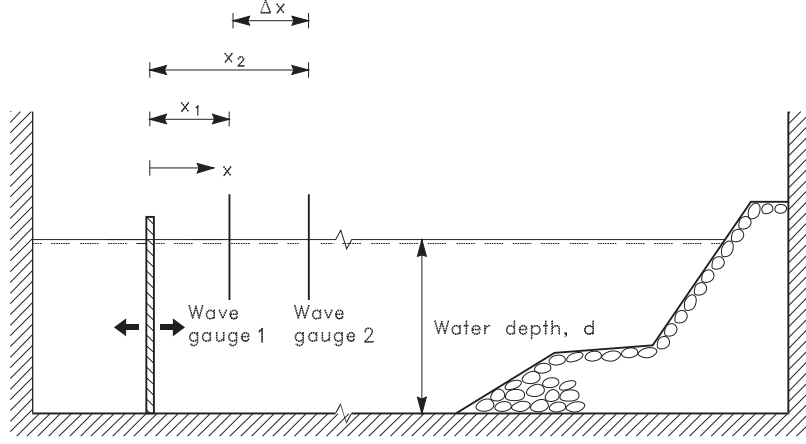
Figure 3.1: *Wave channel with piston-type wave generator.*

the case of monochromatic waves.

$$
\begin{aligned}
\eta(x,t) &= \eta_I(x,t) + \eta_R(x,t) \\
&= a_I cos(2\pi ft - kx + \phi_I) + a_R cos(2\pi ft + kx + \phi_R) \qquad (3.1)
\end{aligned}
$$

where

$$
\begin{array}{ll}
f & : \text{frequency} \\
a = a(f) & : \text{wave amplitude} \\
k = k(f) & : \text{wave number} \\
\phi = \phi(f) & : \text{phase}
\end{array}
$$

and indices I and R denote incident and reflected, respectively.

At the two wave gauges we have:

$$
\begin{aligned}
\eta(x_1,t) &= a_I cos(2\pi ft - kx_1 + \phi_I) + a_R cos(2\pi ft + kx_1 + \phi_R) \quad (3.2) \\
\eta(x_2,t) &= a_I cos(2\pi ft - kx_2 + \phi_I) + a_R cos(2\pi ft + kx_2 + \phi_R) \\
&= a_I cos(2\pi ft - kx_1 - k\Delta x + \phi_I) + \\
&\quad a_R cos(2\pi ft + kx_1 + k\Delta x + \phi_R) \qquad\qquad (3.3)
\end{aligned}
$$

where $x_2 = x_1 + \Delta x$ has been substituted into eq. (3.3).
It is seen that the incident wave is phaseshifted $\Delta\phi = k\Delta x$ from signal
$\eta(x_1,t)$ to signal $\eta(x_2,t)$, and the reflected wave is phaseshifted $\Delta\phi = -k\Delta x$
due to opposite travel directions. These phaseshifts are called the physical
phaseshifts and are denoted ϕ_I^{phys} and ϕ_R^{phys}, respectively.

The idea in the following manipulations of the elevation signals is to phase-shift the signals from the two wave gauges in such ways that the incident parts of the wave signals are in phase while the reflected parts of the signals are in mutual opposite phase. In this case the sum of the two manipulated signals is proportional to and in phase with the incident wave signal.

An amplification C and a theoretical phase shift ϕ^{theo} are introduced into the expressions for $\eta(x,t)$. The modified signal is denoted η^*. For the i'th wave gauge signal the modified signal is defined as:

$$
\begin{aligned}
\eta^*(x_i,t) \;=\; & Ca_I cos(2\pi ft - kx_i + \phi_I + \phi_i^{theo}) + \\
& Ca_R cos(2\pi ft + kx_i + \phi_R + \phi_i^{theo})
\end{aligned}
\tag{3.4}
$$

This gives at wave gauges 1 and 2:

$$
\begin{aligned}
\eta^*(x_1,t) \;=\; & Ca_I cos(2\pi ft - kx_1 + \phi_I + \phi_1^{theo}) + \\
& Ca_R cos(2\pi ft + kx_1 + \phi_R + \phi_1^{theo})
\end{aligned}
\tag{3.5}
$$

$$
\begin{aligned}
\eta^*(x_2,t) \;=\; & Ca_I cos(2\pi ft - kx_2 + \phi_I + \phi_2^{theo}) + \\
& Ca_R cos(2\pi ft + kx_2 + \phi_R + \phi_2^{theo}) \\
\;=\; & Ca_I cos(2\pi ft - kx_1 - k\Delta x + \phi_I + \phi_2^{theo}) + \\
& Ca_R cos(2\pi ft + kx_1 + k\Delta x + \phi_R + \phi_2^{theo})
\end{aligned}
\tag{3.6}
$$

The sum of $\eta^*(x_1,t)$ and $\eta^*(x_2,t)$, which is denoted $\eta^{calc}(t)$, gives:

$$
\begin{aligned}
\eta^{calc}(t) \;=\; & \eta^*(x_1,t) + \eta^*(x_2,t) \\
\;=\; & Ca_I cos(2\pi ft - kx_1 + \phi_I + \phi_1^{theo}) + \\
& Ca_R cos(2\pi ft + kx_1 + \phi_R + \phi_1^{theo}) + \\
& Ca_I cos(2\pi ft - kx_1 - k\Delta x + \phi_I + \phi_2^{theo}) + \\
& Ca_R cos(2\pi ft + kx_1 + k\Delta x + \phi_R + \phi_2^{theo})
\end{aligned}
$$

$$\begin{aligned} &= 2Ca_I cos(0.5(-k\Delta x - \phi_1^{theo} + \phi_2^{theo})) \\ &\quad cos(2\pi ft - kx_1 + \phi_I + 0.5(-k\Delta x + \phi_1^{theo} + \phi_2^{theo})) + \\ &\quad 2Ca_R cos(0.5(-k\Delta x + \phi_1^{theo} - \phi_2^{theo})) \\ &\quad cos(2\pi ft + kx_1 + \phi_R + 0.5(k\Delta x + \phi_1^{theo} + \phi_2^{theo})) \qquad (3.7) \end{aligned}$$

It is seen that $\eta^{calc}(t)$ and $\eta_I(x_1, t) = a_I cos(2\pi ft - kx_1 + \phi_I)$ are identical signals when the following three conditions are met:

$$2C cos(0.5(-k\Delta x - \phi_1^{theo} + \phi_2^{theo})) = 1 \qquad (3.8)$$

$$\begin{aligned} 0.5(-k\Delta x + \phi_1^{theo} + \phi_2^{theo}) &= n \cdot 2\pi & n \in (0, \pm 1, \pm 2, ..) \quad (3.9) \\ 0.5(-k\Delta x + \phi_1^{theo} - \phi_2^{theo}) &= \frac{\pi}{2} + m \cdot \pi & m \in (0, \pm 1, \pm 2, ..) \quad (3.10) \end{aligned}$$

Solving eqs. (3.8) - (3.10) with respect to $\phi_1^{theo}, \phi_2^{theo}$ and C gives eqs (11) - (13). n and m can still be chosen abitrarily.

$$\begin{aligned} \phi_1^{theo} &= k\Delta x + \pi/2 + m\pi + n2\pi & (3.11) \\ \phi_2^{theo} &= -\pi/2 - m\pi + n2\pi & (3.12) \\ C &= \frac{1}{2cos(-k\Delta x - \pi/2 - m\pi)} & (3.13) \end{aligned}$$

All the previous considerations and calculations were done in order to find an amplification and a phaseshift for each of the two elevation signals η_1 and η_2.

Eqs. (3.11) - (3.13) give the result of our efforts, i.e. $\eta_I(x_1, t) = \eta^{calc}(t)$. Remembering that $\phi_1^{theo} = \phi_1^{theo}(f), \phi_2^{theo} = \phi_2^{theo}(f)$ and $C = C(f)$, it is seen that the goal is already reached in the *frequency domain*. However, the implementation of the principle will be done in the *time domain* using digital filters.

It is seen that singularities may occur. The consequences and the handling of the singularities will be treated later on in the paper. Here it should just be mentioned that one way to bypass the singularities is to use a velocity meter instead of one of the two wave gauges. Nevertheless, this paper will concentrate on using elevation signals from two wave gauges.

$$\eta(x_1,t) \longrightarrow \boxed{\text{FILTER 1}} \searrow$$
$$\oplus \longrightarrow \eta_I(x_1,t)$$
$$\eta(x_2,t) \longrightarrow \boxed{\text{FILTER 2}} \nearrow$$
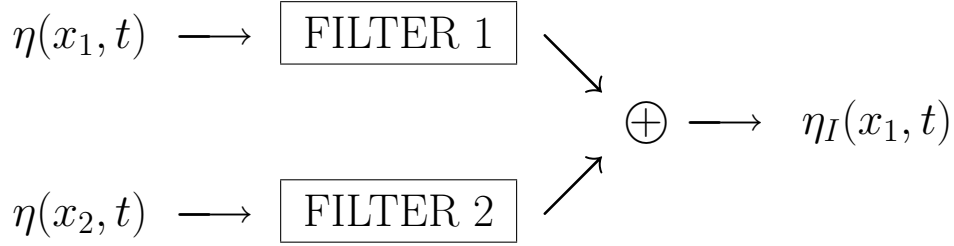
Figure 3.2: *Flow diagram for signals in the SIRW-method.*

The purposes of the filters shown in Fig. 3.2 are exactly a frequency dependent amplification and a frequency dependent phaseshift on each of the two elevation signals.

Taking $n = 0$ and $m = 0$ the frequency response functions $H_1(f)$ for filter 1 and $H_2(f)$ for filter 2 calculated due to eqs. (3.11) - (3.13) are given below in complex notation:

$$Re\{H_1(f)\} = \frac{1}{2cos(-k\Delta x - \pi/2)} \cdot cos(k\Delta x + \pi/2)$$

$$Im\{H_1(f)\} = \frac{1}{2cos(-k\Delta x - \pi/2)} \cdot sin(k\Delta x + \pi/2) \qquad (3.14)$$

$$Re\{H_2(f)\} = \frac{1}{2cos(-k\Delta x - \pi/2)} \cdot cos(-\pi/2)$$

$$Im\{H_2(f)\} = \frac{1}{2cos(-k\Delta x - \pi/2)} \cdot sin(-\pi/2) \qquad (3.15)$$

Based on eqs. (3.14) and (3.15) it is straightforward to design the time domain filters. The design of the filters will be given on the next pages.

3.2 Design of Filters

The impulse response of the filters is found by an inverse *discrete* Fourier transformation, which means that N discrete values of the complex frequency response are used in the transformation, see Fig. 3.3.
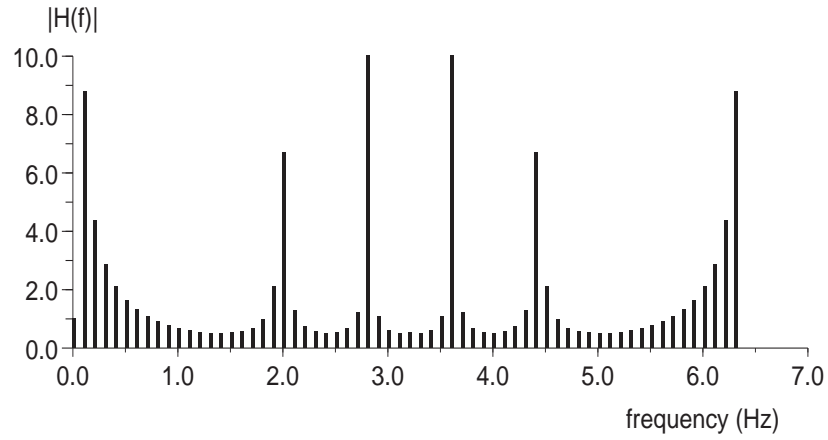
Figure 3.3: *Magnitude (gain) of the frequency responses of a discrete filter. $N = 64$, $d = 0.5$ m, $\Delta f = 0.10$ Hz, $\Delta t_{filter} = 0.16$ sec., $\Delta x = 0.2m$.*

This gives an impulse response of *finite* duration, i.e. the impulse response h^j or the filter coefficients are found by:

$$h^j = h(j \cdot \Delta t_{filter}) = \sum_{r=0}^{N-1} H^r \cdot e^{i \frac{2\pi r j}{N}} \tag{3.16}$$

where
$r = 0,\ldots,$ N-1
$j = 0,\ldots,$ N-1

and H^r is the complex frequency response given by eqs. (3.14) and (3.15) at the frequency $f = r \cdot \Delta f$.

The frequency increment, Δf, in the frequency response is found by

$$\Delta f = \frac{1}{N \cdot \Delta t_{filter}} \tag{3.17}$$

where Δt_{filter} is the time increment of the filter.
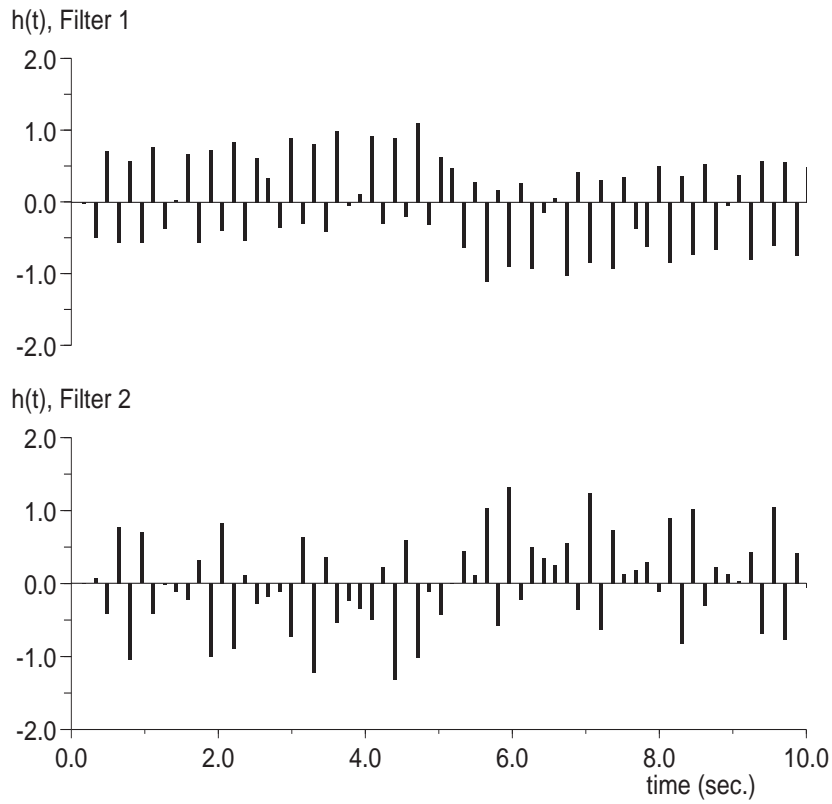
Figure 3.4: *Filter coefficients corresponding to Filter 1 and Filter 2. N = 64, waterdepth = 0.5 m, Δf=0.10 Hz, Δt_{filter} = 0.16 sec.,Δx = 0.2m.*

Fig. 3.4 gives an example on the filters. The price paid for handling only N frequencies in this transformation, is a minor inaccuracy in the performance of the filter at input frequencies, which do not coincide with one of the calculated frequencies in the discrete filter.

If the length of the filter (N) is increased, more frequencies are included,

and in principle the overall accuracy of the filter is improved. In practice, however, there is a limit beyond which the accuracy of the filter starts to decrease due to other effects in the model.

The *convolution* integral (summation), eq. (3.18), describes the input-output relationship for the filters. Notice that the output $\eta^*(x,t)$ is delayed $(N/2)$-1 time steps relative to the input $\eta(x,t)$.

$$\eta^{*p} = \sum_{j=0}^{N-1} h^j \cdot \eta^{p-j} \qquad (3.18)$$

where

$j,p = 0,\dots,$ N-1
η^{p-j} : elevation at time $t = (p-j) \cdot \Delta t_{filter}$
η^{*p} : output from filter at time $t = p \cdot \Delta t_{filter}$
h^j : the filter coefficient corresponding to time $t = j \cdot \Delta t_{filter}$

Fig. 3.3 indicates that in the present example, singularities are present at frequencies of about 2.0 Hz and 2.8 Hz. The figure also shows that due to the fact that the frequency response is calculated only at *discrete frequencies* in the filters, the singularities will not *destroy* the calculations. However, it is recommended to *cut off* the frequency responses whenever the value is larger than around 5. For practical use this means that, if $|H(f)| \geq 5$ when calculated, then $|H(f)|$ should be valued 5. Furthermore, it is recommended to *place* the singularities in a frequency range where the wave spectrum is without significant energy, for example 3 times the peak frequency of the spectrum. This can always be done by choosing appropriate values of Δx and Δt_{filter}, i.e. Δx smaller than a quarter of the shortest wave lengths.

3.3 Results

NUMERICAL EXAMPLES

In order to evaluate the SIRW-method we will look at two numerical examples with known incident and reflected waves. The error is described by the difference between the calculated incident wave signal η^{calc} and the actual incident wave signal η_I.
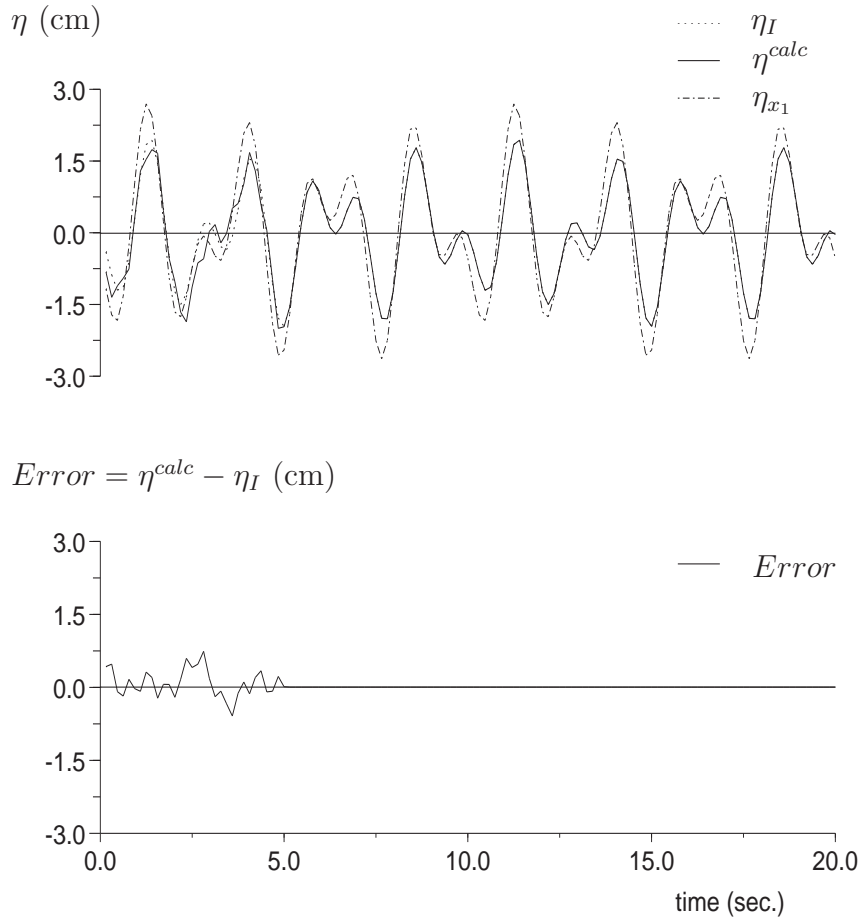
Figure 3.5: *A comparison between η_I, η^{calc} and η_{x_1}. $f_1 = 4\Delta f$, $f_2 = 7\Delta f$.*

39
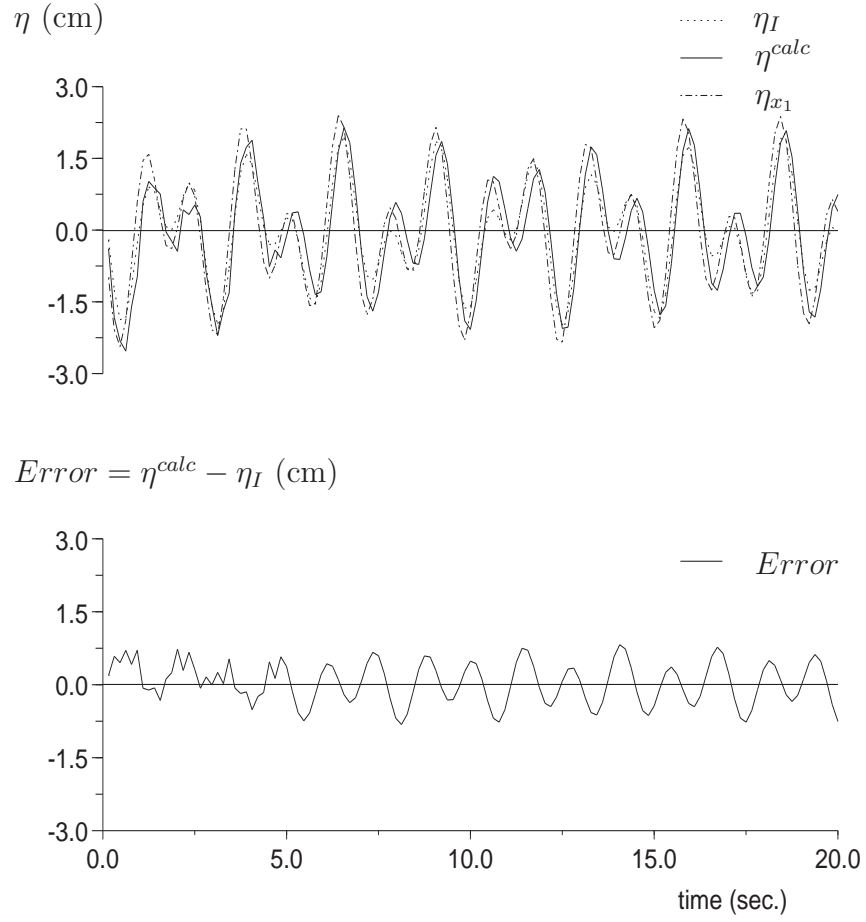
Figure 3.6: *A comparison between η_I, η^{calc} and η_{x_1}. $f_1 = 4.2\Delta f$, $f_2 = 7.5\Delta f$.*

In the examples the total elevation due to two superimposed sine waves is described by eq. (3.19), corresponding to 50 % reflection of the incident waves.

$$
\begin{aligned}
\eta(x,t) \;=\;\; & 0.01 \cdot cos(2\pi f_1 t - k_1 x) + 0.01 \cdot cos(2\pi f_2 t - k_2 x) + \\
& 0.01 \cdot 0.5 \cdot cos(2\pi f_1 t + k_1 x) + \\
& 0.01 \cdot 0.5 \cdot cos(2\pi f_2 t + k_2 x)
\end{aligned}
\tag{3.19}
$$

The signals are sampled with a frequency of 6.4 Hz. Fig. 3.5 illustrates the functionality of the method, when f_1 and f_2 are both coinciding with some

frequencies of the discrete filter, i.e. $n \cdot \Delta f$. As expected the method is exact for signals consisting only of energy placed at the discrete frequencies (Fig. 3.5), though it is seen that errors are present during *warm up* of the filters.
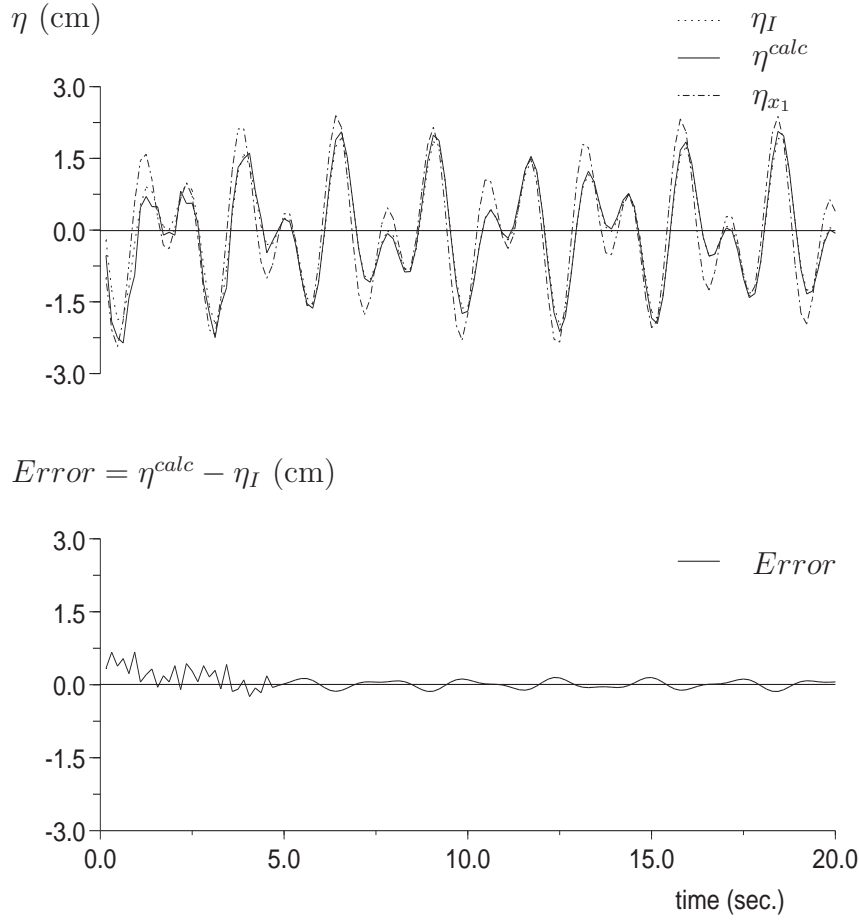
Figure 3.7: *A comparison between η_I, η^{calc} and η_{x_1}. The filters have been cosine tapered. $f_1 = 4.2\Delta f$, $f_2 = 7.5\Delta f$.*

The second example (Fig. 3.6) is identical to the first example except that f_1 and f_2 are not coinciding with frequencies in the digital filter i.e. $f_1 = 4.2\Delta f$, $f_2 = 7.5\Delta f$.

It must be stressed that the output signal shown in Fig. 3.6 corresponds to the worst case situation, where the wave frequencies are placed midway between filter frequencies. One way to improve the results is to apply a tapering of the filter coefficients, because the output from a digital filter is more stable in case the absolute values of the filter coefficients are almost zero in both ends of the filter, Karl (1989). Cosine tapering of the filter coefficients improves the accuracy of the SIRW method as demonstrated in Fig. 3.7.

41

PHYSICAL MODEL TESTS

The SIRW-method previously described was also tested in a laboratory flume at the Hydraulics and Coastal Engineering Laboratory, Aalborg University, cf Fig 3.8.

First, the waves (incident part of the timeseries) were generated and sent towards a spending permeable beach (slope 1:8) with low reflection (app. 5 %) in order to obtain a good estimate of the incident waves. Next, a reflecting wall was mounted in the flume giving a fairly high reflection (app. 50 %) and the same incident waves were reproduced by play back of the same digital steering signal to the wave maker. Notice, that the incident wave fields are identical only until re-reflection occurs.
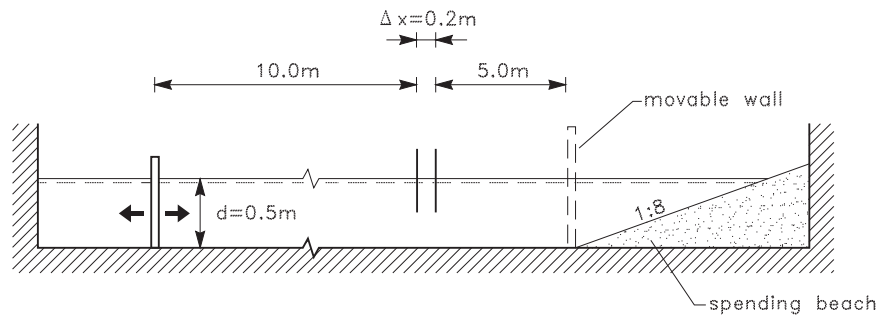
Figure 3.8: *Set-up for physical model tests.*
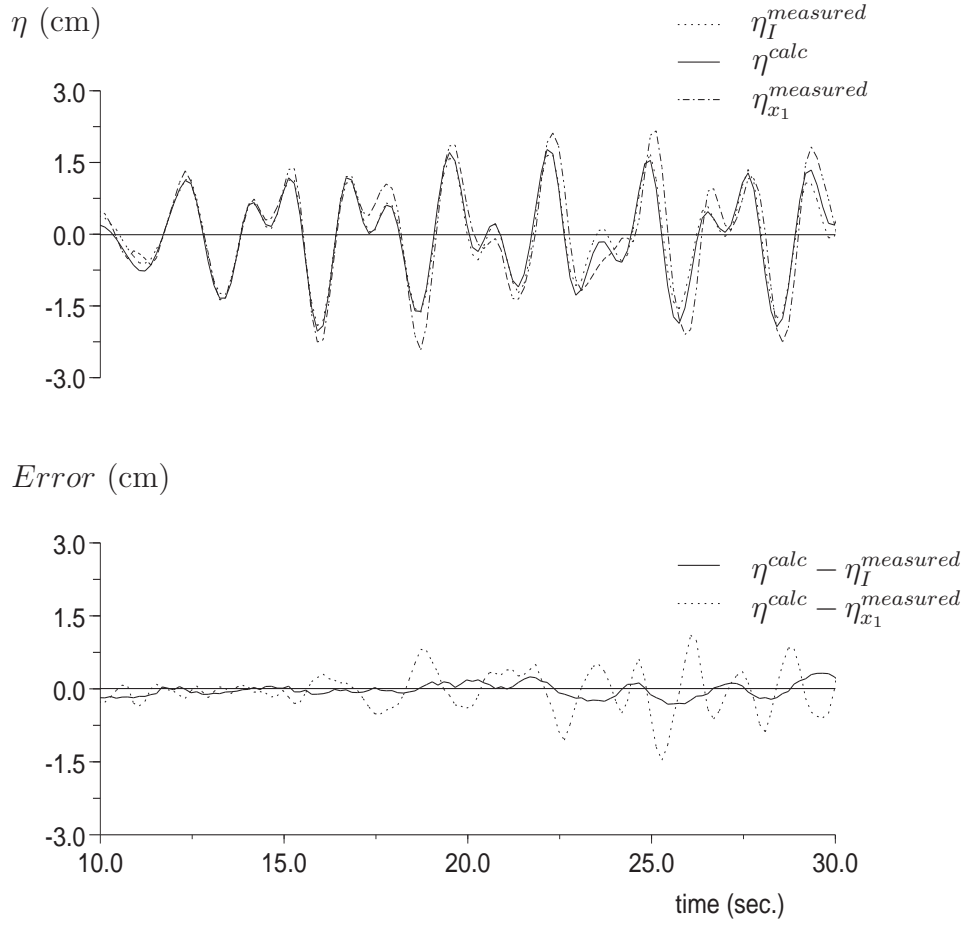
Figure 3.9: *A comparison between $\eta_I^{measured}, \eta^{calc}$ and $\eta_{x_1}^{measured}$. $f_1 = 4.2\Delta f$, $f_2 = 7.5\Delta f$.*

In Fig. 3.9 the output from the SIRW-filters is compared with the incident waves measured in the case of very low reflection. The specific part of the signals, where reflection is present but re-reflection from the wave paddle is still not present, is shown. Two different estimates of the incident waves are used, namely the measured elevation at gauge no 1 ($\eta_{x_1}^{measured}$) and the calculated elevation at gauge no 1 (η^{calc}). In the the specific example the SIRW-method reduces the error (variance of the difference $\eta^{calc} - \eta_{x_1}$) from 30 % of the incident energy to 3 % of the incident energy.

3.4   Conclusions

A time-domain method for Separating Incident and Reflected Irregular Waves (The SIRW-method) has been presented.

By numerical and physical model tests it is demonstrated that the method is quite efficient in separating the total wave field into incident and reflected waves. Please note, that all the tests shown were done with fairly small filters (few filter components), and that longer filters will improve the efficiency of the method. Taking the example shown in Fig. 3.6 and doubling the number of filter coefficients the error (variance) will decrease to 2/3 of the shown example.

The accuracy of the SIRW-method is comparable with the accuracy of the method proposed by Goda and Suzuki (1976), but the SIRW-method has the advantage that where the incident wave signal is wanted in *time domain* (i.e. for zero-crossing analysis) the singularity points are treated more properly than in the Goda-method. The SIRW-method can easily be extended to give the same accuracy as the method proposed by Mansard and Funke (1980).

The greatest advantage of the SIRW-method is that it works in *real time*. Brorsen and Frigaard (1992) previously used digital filters to make an open boundary condition in a Boundary Element Model, based on a filtering of the surface elevation. That boundary condition accumulated errors, because separation of the surface elevation into incident and reflected waves was not possible in *real time* at that moment and, consequently, the Boundary Element Model became unstable and could only run for a limited time. The SIRW-method will make it possible to use digital filters as boundary condition in these models.

At the moment the SIRW-method is implemented at Aalborg Hydraulics Laboratory, Aalborg University and the method is used in active absorption, cf. chapter 4

Chapter 4

Active Absorption of Long-Crested Waves

A comparison of wave gauge based and velocity meter based active absorption systems is presented discussing advantages and disadvantages of the systems. In detail one system based on two surface elevations, one system based on a surface elevation and a horizontal velocity and one system based on a horizontal and a vertical velocity are treated. All three systems are based on digital FIR-filters. For numerical comparison a performance function combining the frequency response of the set of filters for each system is derived enabling discussion on optimal filter design and system setup.

Irregular wave tests with a highly reflective structure with the purely wave gauge based system and the wave gauge velocity meter based system are performed. The wave tests depict the differences between the systems.

4.1 Introduction

Coastal engineering problems are often solved by means of physical and numerical models. Physical and numerical modelling of coastal engineering phenomena require the capability of reproducing natural conditions. One of the problems associated with the modelling of waves in both numerical and laboratory wave flumes is the presence of rereflected waves altering the characteristics of the wave train incident to the model structure repeatedly.

Consequently, an effective absorption of the waves propagating towards the wave generator is necessary. By making the wave generator simultaneously generating the incident wave field and absorbing the reflected wave field the

45
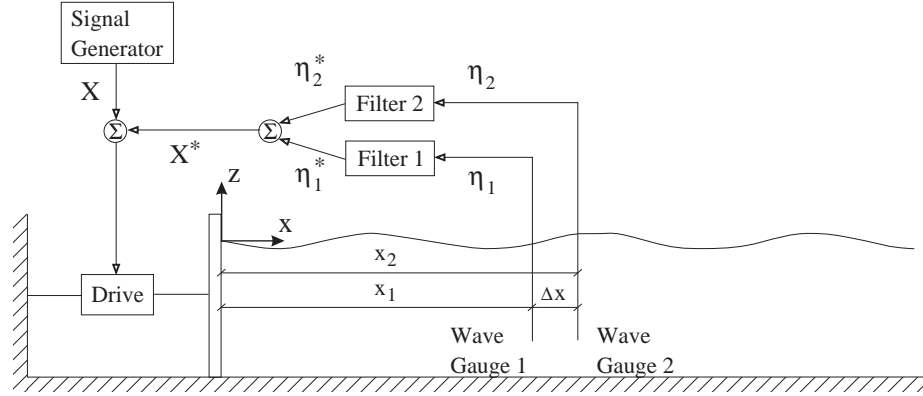
Figure 4.1: Principle of active absorption system.

problems caused by rereflection can be reduced significantly.

The principle in constructing a combined wave generator and active wave absorber requires, Gilbert (1978):

1. A means of detecting reflected waves approaching the wave paddle.

2. A means of making the paddle generate waves that are, in effect, equal and opposite to the reflected waves so that the reflected waves are cancelled out reaching the paddle.

Milgram (1970) presented a system in which waves in a channel were absorbed by means of a moving termination at the end of the channel. The motion of the termination needed for absorption was determined by analog filtering of a surface elevation signal measured in front of the termination. This active wave absorption system was not used in a combined generation and absorption mode.

The common approach to detect the reflected wave when performing simultaneous wave generation and active wave absorption is by measuring the surface elevation with a wave gauge positioned on the face of the paddle. The reflected wave signal is then determined as the difference between the measured surface elevation signal and the generated surface elevation signal estimated from the wave generator control signal. In consequence, the actual reflected wave is not being estimated with the possibility of accumulating errors. Several systems based on this approach have been presented in the litterature, e.g. Bullock and Murton (1989), Hirakuchi et al. (1990) and Schäffer et al. (1994).

46

An active wave absorption system based on real time separation of the wave field in front of the paddle in incident and reflected waves has been installed in a wave flume at Hydraulics & Coastal Engineering Laboratory, Aalborg University (Frigaard (1993)). This open loop system is entirely different from the above described and does not accumulate errors because the actual reflected wave is determined continously. The system shows excellent absorption characteristics, Frigaard and Christensen (1994).

In the following three absorption systems based on the theoretical considerations by Frigaard and Brorsen (1995) are described: one based on two surface elevation signals, one based on a surface elevation and a horizontal velocity signal and one based on a horizontal and a vertical velocity signal. The systems are termed (η, η), (η, u) and (u, w). Based on both numerical and physical tests the systems are compared discussing the differences between the three systems as well as optimal filter design.

4.2   Principle of Active Absorption System

The active absorption system is operated by means of on-line signals from digital FIR-filters. In essence, a digital filter relates N input η^{k-i} with an output x^k by convolving the input data with N precalculated time domain terms h^i called filter coefficients. The input/output relation of the FIR-filter is given by the discrete convolution integral

$$x^k = \sum_{i=-M}^{i=M} h^i \eta^{k-i} \qquad , \quad M = \frac{N-1}{2} \qquad (4.1)$$

with the filter coefficients determining the impulse response of the filter. Given a desired frequency response the corresponding filter impulse response is designed by computing the inverse Fourier transform of the complex frequency response function. Notice that the filter output is delayed $\frac{N-1}{2}$ time steps relative to the input. For systems operating in real time this time delay must be removed.

Calculation of the paddle displacement correction signal needed for absorption of the reflected waves is done by digital filtering and subsequent superposition of two surface elevation or velocity signals measured in front of the wave generator, see principle in Fig. 4.1.

When active absorption is applied the paddle displacement correction signal is added to the input paddle displacement signal read from the signal generator causing the wave generator to operate in a combined gener-

ation/absorption mode.

Having outlined the principle of the system the only remaining problem is to specify the frequency response of the applied filters.

4.3 Frequency Response of Digital Filters

Offspring is taken in the system illustrated in Fig. 4.1 where the wave flume is equipped with two wave gauges.

The surface elevation signal at a position x may be regarded as a sum of harmonic components since the effect of the near field local disturbances disapear when $x > 3d$, with d being the water depth (Biesel (1951)). Considering an isolated component of frequency f the surface elevation arising from this component may be written as the sum of the corresponding incident and reflected wave components

$$
\begin{aligned}
\eta(x,t) &= \eta_I(x,t) + \eta_R(x,t) \\
&= a_I \cos(\omega t - kx + \phi_I) + \\
&\quad a_R \cos(\omega t + kx + \phi_R)
\end{aligned}
\tag{4.2}
$$

where

f	:	frequency
$a = a(f)$	:	wave amlitude
$k = k(f)$	:	wave number
$\phi = \phi(f)$	:	phase

and indices I and R denote incident and reflected, respectively.

Provided a linear relation exists between a given paddle displacement signal and its corresponding surface elevation signal the paddle displacement correction signal $X^*(t)$ which cancels out the reflected component without disturbing the incident component is given by

$$
X^*(t) = Ba_R \cos(\omega t + \phi_R + \phi_B + \pi)
\tag{4.3}
$$

where

B	:	piston stroke/wave height relation
ϕ_B	:	phase shift between paddle displacement and
		surface elevation on the face of the paddle

In the following it is shown that it is possible to amplify and phase shift the

surface elevation signals from the two wave gauges in such a way that their sum is identical to the paddle correction signal corresponding to absorption of the reflected component as given by eq. (4.3).

At the two wave gauges (Fig. 4.1) we have:

$$
\begin{aligned}
\eta(x_1, t) &= a_I \cos(\omega t - kx_1 + \phi_I) + \\
&\quad a_R \cos(\omega t + kx_1 + \phi_R) \\
\eta(x_2, t) &= a_I \cos(\omega t - kx_2 + \phi_I) + \\
&\quad a_R \cos(\omega t + kx_2 + \phi_R) \\
&= a_I \cos(\omega t - kx_1 - k\Delta x + \phi_I) + \\
&\quad a_R \cos(\omega t + kx_1 + k\Delta x + \phi_R)
\end{aligned}
$$

(4.4)

(4.5)

where $x_2 = x_1 + \Delta x$ has been substituted into eq. (4.5).

An amplification of G^η and a theoretical phase shift ϕ^η are introduced into the expressions for $\eta(x, t)$. The modified signal is denoted η^*. For the i'th wave gauge signal the modified signal is defined as

$$
\begin{aligned}
\eta^*(x_i, t) &= G^\eta a_I \cos(\omega t - kx_i + \phi_I + \phi^{\eta_i}) + \\
&\quad G^\eta a_R \cos(\omega t + kx_i + \phi_R + \phi^{\eta_i})
\end{aligned}
$$

(4.6)

This gives at wave gauges 1 and 2

$$
\begin{aligned}
\eta^*(x_1, t) &= G^\eta a_I \cos(\omega t - kx_1 + \phi_I + \phi^{\eta_1}) + \\
&\quad G^\eta a_R \cos(\omega t + kx_1 + \phi_R + \phi^{\eta_1})
\end{aligned}
$$

(4.7)

$$
\begin{aligned}
\eta^*(x_2, t) &= G^\eta a_I \cos(\omega t - kx_1 - k\Delta x + \phi_I + \phi^{\eta_2}) + \\
&\quad G^\eta a_R \cos(\omega t + kx_1 + k\Delta x + \phi_R + \phi^{\eta_2})
\end{aligned}
$$

(4.8)

The sum of $\eta^*(x_1, t)$ and $\eta^*(x_2, t)$ which is termed $\eta^{calc}(t)$ is

$$
\begin{aligned}
\eta^{calc}(t) &= \eta^*(x_1, t) + \eta^*(x_2, t) \\
\\
&= 2G^\eta a_I \cos\left(\frac{k\Delta x + \phi^{\eta_1} - \phi^{\eta_2}}{2}\right) \\
&\quad \cos\left(\omega t - kx_1 + \phi_I + \frac{-k\Delta x + \phi^{\eta_1} + \phi^{\eta_2}}{2}\right) +
\end{aligned}
$$

49

$$2G^\eta a_R \cos(\frac{-k\Delta x + \phi^{\eta_1} - \phi^{\eta_2}}{2})$$
$$\cos(\omega t + kx_1 + \phi_R + \frac{k\Delta x + \phi^{\eta_1} + \phi^{\eta_2}}{2}) \tag{4.9}$$

It is seen that $\eta^{calc}(t)$ and $X^*(t) = Ba_R \cos(\omega t + \phi_R + \phi_B + \pi)$ are identical signals in case

$$2G^\eta \cos(\frac{k\Delta x - \phi^{\eta_1} + \phi^{\eta_2}}{2}) = B \tag{4.10}$$
$$kx_1 + \frac{k\Delta x + \phi^{\eta_1} + \phi^{\eta_2}}{2} = \phi_B + \pi + n2\pi \tag{4.11}$$
$$\frac{k\Delta x + \phi^{\eta_1} - \phi^{\eta_2}}{2} = \frac{\pi}{2} + m\pi \tag{4.12}$$

where $n, m \in (0, \pm 1, \pm 2, ..)$.

Solving eqs. (4.10)-(4.12) with respect to ϕ^{η_1}, ϕ^{η_2} and G^η with $n = m = 0$ gives

$$\phi^{\eta_1} = \phi_B - k\Delta x - kx_1 + 3\pi/2 \tag{4.13}$$
$$\phi^{\eta_2} = \phi_B - kx_1 + \pi/2 \tag{4.14}$$
$$G^\eta = \frac{B}{2\cos(-k\Delta x + \pi/2)} \tag{4.15}$$

Eqs. (4.13)-(4.15) specify the frequency responses, i.e. the amplification factors and phase shifts of filters 1 and 2 in Fig. 4.1.

Considering a situation with a spatially co-located wave gauge and velocity meter measuring the horizontal velocity this gives for the two input signals

$$\eta(x_1, t) = a_I \cos(\omega t - kx_1 + \phi_I) +$$
$$a_R \cos(\omega t + kx_1 + \phi_R) \tag{4.16}$$
$$u(x_1, z, t) = a_I \omega \frac{\cosh(k(z+d))}{\sinh(kd)} \cos(\omega t - kx_1 + \phi_I) -$$
$$a_R \omega \frac{\cosh(k(z+d))}{\sinh(kd)} \cos(\omega t + kx_1 + \phi_R) \tag{4.17}$$

By similar calculations as for the (η,η)-system the amplification G^η of the surface elevation signal, the amplification G^u of the velocity signal and the

theoretical phase shift $\phi^\eta = \phi^u$ of both the surface elevation and the velocity signal are found for the (η,u)-system

$$G^\eta = \frac{B}{2} \tag{4.18}$$

$$G^u = -\frac{B}{2\omega}\frac{\sinh(kd)}{\cosh(k(z+d))} \tag{4.19}$$

$$\phi^\eta = \phi_B + \pi - kx_1 \tag{4.20}$$

$$\phi^u = \phi_B + \pi - kx_1 \tag{4.21}$$

Finally, for spatially co-located horizontal and vertical velocity signals the two input signals are

$$w(x_1, z, t) = -a_I\omega\frac{\sinh(k(z+d))}{\sinh(kd)}\sin(\omega t - kx_1 + \phi_I) -$$
$$a_R\omega\frac{\sinh(k(z+d))}{\sinh(kd)}\sin(\omega t + kx_1 + \phi_R) \tag{4.22}$$

$$u(x_1, z, t) = a_I\omega\frac{\cosh(k(z+d))}{\sinh(kd)}\cos(\omega t - kx_1 + \phi_I) -$$
$$a_R\omega\frac{\cosh(k(z+d))}{\sinh(kd)}\cos(\omega t + kx_1 + \phi_R) \tag{4.23}$$

The (u,w)-system is very similar to the (η,u)-system since an amplification of the vertical velocity signal by $-\frac{\sinh(kd)}{\omega\sinh(k(z+d))}$ and a phase shift of $\frac{\pi}{2}$ simply give the surface elevation (cf. eq. (4.22)). Considering the frequency responses of the two filters this gives

$$G^u = -\frac{B}{2\omega}\frac{\sinh(kd)}{\cosh(k(z+d))} \tag{4.24}$$

$$G^w = -\frac{B}{2\omega}\frac{\sinh(kd)}{\sinh(k(z+d))} \tag{4.25}$$

$$\phi^u = \phi_B + \pi - kx_1 \tag{4.26}$$

$$\phi^w = \phi_B + \pi - kx_1 - \frac{\pi}{2} \tag{4.27}$$

Even though the theoretical frequency response of the different filters easily can be calculated from the eqs. (4.13)-(4.15), eqs. (4.18)-(4.21) and eqs. (4.24)-(4.27) actual realization or fitting of the theoretical frequency responses in
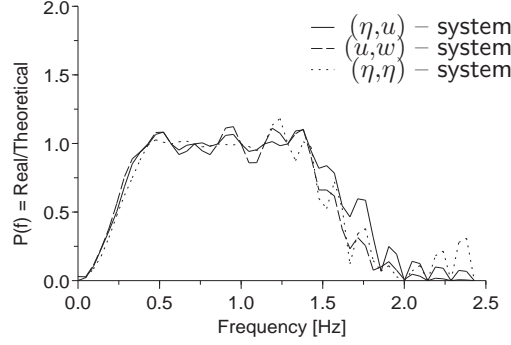
Figure 4.2: Performance of absorption systems.

FIR-filters is rather difficult. Any fitting of the filter coefficients to the above derived theoretical frequency responses obviously involves some error to be minimized in order to obtain the best possible performance. The fitting error is strongly dependent on: Water depth d, location of wave gauges x_1, x_2 and/or velocity meters x_1, z, number of filter coefficients N and the sample frequency of the filter f_s. This means that the actual performance of the systems is very depending on the setup of the filters.

4.4   Optimal Filter Design

To evaluate the efficiency and to enable optimization of an active absorption system the effect of the fitting error over some frequency area has to be quantified for the filter sets. The combined frequency response of the two filters can be determined by considering a simple cosine input

$$\eta(t) = \cos(\omega t) \tag{4.28}$$

and the frequency response functions of the two filters

$$\mathcal{H}_1(\omega) = G_1(\cos(\phi_1) + i\sin(\phi_1)) \tag{4.29}$$
$$\mathcal{H}_2(\omega) = G_2(\cos(\phi_2) + i\sin(\phi_2)) \tag{4.30}$$

By convolution of the input cosine with the two frequency response functions and subsequent addition of the outputs the following output is obtained

$$X(t) = G_1\cos(\omega t + \phi_1) + G_2\cos(\omega t + \phi_2)$$

$$= \{G_1 \cos(\phi_1) + G_2 \cos(\phi_2)\} \cos(\omega t) -$$
$$\{G_1 \sin(\phi_1) + G_2 \sin(\phi_2)\} \sin(\omega t) \qquad (4.31)$$

The gain corresponding to this combined input/output relation is

$$G_X = \{(G_1 \cos(\phi_1) + G_2 \cos(\phi_2))^2 +$$
$$(G_1 \sin(\phi_1) + G_2 \sin(\phi_2))^2\}^{\frac{1}{2}} \qquad (4.32)$$

Calculating G_X for both the theoretical frequency response functions corresponding to eqs. (4.13)-(4.15), eqs. (4.18)-(4.21) or eqs. (4.24)-(4.27) as well as for the realized impulse response functions corresponding to the filter coefficients, the ratio $P(f)$ signifies the performance of the actual system

$$P(f) = \frac{G_{X,real}}{G_{X,theo}} \qquad (4.33)$$

This ratio is termed the performance function and gives the actual degree of absorption on every frequency desired. In case of 100% absorption $P(f) = 1$.

By calculating the error ϵ defined as

$$\epsilon = \int_{f_{low}}^{f_{high}} (1 - P(f))^2 df \qquad (4.34)$$

setup parameters for each of the systems can be evaluated. f_{low} and f_{high} are two prespecified low and high cutoff frequencies between which the filters are fitted.

In Fig. 4.2 the performance function is plotted for the setup parameters given in Table 4.1. All systems show excellent absorption characteristics within the frequency area [0.3;1.5] and are basically very similar in performance.

Generally, to obtain the best possible fit Δf must be small. On the other hand a small Δf results in a large filter delay that must be compensated for in the filters. In order to compensate for this delay the wave gauges or velocity meters have to be positioned far away from the paddle with the risk that accumulated phase errors due to the dispersion relation (correct to 2nd order) effect the system more. Both limitations must be considered when selecting Δf.

The main difference between the systems is not seen in Fig. 4.2, but is found in the sensitivity to the internal gauge spacing $x_2 - x_1$ for the (η, η)-system.

system		(η, η)	(η, u)	(u, w)
Δf	[Hz]	0.143	0.143	0.143
x_1	[m]	3.1	3.1	3.1
x_2	[m]	3.3	-	-
z	[m]	-	-0.15	-0.15
d	[m]	0.55	0.55	0.55

Table 4.1: Setup parameters.
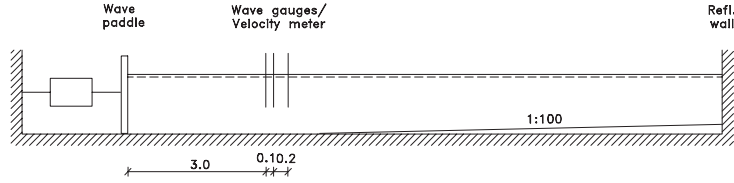
Figure 4.3: Wave flume and model test setup.

The frequency response of the (η, η)-system is very sensitive to changes in the internal gauge spacing since a singularity occurs because of the phase difference between the two input signals. Opposite, the (η, u)-system and the (u, w)-system are based on colocated input signals with no singularities occuring making the filters easier to realize.

A disadvantage of the two velocity meter based systems compared to the (η, η)-system is the higher sensitivity to non-linear waves.

For the tested setup the absorption frequency range covers the frequency range in which the main part of the energy is concentrated in the wave spectrum - only low frequency or long periodic waves are not covered.

In case another sea state with another peak wave length (or peak frequency) than those covered by the system described in Table 4.1 is desired. The system setup parameters in Table 4.1 are simply Froude scaled with a length scale determined by the ratio between the new and the old peak wave length (or peak frequency). The more elaborate procedure calculating ϵ and $P(f)$ for the different parameters is of course still applicable.

It should be noted that the gauge spacing from the wave paddle must be large than three water depth for the gauges to be placed in the Biesel far field, since the elevation model in eq. (4.2) neglects the near field local disturbances.

54

4.5 Physical Model Test Comparisons

In order to determine the performances of the different active absorption methods described above, the (η,η)-system and the (η,u)-system were implemented in the control system of a piston-type wave generator in Hydraulics & Coastal Engineering Laboratory, Aalborg University.

The geometry and test setup of the wave flume are given in Fig. 4.3 and the setup parameters for the two systems are those listed in Table 4.1.

The Biesel phase ϕ_B and gain B (see eq. (4.3)) are determined using the linear transfer functions derived by Biesel (1951).

When active absorption was applied, the surface elevation time series were recorded and digitized by means of a PC equipped with an A/D-D/A-card, digital filtering and superposition were performed, and the resulting paddle displacement correction signal was added to the input signal read from the signal generator.

At the far end of the flume a vertical fully reflecting wall was mounted. The flume is equipped with three pairs of wave gauges mounted on a beam at distances of 3.0 m, 3.1 m and 3.3 m from the wave paddle. These gauges are used for reflection measurements as well as absorption. A water depth of d = 0.55 m was maintained throughout the test series.

All tests were performed with exactly the same input from the signal generator: a wave paddle displacement signal corresponding to a JONSWAP-spectrum with significant wave height $H_s = 0.08$ m, peak period $T_p = 1.2$ sec and peak enhancement factor $\gamma = 3.3$, sampled at a frequency of $f_s = 40$ Hz, and generated by means of digital filtering of Gaussian white noise in the time domain. All tests were run for 10 min.

The 0.08 m significant wave height is fairly high resulting in non-linear waves with some breaking in form of white capping. Furthermore, severe cross mode wave action was observed. These severe wave conditions should accentuate eventual differences between the systems.

In each test the incident and reflected spectra were resolved as described by Mansard and Funke (1980) and for the systems (η, η) and (η, u) the incident wave spectra are given in Figs. 4.4 - 4.6.

Comparing the significant wave height for the two systems these are in the same order of magnitude though slightly higher than the target wave height. The differences between the two systems must be derived from the energy spectra showing more long periodic energy for the (η, η)-system than the (η, u)-system signifying that the purely wave gauge based system tends to

generate long periodic waves. Also when comparing with the case of no absorption more long periodic energy is observed. Regarding the (η, u)-system the wave energy spectrum is far more peaked.

The tendency to generate long periodic energy can be explained by the high sensitivity of the (η, η)-system to uncorrelated pink noise on the two input signals, see Figs. 4.7 and 4.8. Uncorrelated pink noise could be electrical noise or surface fluctuations due to breaking.

Since severe cross mode action occured during testing, the sensitivity to cross mode action is simulated for both systems by adding correlated pink noise to the two input signals. Because of the surface elevation model in eq. (4.2) the two sensors (surface elevation or velocity) will recognice cross mode action as correlated noise. The amplitude amplification for the two systems are shown in Figs. 4.9 and 4.10.

Surprisingly, the sensitivity of the two systems is in the same order of magnitude. For the wave flume used, the cross mode of 1st order corresponds to a frequency of $1\,\mathrm{Hz}$ and as noted from Figs. 4.4 and 4.5 this corresponds very well with the frequency at the energy peak.

A matter that is not depicted in Fig. 4.10 is that the actual separation of incident and reflected waves for this system is erroneous because the cross mode action only influences the wave gauge. This is not the case for the (η, η)-system and might explain the peaked incident wave spectrum for the (η, u)-system.

system	$H_{s,target}$ [cm]	$H_{s,inci}$ [cm]
(η, η)	8.4	8.5
(η, u)	8.4	8.6
no abs.	8.4	11.4

Table 4.2: Spectral wave characteristics.
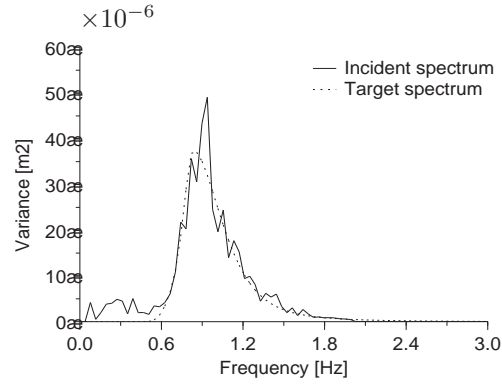
Figure 4.4: Incident spectra for (η, η)-system.
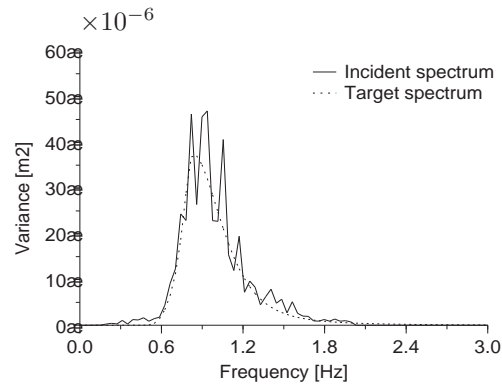
Figure 4.5: Incident spectra for (η, u)-system.
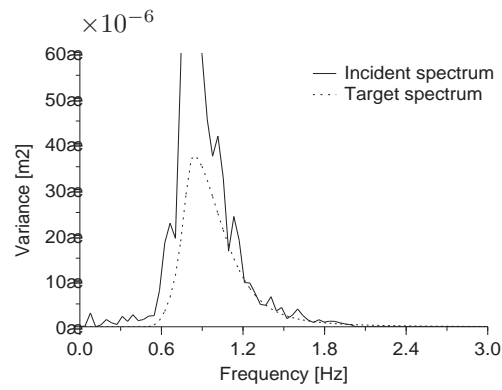
Figure 4.6: Incident spectra with no absorption.
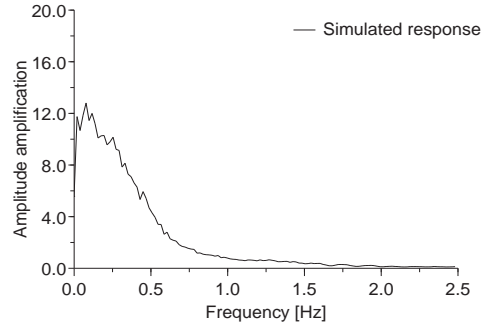
Figure 4.7: Amplitude amplification for uncorrelated pink noise for (η, η)-system.
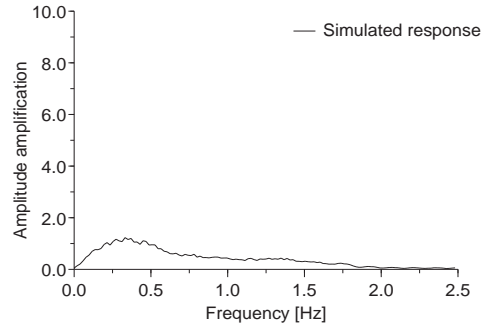
Figure 4.8: Amplitude amplification for uncorrelated pink noise for (η, u)-system.
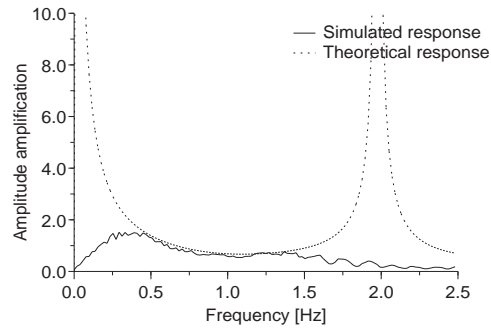
Figure 4.9: Amplitude amplification for simulated cross mode action for (η, η)-system.
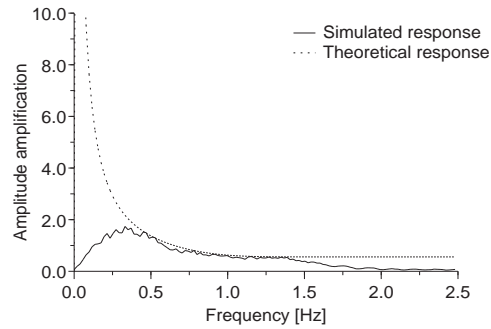
Figure 4.10: Amplitude amplification for simulated cross mode action for (η, u)-system.

4.6 Conclusion

Three types of active absorption systems are described. A purely wave gauge based system termed (η, η), a combined wave gauge, velocity meter based system termed (η, u) and a purely velocity meter based system termed (u, w). For each system the theoretical frequency response of the filter systems is presented.

To optimize the frequency response of the filters a performance function has been derived. Numerical tests with the (η, η)-system, the (η, u)-system and the (u, w)-system demonstrate that all three filter systems easily are realized with excellent frequency response in the relevant frequency area. All systems show similar absorption characteristics

Tests performed with both the (η, η)-system and the (η, u)-system imply good absorption characteristics even at very high levels of reflection. Furthermore, both systems appear to be very stable.

Regarding the (η, u)-system the incident wave spectrum is more peaked than that of the (η, η)-system. Regarding the (η, η)-system some long periodic waves tend to be generated. A possible solution to these problems might be by demanding zero gain at $f = 0.0$ and averaging measured surface elevations over the width of the flume.

Converting a conventional wave generator to an absorbing wave generator based on the principle presented above is relatively inexpensive considering the improvements achieved: the only requirement in its most simple form is two conventional wave gauges and a PC equipped with an A/D-D/A-card. These facilities will normally be available in most laboratory environments. If a PC equipped with an A/D-D/A-card is used as signal generator for the wave generator, the wave gauges can simply be connected to this computer, allowing to perform signal generation and correction signal calculation simultaneously.

Chapter 5

Wave Groups

A wave group is generally defined as a sequence of consecutive high waves in a random wave train.

In sea wave recordings, group formations of high waves occur from time to time. This phenomenon corresponds to a non-zero correlation between succesive waves. Information concerning this correlation is of importance when reproducing waves in the laboratory in order to determine the response of the modelled structure. Normally, irregular waves are reproduced in accordance with a specific energy spectrum solely defining the distribution of the variances. The grouping of waves is determined by the distribution of the phases. Hitherto, independence between succesive waves have been applied and the phases are treated as independent random variables, each with a uniform probability density on the interval $[0;2\pi]$ leading to a sea surface that is Gaussian distributed. However, if the waves during wave propagation become more non-linear there will be some coupling and thus dependence of the phases of the component waves at different frequencies, which eventually will modify the wave grouping.

To illustrate the effect of randomly assigned phases two wave trains are generated from the same energy spectrum. These two wave conditions are depicted in figure 5.1.

Figure 5.1 shows different groupiness characteristics, and clearly it is important to have informations on the wave grouping when coastal structures respond differently when exposed to the distinctive wave patterns. Especially, the stability of rubble mound structures appears to be significantly affected by the wave grouping, but also the slow drift oscillations of moored vessels is highly dependent on the wave grouping.

Burcharth (1979) and Johnson et al. (1978) found that the wave grouping
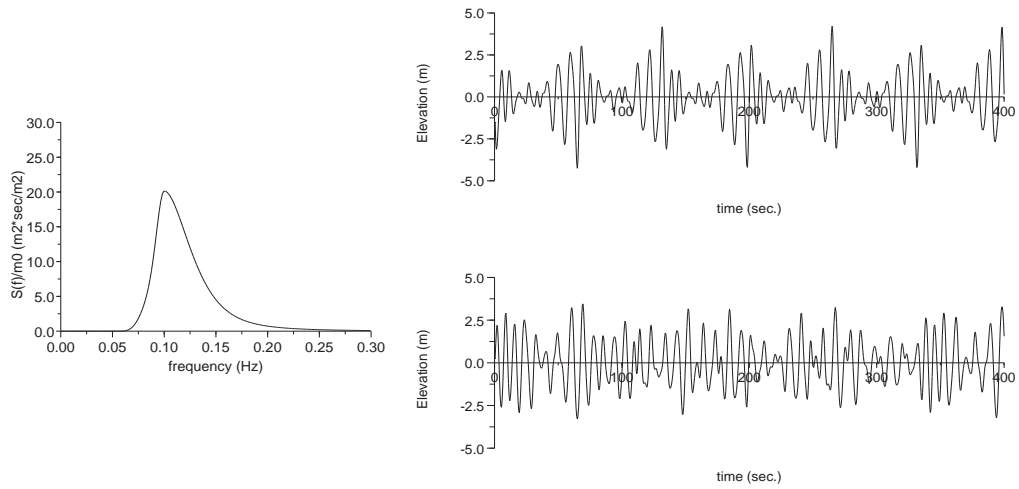
Figure 5.1: *Wave energy spectrum and generated grouped and non-grouped wave trains.*

significantly affects the stability of rubble mound breakwaters as well as the run-up. Johnson et al., (1978) compared the effects of a grouped and a non-grouped time series generated from the same energy spectrum, thus having the same statistical properties. Conclusively, the model tests showed that the breakwater response to the two different wave trains was quite different, with the grouped wave train causing severe damage and the non-grouped only causing minor rocking of the armour units. Similar significant influence on the wave grouping was found in the tests performed by Burcharth (1979).

In irregular seas, model tests by Spangenberg (1980) showed that the wave grouping has a significant influence on the slow drift motion of moored platforms and vessels. This influence might be explained by the fact that the period of the slow drift oscillations practically corresponds to the wave group period where the wave grouping is pronounced.

Both examples illustrate the importance of a correct modelling of natural sea waves in the laboratory if the structural responses are sensitive to the wave grouping. A characterization of the wave grouping seems therefore evident.

5.1 Description of Wave Groups

A measure of the wave grouping is obtained by defining the wave envelope to the time signal. Due to the presence of small waves in the signal the wave envelope is difficult to determine. However, if the time signal is squared, the squaring procedure will supress the relative influence of the small waves present, and furthermore, a slowly varying part appears which may be inter-

preted as the square envelope.

Assuming that the sea surface elevation at a given point is a realization of a linear stationary Gaussian process defined by its one-sided spectrum $S_\eta(f)$, it can be represented by an ordinary sum of a finite number of waves

$$\eta(t) = \sum_{n=1}^{N} c_n \cos(\omega_n t + \varepsilon_n) \tag{5.1}$$

where c_n = amplitude, ω_n = cyclic frequency, and ε_n = phase angle. By squaring the time signal following equation is obtained

$$
\begin{aligned}
\eta^2(t) &= \sum_{n=1}^{N} \sum_{m=1}^{N} c_n c_m \cos(\omega_n t + \varepsilon_n) \cos(\omega_m t + \varepsilon_m) \tag{5.2} \\
&= \sum_{n=1}^{N} \sum_{m=1}^{N} \{ c_n c_m (\frac{1}{2} \cos((\omega_n + \omega_m)t + (\varepsilon_n + \varepsilon_m)) + \\
&\quad \frac{1}{2} \cos((\omega_n - \omega_m)t + (\varepsilon_n - \varepsilon_m))) \} \tag{5.3}
\end{aligned}
$$

Equation (5.3) represents a splitting of $\eta^2(t)$ into a slowly varying part (represented by the difference-frequencies) and a more rapid oscillating part (represented by the summation-frequencies).

By use of symmetry of the double summation, equation (5.3) can be expressed in terms of four separate contributions

$$
\begin{aligned}
\eta^2(t) &= \frac{1}{2} \sum_{n=1}^{N} c_n^2 + \frac{1}{2} \sum_{n=1}^{N} c_n^2 \cos(2\omega_n t + 2\varepsilon_n) \\
&\quad + \sum_{n=1}^{N} \sum_{m=n+1}^{N} c_n c_m \cos((\omega_n + \omega_m)t + (\varepsilon_n + \varepsilon_m)) \\
&\quad + \sum_{n=1}^{N} \sum_{m=n+1}^{N} c_n c_m \cos((\omega_n - \omega_m)t + (\varepsilon_n - \varepsilon_m))) \tag{5.4}
\end{aligned}
$$

The four terms on the right-hand side of equation (5.4) are identified as follows: The first term consists of a constant off-set component. The second and third term constitutes the superharmonic components, i.e. the summation-frequency terms, and the fourth term constitutes the subharmonic components, i.e. the difference-frequency terms. It is the latter that describes the slowly varying part of the squared time signal and the term which may be interpreted as the square envelope. By means of Bartlett filtering the su-

perharmonic components on the right-hand side of equation (5.4) may be filtered out after subtraction of the constant off-set as done by Funke and Mansard (1979).

Funke and Mansard denoted the filtered square of the time signal the SIWEH (Smoothed Instantaneous Wave Energy History) function as the function provides a measure of the instantaneous wave energy in the time signal.

The effect of the Bartlett filtering corresponds to a digital low pass filtering and the efficiency of the SIWEH analysis can best be interpreted by examination of the energy spectrum of the stochastic process in (5.1) and the energy spectrum of the squared process.
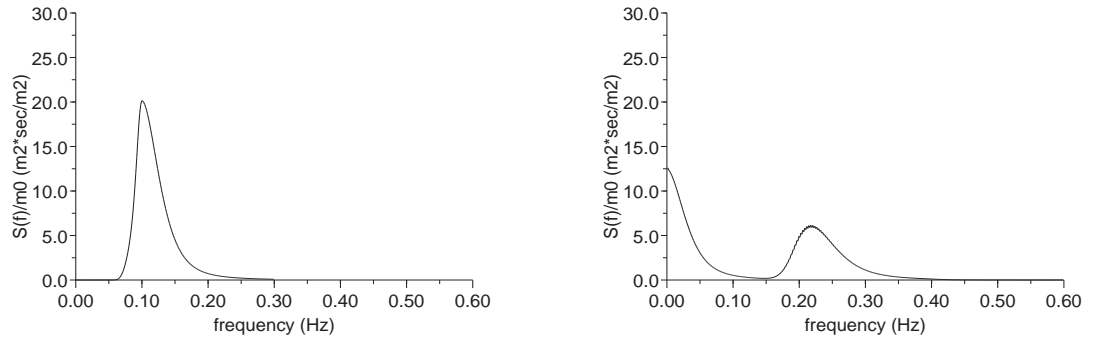
Figure 5.2: a) *JONSWAP energy spectrum for a linear stochastic process and* b) *energy spectrum for the squared process.*

From figure 5.2 it is understood that the SIWEH analysis does not exactly isolate the slowly varying part; also contributions from the superharmonic components occur and not the complete amount of energy from the subharmonic components is included. Only when the process is narrow-banded does the SIWEH analysis perform well but as the process becomes more and more broad-banded the SIWEH function is a poor estimator of the wave envelope, see Hupspeth and Medina (1988).

Instead of using a Bartlett window to isolate the subharmonic components, a wave envelope function defined on basis of the time series and its Hilbert transform isolates exactly the subharmonic components.

5.2 Hilbert Transform Technique

From the sea surface elevation $\eta(t)$ a conjugate signal $\hat{\eta}(t)$ is uniquely obtained by shifting the phase of each elementary harmonic component of $\eta(t)$ by $\pm\frac{\pi}{2}$. When the phase angles of all components of a given signal are shifted

$\pm\frac{\pi}{2}$, the resulting function $\hat{\eta}(t)$ is known as the Hilbert transform of the original signal $\eta(t)$. The Hilbert transform is defined by

$$\hat{\eta}(t) = \frac{1}{\pi}\int_{-\infty}^{\infty}\frac{\eta(t)}{t-\tau}d\tau \tag{5.5}$$

From the definition of the Hilbert transform it is noted that $\hat{\eta}(t)$ is simply the convolution of $\eta(t)$ with a linear filter with the impulse response function $h(t) = \frac{1}{\pi t}$ [1]. Since a convolution of two functions in the time domain are transformed into a multiplication of their Fourier transforms in the frequency domain [2] a frequency response function $H(f)$ is related to the impulse response function. The frequency response function provides an equally characterization of the linear time-invariant input and output system in (5.5) and does furthermore visualize the effect of the Hilbert transform operation. Through the Fourier transform the frequency response of the Hilbert transformer becomes

$$H(f) = \mathcal{F}[\frac{1}{\pi t}] = -i\,\text{sgn}(f) = \begin{cases} -i & f > 0 \\ 0 & f = 0 \\ i & f < 0 \end{cases} \tag{5.6}$$

The gain of this frequency response function is $\sqrt{\text{re}^2(H(f)) + \text{im}^2(H(f))}$ resulting in unity in magnitude, and thus, the amplitudes of the signal does not change. The phase angle is $\arctan(\frac{\text{im}(H(f))}{\text{re}(Hf))})$ resulting in a phase angle of $-\frac{\pi}{2}$ for $f > 0$ and $+\frac{\pi}{2}$ for $f < 0$. Such a system is denoted an ideal 90-degree phase shifter.

Consequently, applying the Hilbert transform operation to the sea surface elevation in (5.1) the cosine function simply shifts to the sine function

$$\hat{\eta}(t) = \sum_{n=1}^{N} c_n \sin(\omega_n t + \varepsilon_n) \tag{5.7}$$

---

[1]The convolution of two functions, denoted $g(t) * h(t)$, is defined

$$g(t) * h(t) \equiv \int_{-\infty}^{\infty} g(\tau)h(t-\tau)d\tau$$

[2]The convolution theorem

$$g(t) * h(t) \Leftrightarrow G(f)H(f)$$

Associated with the Hilbert transform is the complex analytical signal defined from the original signal $\eta(t)$ and the Hilbert transform $\hat{\eta}(t)$

$$
\begin{aligned}
\tilde{\eta}(t) &= \mid \tilde{\eta}(t) \mid \; \exp(i\psi(t)) = \mid \tilde{\eta}(t) \mid \; \cos(\psi(t)) + i \mid \tilde{\eta}(t) \mid \; \sin(\psi(t)) \\
&= \eta(t) + i\hat{\eta}(t) \quad\quad (5.8)
\end{aligned}
$$

where the envelope or the modulation $\mid \tilde{\eta}(t) \mid = \sqrt{\eta^2(t) + \hat{\eta}^2(t)}$ and the associated phase $\psi(t) = \arctan(\frac{\hat{\eta}(t)}{\eta(t)})$. The properties of the Hilbert transform operation entail that the slowly varying difference-frequency terms in the second order expression $\eta^2(t)$ are separated mathematically by the expression

$$
E(t) \equiv \mathrm{re}(\tilde{\eta}^*(t)\tilde{\eta}(t)) = \mid \tilde{\eta}(t) \mid^2 \quad\quad (5.9)
$$

where $\tilde{\eta}^*(t)$ = the complex conjugate and $E(t)$ = the square wave envelope function.

In order to visualize the effect of the defined envelope function the Hilbert transform of the sea surface elevation is squared and rewritten by use of trigonometry and symmetry of the double summation similar to $\eta^2(t)$

$$
\begin{aligned}
\hat{\eta}^2(t) &= \sum_{n=1}^{N}\sum_{m=1}^{N} c_n c_m \sin(\omega_n t + \varepsilon_n)\sin(\omega_m t + \varepsilon_m) \quad\quad (5.10)\\
&= \sum_{n=1}^{N}\sum_{m=1}^{N}\{c_n c_m (\frac{1}{2}\cos((\omega_n - \omega_m)t + (\varepsilon_n - \varepsilon_m)) - \\
&\quad \frac{1}{2}\cos((\omega_n + \omega_m)t + (\varepsilon_n + \varepsilon_m)))\} \quad\quad (5.11)\\
&= \frac{1}{2}\sum_{n=1}^{N} c_n^2 - \frac{1}{2}\sum_{n=1}^{N} c_n^2 \cos(2\omega_n t + 2\varepsilon_n) \\
&\quad - \sum_{n=1}^{N}\sum_{m=n+1}^{N} c_n c_m \cos((\omega_n + \omega_m)t + (\varepsilon_n + \varepsilon_m)) \\
&\quad + \sum_{n=1}^{N}\sum_{m=n+1}^{N} c_n c_m \cos((\omega_n - \omega_m)t + (\varepsilon_n - \varepsilon_m))) \quad\quad (5.12)
\end{aligned}
$$

Remembering that the squared time signal is given by (5.4), the square wave envelope function, according to (5.9), then becomes

$$
E(t) = \sum_{n=1}^{N} c_n^2 + 2\sum_{n=1}^{N}\sum_{m=n+1}^{N} c_n c_m \cos((\omega_n - \omega_m)t + (\varepsilon_n - \varepsilon_m)) \quad\quad (5.13)
$$

Introducing $\frac{1}{\sqrt{2}}$ in the complex analytical signal $\tilde{\eta}(t) = \frac{1}{\sqrt{2}}(\eta(t) + i\hat{\eta}(t))$ leads to the definition of an envelope function which may be interpreted as half the square envelope.

$$E(t) = \mid \tilde{\eta}(t) \mid^2 = \frac{1}{2}(\eta^2(t) + \hat{\eta}^2(t)) \tag{5.14}$$

This envelope function isolates exactly the slowly varying part of the squared time signal plus the constant off-set similar to what approximately is achieved by the SIWEH analysis.

The present method seems to be more convenient than the SIWEH analysis and it does not require the narrow-band spectrum assumption. The disadvantage of this method is however that the sea surface must be described by a linear model.

Computation of half the square envelope

To compute the Hilbert transform numerically the continuous-time convolution integral in (5.5) is approximated by a discrete-time Hilbert transformation. Furthermore, as the Hilbert transformation is non-banded, approximations limiting the impulse response function are made. A tool to handle the ideal Hilbert transformation of the sea surface elevation is by using FIR approximations. In such approximations the 90-degree phase shift is conserved exactly.

The principle in the FIR approximation is that the convolution integral in (5.5) is represented by a summation over a finite number of coefficients where the coefficients are fitted to represent the impulse response function. Taking an even number of coefficients, easily extended to an odd number, the non-causal FIR approximation can be written

$$\hat{\eta}_j = \sum_{k=-N_c/2}^{N_c/2-1} c_k \eta_{j-k} = \sum_{k=0}^{N_c-1} c_k \eta_{j+k-N_c/2} \tag{5.15}$$

where c_k = the k'th coefficient, N_c = number of coefficients or filter length, $\hat{\eta}_j$ is the Hilbert transform corresponding to the time step j, and $\eta_{j+k-N_c/2}$ are the input elevations to the filter system. The reason why the index on the filter coefficients remain unchanged is that the coefficients are mirrored in the Nyquist frequency, i.e. the frequency corresponding to half the filter length. The coefficients are derived from the frequency response function by FFT to obtain a least-square fit of the coefficients. Opposite the centered format definition of the Fourier transformation, the FFT is based on a one-sided

format

$$c_k = \frac{1}{N_c} \sum_{j=0}^{N_c-1} X_j \exp(i\omega_j k \Delta t) = \frac{1}{N_c} \sum_{j=0}^{N_c-1} X_j \exp(i\frac{2\pi jk}{N_c}) \qquad (5.16)$$

where ω_j is the cyclic frequency corresponding to the j'th coefficient and X_j is the desired sampled frequency response of the system. By using the one-sided format a time delay corresponding to half the filter length is introduced

$$\tau = \frac{N_c}{2} \Delta t \qquad (5.17)$$

The corresponding phase delay may then be found as

$$\psi_\tau = \tau \omega_j = \tau \frac{2\pi j}{N_c \Delta t} = \pi j \qquad (5.18)$$

To compensate for the phase delay the original frequency response function given by (5.6) only needs to be multiplied by a linear phase shift operator $\exp(-i\pi k)$ and X_j might be interpreted as

$$X_j = H(f_j)\exp(-i\pi j) = G(f_j)\cos(\psi_j - \pi j) + iG(f_j)\sin(\psi_j - \pi j) \qquad (5.19)$$

where $G(f_j)$ is the gain of the input amplitude to equal the output amplitude and $\psi_j - \pi j$ is the phase difference between the input and the output signal.

To sample the frequency response function the frequency band is subdivided into N_c discrete frequencies where $f_j = j\frac{f_s}{N_c}$ and f_s is the sample frequency. Since the phase $\psi_j = -\frac{\pi}{2}$ for $0 < f_j < f_{Nq}$ and $\psi_j = \frac{\pi}{2}$ for $f_{Nq} < f_j < 2f_{Nq}$ the sampled discrete frequency response function becomes

$$H(f_j) = \begin{cases} G(f_j)\cos(-\frac{\pi}{2} - \pi j) + iG(f_j)\sin(-\frac{\pi}{2} - \pi j) & 0 < f_j < f_{Nq} \\ 0 & f_j = 0, f_{Nq} \\ G(f_j)\cos(-\frac{\pi}{2} - \pi j) - iG(f_j)\sin(-\frac{\pi}{2} - \pi j) & f_{Nq} < f_j < 2f_{Nq} \end{cases} \qquad (5.20)$$

Due to the truncation of the Fourier transformation, the filter frequency response will differ from the desired frequency response. To illustrate the effect of the least-square fit, both the gain and phase characteristic of a linear FIR Hilbert filter are plotted in figure 5.3.
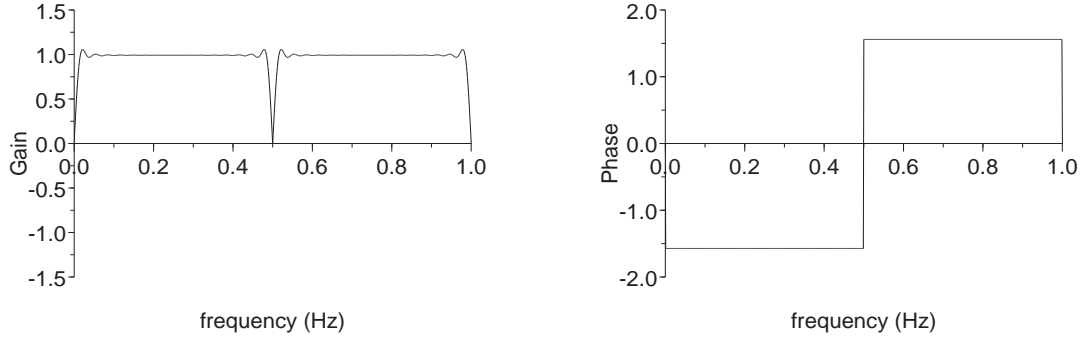
Figure 5.3: *Gain and phase characteristic of linear FIR Hilbert filter with a filter length $N_c = 64$ and $f_s = 1.0$ Hz.*

To compare the FIR approximated Hilbert transform with the theoretical Hilbert transform an irregular time signal is generated from the JONSWAP spectrum and the two transforms are depicted in figure 5.4. Generally very good accordance is observed also at the edges where a zone of half the filter length normally is disturbed.
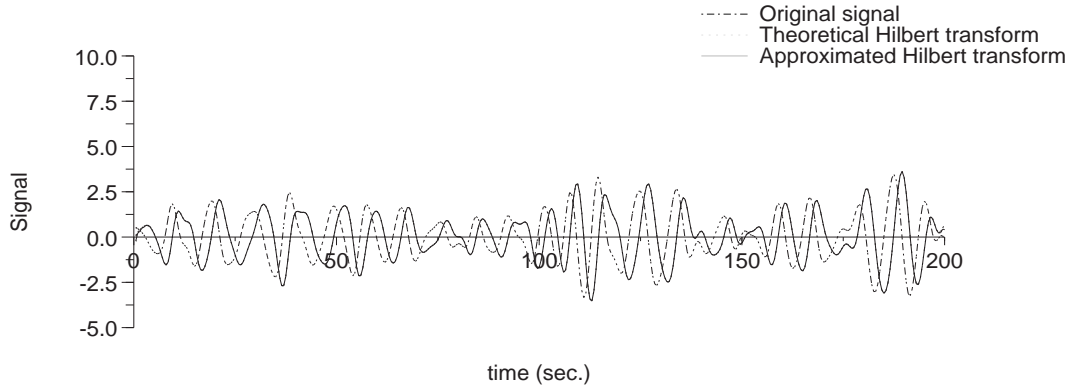
Figure 5.4: *Comparison of theoretical and FIR approximated, $N_c = 64$, Hilbert transform. The signal is generated from the JONSWAP spectrum, $f_p = 0.1$ Hz and $\gamma = 3.3$.*

To illustrate the envelope function, $E(t)$ is plotted together with half the squared elevation in figure 5.5 for a time signal generated from the JONSWAP spectrum.

5.3 Groupiness Factor

To characterize the actual groupiness of a wave train the energy spectrum $S_{\hat{\eta}}(f)$ of half the square envelope function can be evaluated. However, a sim-
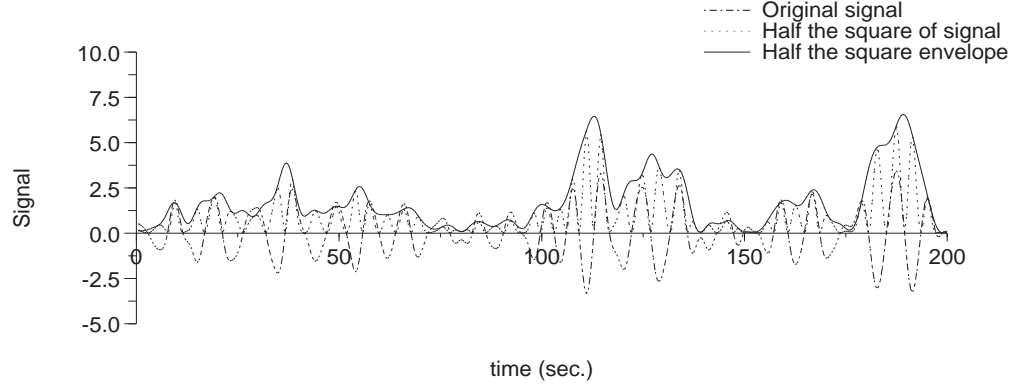
Figure 5.5: *Comparison of half the square envelope $E(t)$ and $\frac{1}{2}\eta^2(t)$ for signal generated from a JONSWAP spectrum, $f_p = 0.1$ Hz, $\gamma = 3.3$, and $N_c = 64$.*

pler measure is the groupiness factor that is defined as the standard deviation of half the square envelope relative to the variance of the original time signal

$$GF = \frac{\sigma[E(t)]}{\sigma^2[\eta(t)]} \tag{5.21}$$

For a monochromatic (sinusoidal) signal the envelope function $E(t)$ is constant leading to a groupiness factor $GF = 0$. Taking a completely Gaussian signal the expected value of the groupiness factor can be shown to be equal to 1.0 independent of the spectrum shape. The actual values for time signals generated from a JONSWAP spectrum including approximately 500 periods are approximately 1.0 in mean with a standard deviation of approximately $\sigma = 0.13$.

Instead of computing one value of the groupiness factor over the complete length of the time signal, the groupiness factor can be evaluated as instantaneous values by computing an average groupiness factor over a time moving window. The length of the window in time is dependent on the desired degree of smoothing of the computed groupiness factor function.

In figure 5.6 to figure 5.9 the groupiness factor function is plotted for both a narrow-banded and a broad-banded JONSWAP spectrum for two different window sizes.
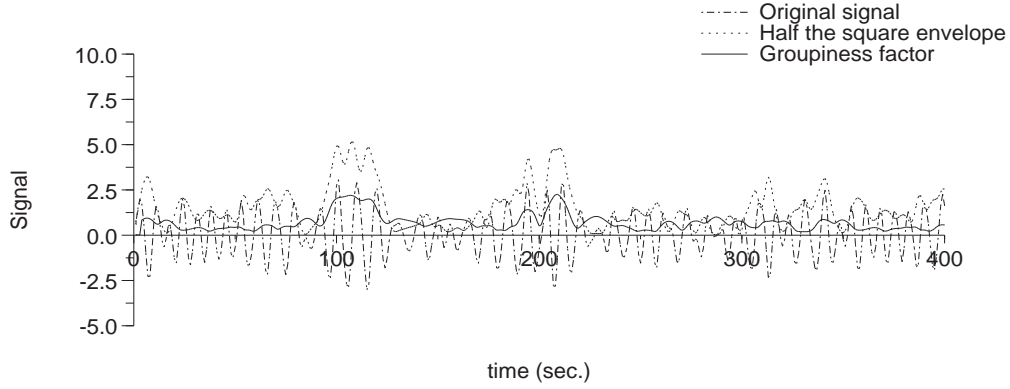
Figure 5.6: *Groupiness factor function GF(t) for signal generated from JON-SWAP spectrum, $f_p = 0.1$ Hz, $f_s = 1.0$ Hz, $\gamma = 10.0$, $N_c = 64$, and window size $= T_m$.*
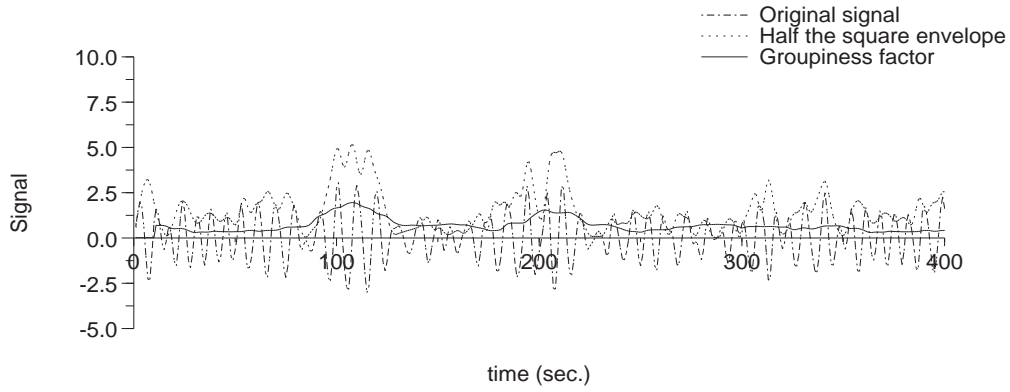
Figure 5.7: *Groupiness factor function GF(t) for signal generated from JON-SWAP spectrum, $f_p = 0.1$ Hz, $f_s = 1.0$ Hz, $\gamma = 10.0$, $N_c = 64$, and window size $= 3T_m$.*

Generally, a more smooth groupiness factor function is obtained for a window size of 3 mean periods and only the largest wave groups are separated as high and smooth peaks. It should though be noted that the sample frequency is 1.0 Hz and that a higher sample frequency eventually will lead to smoother groupiness factor function for smaller window sizes.

71
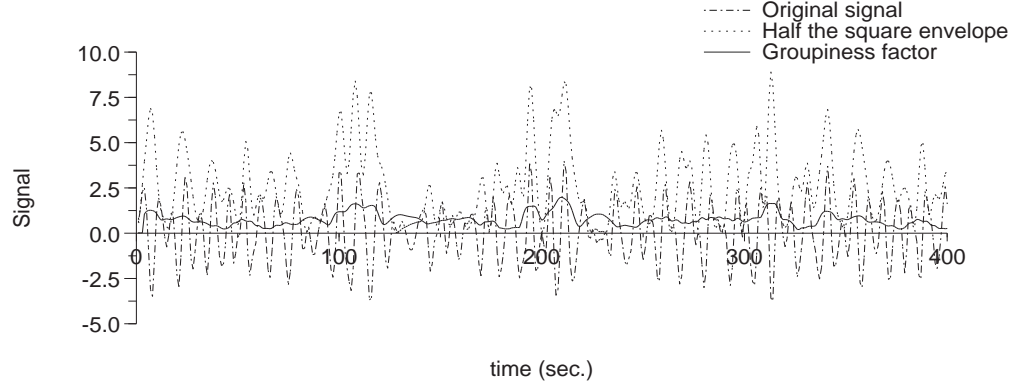
Figure 5.8: *Groupiness factor function GF(t) for signal generated from JON-SWAP spectrum, f_p = 0.1 Hz, f_s = 1.0 Hz, γ = 1.0, N_c = 64, and window size = T_m.*
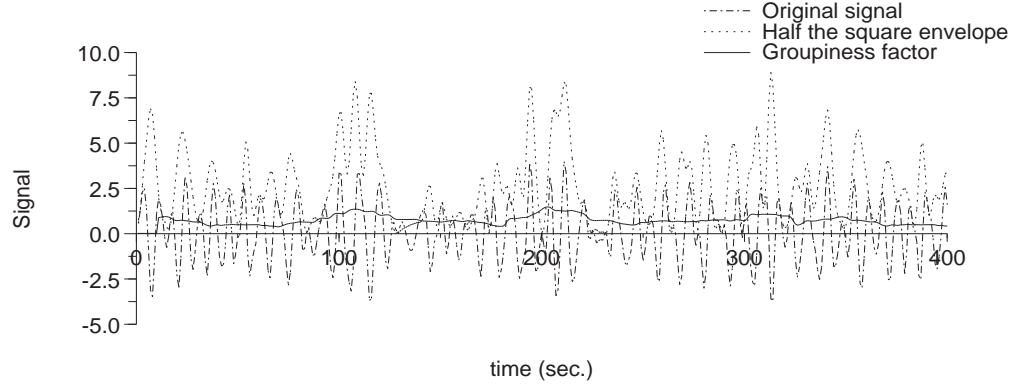
Figure 5.9: *Groupiness factor function GF(t) for signal generated from JON-SWAP spectrum, f_p = 0.1 Hz, f_s = 1.0 Hz, γ = 1.0, N_c = 64, and window size = $3T_m$.*

5.4 Conclusions and Further Use

Based on a linear assumption a method for calculating the instantaneous wave energy history and the groupiness factor function has been presented. The method is based on a temporal Hilbert filter and this approach enables an exact isolation of the 2nd order subharmonics which describe the slowly varying part of the time signal. This Hilbert filter approach is thus more efficient than the SIWEH analysis. The groupiness factor has proven to be ineffective in describing Gaussian distributed sea surfaces and the groupiness factor function is defined. Also discussions regarding the implementation of the Hilbert filter using FIR approximations and choice of window sizes for computing the groupiness factor functions are made.

The method can easily be extended to a three-dimensional motion but a physical interpretation of the more slowly varying part must then be revised.

The groupiness factor function enables computations of instantaneous groupiness factors in time and hence, the function is suitable for comparing the correlation between the damage development of e.g. a breakwater and the wave grouping in the wave train causing the damage.

A further application is the possibility to evaluate the change in wave grouping due to shoaling and thus also the change in phase distribution from deep to shallow water.

Chapter 6

Bounded Long Waves

Non-linear interaction between individual wave components in irregular wave trains give rise to so-called group bounded long waves. These waves are of second order and therefore they cannot be reproduced by means of the linear (first order) wave generation theory presented by Biésel. Consequently, socalled spurious long wave components will occur when a first order paddle displacement signal is applied to the wave generator. The presence of spurious long waves (free long waves) in physical model tests often leads to unrealistic responses of the test structures because of the dominant influence of the long waves on e.g. mooring forces and slow-drift oscillations.

The physical reason for the presence of bounded long waves in natural wave trains is the "wave pressure force" or with another name the "wave reaction force" described by Fredsø (1990).

The problem of correctly reproducing the bounded long waves in physical model tests was solved by Sand (1982). By means of a perturbation analysis of the Laplace equation correct to second order, he derived the second order piston positions for correct reproduction of the bounded long waves.

In the following, the results derived by Sand are outlined.

Both the calculations of second order long waves and second order piston positions are based on a Fourier decomposition of the first order wave train. The long wave elevations $\zeta(t)$ are determined as the sum of the terms arising from interaction between individual components in the first order wave train

$$\zeta(t) \;=\; \sum_{n-m=1}^{\infty} \sum_{m=m^*}^{\infty} \zeta_{nm}(t), \quad m^* = \frac{\omega^*}{\omega_0}$$

where ω_0 is the frequency interval in the Fourier decomposition and ω^* is the lowest frequency in the first order spectrum.

Consider a pair of regular wavelets with frequencies ω_n and ω_m. Such a pair of wavelets constitutes a regular wave group, i.e.

$$
\begin{aligned}
\eta_{nm} &= \eta_n + \eta_m \\
&= a_n \cos(\omega_n t - k_n x) + b_n \sin(\omega_n t - k_n x) \\
&\quad + a_m \cos(\omega_m t - k_m x) + b_m \sin(\omega_m t - k_m x)
\end{aligned}
$$

The second order long wave generated by this wave group becomes

$$
\begin{aligned}
\frac{\zeta_{nm}}{h} &= G_{nm}h\left[\left(\frac{a_n a_m + b_n b_m}{h^2}\right)\cos(\Delta\omega_{nm}t - \Delta k_{nm}x)\right. \\
&\quad \left. + \left(\frac{a_m b_n - a_n b_m}{h^2}\right)\sin(\Delta\omega_{nm}t - \Delta k_{nm}x)\right]
\end{aligned}
$$

where

$$
\begin{aligned}
\Delta\omega_{nm} &= \omega_n - \omega_m \\
\Delta k_{nm} &= k_n - k_m
\end{aligned}
$$

and the transfer function G_{nm} is given by

$$
\begin{aligned}
G_{nm}h &= \left[\frac{4\pi^2 D_n D_m \Delta k_{nm} h \cosh(\Delta k_{nm}h)}{\cosh(k_n h + k_m h) - \cosh(\Delta k_{nm}h)} - 2\pi^2(D_n - D_m)^2 \Delta k_{nm}h\right. \\
&\quad \left. + \frac{\Delta k_{nm}h(D_n - D_m)(k_n h D_m + k_m h D_n)\coth(\Delta k_{nm}h)}{2_n D_m}\right] \\
&\quad / \left[4\pi^2(D_n - D_m)^2 \coth(\Delta k_{nm}h) - \Delta k_{nm}h\right]
\end{aligned}
$$

where

$$
\begin{aligned}
D_n &= \sqrt{h/g} \cdot \omega_n/2\pi \\
D_m &= \sqrt{h/g} \cdot \omega_m/2\pi
\end{aligned}
$$

The second order piston positions for correct reproduction of the group

bounded long waves given above are

$$X^{(2)}(t) \;=\; \sum_{n-m=1}^{\infty} \sum_{m=m^*}^{\infty} X_{nm}^{(2)}(t), \quad m^* = \frac{\omega^*}{\omega_0}$$

where

$$
\begin{aligned}
\frac{X_{nm}^{(2)}}{h} \;=\; & \left[\left(\frac{a_n b_m - a_m b_n}{h^2} \right) F_1 h + \left(\frac{a_n a_m + b_n b_m}{h^2} \right) F_{23} h \right] \cos(\Delta\omega_{nm} t) \\
& + \left[\left(\frac{a_n a_m + b_n b_m}{h^2} \right) F_1 h + \left(\frac{a_m b_n - a_n b_m}{h^2} \right) F_{23} h \right] \sin(\Delta\omega_{nm} t)
\end{aligned}
$$

where the transfer function F_1 is given by

$$F_1 h = F_{11} h + F_{12} h$$

in which

$$F_{11}h \;=\; \frac{G_{nm}h\,\Delta k_f h (\Delta k_{nm}h - \Delta k_f h)\sinh(\Delta k_{nm}h + \Delta k_f h) + (\Delta k_{nm}h + \Delta k_f h)\sinh(\Delta k_{nm}h - \Delta k_f h)}{2((\Delta k_{nm}^2 h^2 - \Delta k_f^2 h^2)\sinh(\Delta k_{nm}h)\sinh(\Delta k_f h)}$$

and

$$
\begin{aligned}
F_{12}h \;=\; & \frac{f_m \Delta k_f h\, k_m h (1 + G_n)\left[\delta k_m^- h \sinh(\delta k_m^+ h) + \delta k_m^+ h \sinh(\delta k_m^- h)\right]}{\Delta f 8 (k_m^2 h^2 - \Delta k_f^2 h^2)\sinh(\Delta k_f h)\sinh(k_m h)\tanh(k_n h)} \\
& + \frac{f_m \Delta k_f h\, k_n h (1 + G_m)\left[\delta k_m^- h \sinh(\delta k_m^+ h) + \delta k_m^+ h \sinh(\delta k_m^- h)\right]}{\Delta f 8 (k_n^2 h^2 - \Delta k_f^2 h^2)\sinh(\Delta k_f h)\sinh(k_n h)\tanh(k_m h)}
\end{aligned}
$$

where the free long wave number , Δk_f is derived from the dispersion relation

$$(\Delta\omega_{nm})^2 \;=\; g\Delta k_f \tanh(\Delta k_f h)$$

and

$$
\begin{aligned}
\delta k_m^+ &= k_m + \Delta k_f \\
\delta k_m^- &= k_m - \Delta k_f
\end{aligned}
$$

The transfer function $F_{23}h$ is negligible relative to $F_1 h$.

Frequency domain solution:

When waves are simulated in the frequency domain (i.e. when the Random Phase Method or Random Complex Spectrum Method is applied), the correct reproduction of group bounded long waves is obtained by superposition of the complex Fourier coefficients corresponding to the 1. and 2. order wave paddle displacement signals before performing InvFFT. The resulting wave paddle displacement signal will be correct to second order, and free long waves will therefore not exist.

Calculation of the second order correction corresponding to a certain frequency Δf_{nm} is illustrated in the figure abowe.
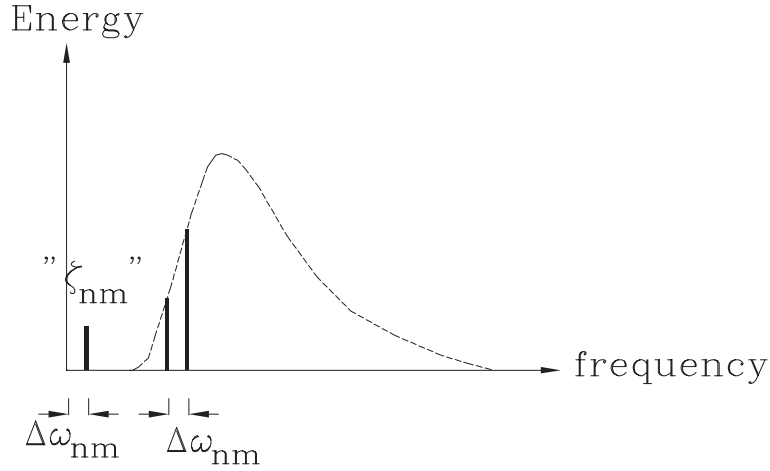
Figure 6.1: Calculation of second order correction term.

Time domain solution:

Consider a non-linear process $Y(t)$:

$$\mathbf{Y} = Y(t) = X(t) + \alpha X^2(t)$$

Remembering that α normally is frequency dependent $\alpha = \alpha(\omega_n, \omega_m)$, we can insert $X(t) = a_n cos(\omega_n t) + a_m cos(\omega_m t)$ and write the equation again:

$$\mathbf{Y} = a_n cos(\omega_n t) + a_m cos(\omega_m t) +$$
$$\alpha \left[a_n^2 cos^2(\omega_n t) + a_m^2 cos^2(\omega_m t) + 2a_n a_m cos(\omega_n t)cos(\omega_m t) \right]$$

Reformulating the equation given above using the cosine relations we obtain:

$$
\begin{aligned}
\mathbf{Y} \;=\; & a_n cos(\omega_n t) + a_m cos(\omega_m t)+ && \textit{(linear terms)} \\[4pt]
& \tfrac{1}{2}\alpha a_n^2 + \tfrac{1}{2}\alpha a_m^2 + && \textit{(offset)} \\[4pt]
& \tfrac{1}{2}\alpha a_n^2 cos(2\omega_n t) + \tfrac{1}{2}\alpha a_m^2 cos(2\omega_m t)+ && \\[4pt]
& \tfrac{1}{2}\alpha a_n a_m cos((\omega_n + \omega_m)t)+ && \textit{(2.order super harmonics)} \\[4pt]
& \tfrac{1}{2}\alpha a_n a_m cos((\omega_n - \omega_m)t) && \textit{(2.order sub harmonics)}
\end{aligned}
$$

In the terminology of water waves the non-linear terms are named *Bounded Long Waves* (2.order sub harmonics), *Stokes 2.order Waves* (2.order super harmonics) and *2.order super harmonic waves* (2.order super harmonics).

An ordinary 2.order FIR filter will reproduce all the terms: Offset, 2.order super harmonics and 2.order sub harmonics given above.

The discrete frequency domain equation for a non-linear filter is:

$$
G^*(\omega_n, \omega_m, \Delta\omega_{nm}) = H(\omega_n) \cdot F(\Delta\omega_{nm}) \cdot H(\omega_m)
$$

where
G^*:   Transfer function for filter in frequency domain
H, F: Two arbitrary functions (frequency domain)

This equation simply expresses that if G^* can be separated into the two functions H and F then the non-linear process is identically described by the process Y given above.

The *problem* with the FIR-filter is that it will generate all 2.order terms. In order to generate specified waves, i.e. bounded long waves, Stokes 2.order waves and 2.order super harmonic waves $\alpha(\omega_n, \omega_m)$ or in other words $H(\omega)$ and $F(\Delta\omega)$ must be found according to the requirements from the transfer-function.

In the case where only the bounded long waves is required the transfer function G^* must be *fitted* to the long wave transfer function. The frequency range and the Δfrequency range (for the fitting must be controlled through the fitting algorithm in order to only have long waves. Small values (frequencies) of the Δfrequency vector are sub–harmonics, and large values (frequencies) are super–harmonics.

The frequency range for H is the part of the wave spectrum with significant energy. The Δfrequency range for F is from zero to the frequency where
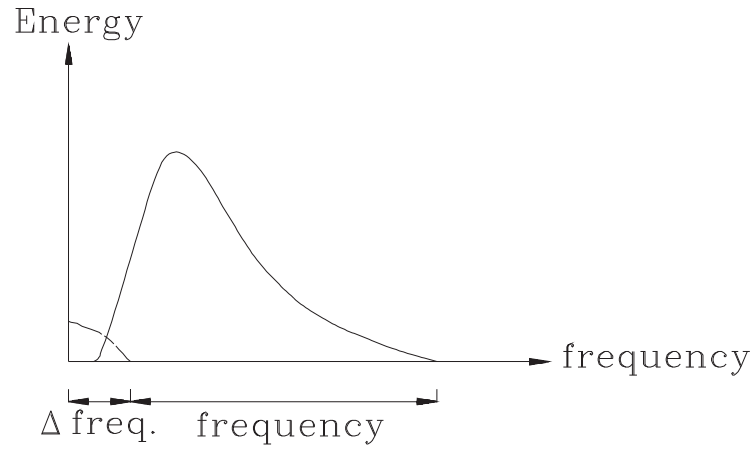
Figure 6.2: Frequency range for calculating *long wave* filters.

energy starts to exist in the spectrum. For all other frequencies the values of H and F are zero.

When the filter coefficients are found the bounded long waves are added to the linear wave signal simply by filtering the linear wave signal through the filters *(Take linear wave signal and convolve with H-filter, take result of convolution and convolve with F-filter).*

Chapter 7

White Noise Wave Generation with Long Wave Compensation

In the last two decades 2nd order wave generation theory has been treated extensively by several authors, cf. Schaeffer (1993) for a comprehensive historical summary. For irregular waves methods for calculating the correct 2nd order bounded sub and superharmonic terms in the surface elevation or paddle displacement signal given the 1st order surface elevation, $\eta^{(1)}$, have been presented:

Ottesen–Hansen (1978) derived a transfer function which in the frequency domain enables a direct calculation of the 2nd order bounded subharmonic terms in the surface elevation. The transfer function was derived for the 2nd order bounded superharmonic terms by Sand and Mansard (1986). A general and compact form of the 1st order elevation to 2nd order elevation transfer function was rederived by Schaeffer (1993).

Transfer functions enabling the 2nd order bounded subharmonic terms in the paddle displacement to be calculated were presented by Sand (1982) for a piston type wave maker. Sand and Mansard (1986) presented the corresponding transfer functions for the 2nd order bounded superharmonic terms. A general and compact form of the 1st order elevation to 2nd order paddle displacement transfer function was rederived by Schaeffer (1993).

The present chapter concentrates on the bounded subharmonic terms as they generally are considered to be the most important in practical applications. Because the formulations presented by Ottesen–Hansen (1978) and Sand (1982), the latter especially after correcting the formula as described in Sand and Mansard (1986), generally are rather complex the formulations suggested by Schaeffer (1993) are adopted herein.

7.1 Application of Existing Theory

The goal is to calculate the correct bounded 2nd order subharmonic terms in the surface elevation, $\eta^{(2)-}$, and the corresponding paddle displacement, $x^{(2)-}$. The calculations are performed using the 1st order surface elevation signal, $\eta^{(1)}$.

Discrete Fourier transform of $\eta^{(1)}$ decomposes the irregular surface elevation into, say N regular wavelets. Let y be the general 2nd order subharmonic signal, that is $y = \eta^{(2)-}$ when considering the surface elevation and $y = x^{(2)-}$ when considering the paddle displacement. The contribution to y by each pair of regular wavelets with complex amplitudes A_n and A_m and wave frequencies f_n and f_m, where $f_n > f_m$, can then be calculated. In the frequency domain:

$$Y(f) = \begin{cases} \frac{1}{2} K(f_n, f_m) A_n A_m^* & , f = f_n - f_m \\ \frac{1}{2} K^*(f_n, f_m) A_n^* A_m & , f = f_m - f_n \end{cases} \tag{7.1}$$

where Y is the discrete Fourier transform of y, * denotes complex conjugation and K for $y = \eta^{(2)-}$ equals the $\eta^{(1)}$ to $\eta^{(2)-}$ transfer function G^- derived by Ottesen–Hansen (1978) and for $y = x^{(2)-}$ equals iF^- in which i is the imaginary unit and F^- is the $\eta^{(1)}$ to $x^{(2)-}$ transfer function derived by Schaeffer (1993).

By adding the calculated y to the appropriate 1st order signal, $\eta^{(1)}$ or $x^{(1)}$, the surface elevation or paddle displacement correct to 2nd order, for linear and subharmonic components only, is obtained.

7.2 Transfer Functions

Introducing the formulations by Schaeffer (1993) the progressive part of the the $\eta^{(1)}$ to $\eta^{(2)-}$ transfer function G^- may be rewritten

$$G^-(f_n, f_m) = \frac{1}{g} \left\{ (\omega_n - \omega_m) \frac{C_1}{C_2} - C_3 \right\} \tag{7.2}$$

where

$$C_1 = (\omega_n - \omega_m) \left((-\omega_n \omega_m) - \frac{g^2 k_n k_m}{\omega_n \omega_m} \right) + \frac{\omega_n^3 - \omega_m^3}{2} - \frac{g^2}{2} \left(\frac{k_n^2}{\omega_n} - \frac{k_m^2}{\omega_m} \right) \tag{7.3}$$

$$C_2 = g(k_n - k_m)\tanh(k_n - k_m)h - (\omega_n - \omega_m)^2 \tag{7.4}$$

$$C_3 = \frac{1}{2}\left\{\frac{g^2 k_n k_m}{\omega_n \omega_m} + \omega_n \omega_m - (\omega_n^2 + \omega_m^2)\right\} \tag{7.5}$$

in which k is the wave number, ω is the cyclic wave frequency, g is the gravitational acceleration and h is the water depth.

Compared to G^- the complex $\eta^{(1)}$ to $x^{(2)-}$ transfer function, F^-, is more complicated, in general

$$F^- = (F_{11} + F_{12} + F_{13}) + i(F_{22} + F_{23} + F_{24}) \tag{7.6}$$

Each of the 6 functions eliminates free waves which otherwise would be emitted from the wave paddle due to interaction between two 1st order terms:

F_{11}	progressive wavelet and progressive wavelet,
F_{12}	component of paddle position and progressive wavelet,
F_{23}	component of paddle position and local disturbance wavelet,
F_{13} and F_{24}	progressive wavelet and local disturbance wavelet and
F_{22}	local disturbance wavelet and local disturbance wavelet

Cf. Schaeffer (1993) for details. Sand (1982) showed that it is reasonable for laboratory applications, where only subharmonic components are considered, to omit 2nd order effects originating from any 1st order interaction with the local disturbance wavelets. Hence F^- reduces to

$$F_1^- = F_{11} + F_{12} \tag{7.7}$$

where

$$F_{11} = C_4 \frac{k_n - k_m}{(k_n - k_m)^2 - k_{nm}^2} C_1 \tag{7.8}$$

$$F_{12} = C_4 g\left\{\frac{\omega_n^2 - (\omega_n - \omega_m)^2}{c_m 2\omega_n}\frac{k_n^2}{k_n^2 - k_{nm}^2} + \frac{\omega_m^2 - (\omega_n - \omega_m)^2}{c_n 2\omega_m}\frac{k_m^2}{k_n^2 - k_{nm}^2}\right\} \tag{7.9}$$

$$C_4 = \frac{k_{nm}^2}{(\omega_n - \omega_m)^3} \tag{7.10}$$

in which k_{nm} is the solution to $(\omega_n - \omega_m)^2 = g k_{nm} \tanh k_{nm} h$ and c is the linear Biesel transfer function for the actual type of wave paddle. This simplified formulation is adopted herein.

7.3 Approximation

The exact method outlined in the previous section is efficient and straight forward to use and have been successfully implemented in several hydraulic laboratories. The method is, however, limited to applications where the 1st order elevation can be frequency analysed, or already is available in the frequency domain. This makes it inadequate for real-time applications, for example where the 1st order elevation is generated on-line by means of digital filtering of white noise, to produce a wave spectrum of a given shape but with built-in stochastic variability (non-deterministic spectral amplitude model).

The scope of the present paper is to present an approximative method for including the 2nd order subharmonic components in the surface elevation or paddle displacement in such applications. Two in principle different schemes can be considered: internal correction, where the approximative method is build into a real-time wave generation software, and external correction, where the analog 1st order paddle control signal is sampled from an existing wave generation system, manipulated to include the correct subharmonics and send to the wave paddle. In the following only the internal correction will be thoroughly described, but how to change it into an external correction will be briefly outlined.

The study took its offspring in an internal correction method build into the wave generating software in the Hydraulics & Coastal Engineering Laboratory at Aalborg University.

7.4 2nd Order Process

Consider a function z which is the sum of two regular wavelets with complex amplitudes A_n and A_m and wave frequencies f_n and f_m, respectively. Let $Z^{(2)}$ denote the discrete Fourier transform of z^2. According to the convolution theorem for Fourier transforms multiplication in the time domain corresponds to convolution in the frequency domain, and vice versa, hence $Z^{(2)}$ can be written

$$Z^{(2)}(f) = \begin{cases} \frac{1}{2}(A_n A_n^* + A_m A_m^*) & , f = 0 \\ \frac{1}{2} A_n A_m^* & , f = f_n - f_m \\ \frac{1}{4} A_m A_m & , f = 2f_m \\ \frac{1}{2} A_n A_m & , f = f_n + f_m \\ \frac{1}{4} A_n A_n & , f = 2f_n \end{cases} \tag{7.11}$$

Keeping in mind that $Z^{(2)}(-f) = Z^{(2)*}(f)$ it is seen that all phases and frequencies in Equation 7.11 correspond, except for the off-set ($f = 0$), to the subharmonics in Equation 7.1 ($f = f_n - f_m$ and $f = f_m - f_n$), the superharmonic components from Stokes 2nd order regular wave theory ($f = 2f_m$ and $f = 2f_n$) and the superharmonic 2nd order components from wave-wave interaction as described by Sand and Mansard (1986) ($f = f_m + f_n$ and $f = -f_m - f_n$).

7.5   Hilbert Transform

The Hilbert transform relates the real and imaginary part of an analytic function. That is, the imaginary part is the Hilbert transform of the real part, and vice versa. Hence, in the frequency domain the Hilbert transform, $\mathcal{H}$, is defined by

$$H(f) = \begin{cases} -i & , f > 0 \\ 0 & , f = 0 \\ i & , f < 0 \end{cases} \tag{7.12}$$

Now consider the function $z^{(2)-}$

$$z^{(2)-}(t) = \frac{1}{2} \left(z^2(t) + \mathcal{H}^2[z(t)] \right) \tag{7.13}$$

in which z is given in the previous section. The discrete Fourier transform of $z^{(2)-}$, $Z^{(2)-}$, is then

$$Z^{(2)-}(f) = \begin{cases} \frac{1}{2} A_n^* A_m & , f = f_m - f_n \\ \frac{1}{2} (A_n A_n^* + A_m A_m^*) & , f = 0 \\ \frac{1}{2} A_n A_m^* & , f = f_n - f_m \end{cases} \tag{7.14}$$

By comparing Equation 7.14 to Equation 7.1 it is evident that $z^{(2)-}$, except for a linear transfer function and an off-set equals the 2nd order subharmonic function y when considering interaction between two regular wavelets.

7.6 Filter Approach

Assume that the transfer functions G^- and F_1^- can be approximated by $\mathcal{G}^-$ and $\mathcal{F}_1^-$, respectively, which both can be separated into two real functions, H_1 and H_2, in the following manner (in the following only the approximation of F_1^- by $\mathcal{F}_1^-$ is discussed, but the method equally applies to G^-):

$$\mathcal{F}^-(f_n, f_m) = H_1(f_n)H_2(f_n - f_m)H_1(f_m) \tag{7.15}$$

where $H_2(0) = 0$. The Fourier transform of y, Y may then be approximated by Y'

$$Y'(f) = \begin{cases} \frac{1}{2}H_1(f_n)H_2(f)H_1(f_m)\delta A_n A_m^* & , f = f_n - f_m \\ \frac{1}{2}H_1(f_n)H_2(f)H_1(f_m)\delta^* A_n^* A_m & , f = f_m - f_n \end{cases} \tag{7.16}$$

where $\delta = 1$ for $y = \eta^{(2)-}$ and $\delta = i$ for $y = x^{(2)-}$. Hence the inverse Fourier transform of Y', y', will approximate y. Using the convolution theorem for Fourier transforms and Equations 7.13 and 7.14, y' may be written:

$$y'(t) = \frac{1}{2}h_2 * \left\{ (h_1 * \eta^{(1)})^2 + (h * h_1 * \eta^{(1)})^2 \right\} \tag{7.17}$$

where h, h_1 and h_2 are filters defined by their Fourier transforms: $H(f)$, $H_1(f)$ and $\delta H_2(f)$, respectively.

Hence, $\eta^{(1)}$ may be filtered digitally to give $\eta^{(2)-}$ or $x^{(2)-}$. Using discrete FIR filters of equal odd finite length, say M, the delay between the last calculated or sampled 1st order surface elevation and the calculated 2nd order elevation or paddle displacement will be $3(M-1)/(2f_s)$ in which f_s is the frequency by which the surface elevation is calculated or sampled. The scope of the present paper is not to discuss the choice of filter length, tapering etc., reference is made to existing literature on the subject.

If calculation time is a problem it may be decided only to generate 2nd order bound subharmonic waves below a certain frequency, say the lowest 1st order wave frequency. In this case there is no need to include the Hilbert filter h in Equation 7.17, because h_2 will act as a low-pass filter, removing any super harmonic components. Hence the calculation time will be reduced by 33 %, if the filter lengths are unchanged.

From Equations 7.2 to 7.10 it is obvious that the variables in the theoretical transfer functions generally cannot be separated as suggested in Equation

7.15 which means that in general $\mathcal{F}_1^- \neq F_1^-$. Only when considering a surface elevation consisting of wavelets with frequencies that ensure that the corresponding subharmonic components have different frequencies will the approximation be exact. However, it is possible, using a steepest descent fitting method as outlined below, to calculate a $\mathcal{F}_1^-$ that makes the filter approach generally applicable as will be shown.

The filters are fitted by minimizing the merit function, χ^2

$$\chi^2 = \sum_{m=1}^{n-1} \sum_{n=2}^{N} \left\{ F_1^-(f_n, f_m) - H_1(f_n)H_2(f_n - f_m)H_1(f_m) \right\}^2 \qquad (7.18)$$

in which N is the number of frequency components, $N = (M + 1)/2$, by successive calculations of the gradient to χ^2, $\nabla \chi^2$, in each point on the $n - m$ plane and subsequent adjustment of $H_1(f_n)$, $H_2(f_n - f_m)$ and $H_1(f_m)$ by a small amount down this gradient, until χ^2 converges. The converge of the iteration is quite sensitive to choosing proper starting values of H_1 and H_2

To take into account the actual distribution of wave energy in the 1st order surface elevation and the actual shape of the transfer function a weighting function, W, is introduced. W is chosen as the relative long wave energy induced by each pair of wavelets in the irregular 1st order wave spectrum S_η, that is:

$$W(f_n, f_m) = \frac{S_\eta(f_n)S_\eta(f_m)(G^-(f_n, f_m))^2}{|S_\eta(f_n)S_\eta(f_m)(G^-(f_n, f_m))^2|_{max}} \qquad (7.19)$$

in which max denotes the maximum value. Hence the small step down the gradient is chosen as $\Delta W(f_n, f_m)(F_1^-(f_n, f_m) - H_1(f_n)H_2(f_n - f_m)H_1(f_m))$, in which Δ is sufficiently small to avoid instability.

To evaluate the quality of fitting, the relative long wave error induced by each pair of wavelets, $\varepsilon(f_n, f_m) = (1 - \mathcal{F}_1^-(f_n, f_m)/F_1^-(f_n, f_m))W(f_n, f_m)$ and the sum of ε relative to the total long wave energy, ε_{tot}, are calculated. In Figure 7.3 ε is shown for a JONSWAP type wave spectrum. As observed the overall error is quite small, $\varepsilon_{tot} = 2.3$ %, and $\mathcal{F}_1^-$ only differs slightly from F_1^- in this case. Fitting the corresponding $\mathcal{G}^-$ to G^- leads to $\varepsilon_{tot} = 3.0$ %. It is in fact the general observation that $\mathcal{F}_1^-$ fits better to F_1^- than $\mathcal{G}^-$ does to G^-.

7.7 Example

Two examples of applying the presented approach to a JONSWAP type wave spectrum and piston type wave maker are described in this section.
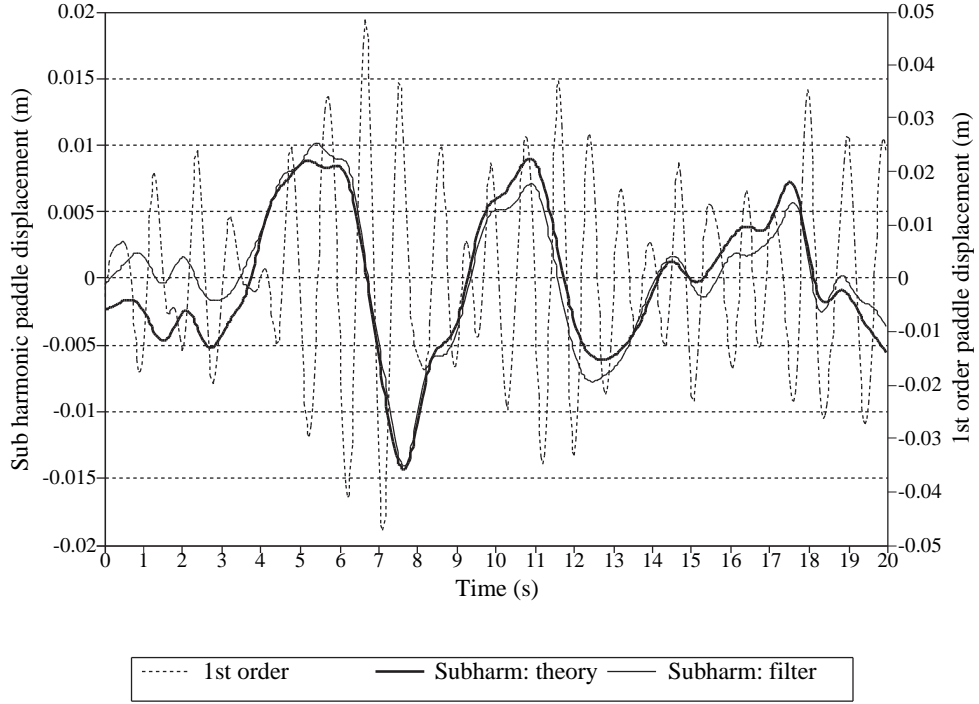

Figure 7.1: Calculated 1st and 2nd order piston displacement, $x^{(1)}$ and $x^{(2)-}$. JONSWAP spectrum, peak frequency, $f_p = 1.0$ Hz, $\gamma = 10$ and $h = 0.5$ m. 2nd order subharmonic components calculated using filter approach (filter) and existing theory (theory).

Figure 7.1 shows the 1st order paddle displacement signal $x^{(1)}$ and the corresponding 2nd order subharmonic signal, $x^{(2)-}$, calculated using the filter approach and the existing theory. From the figure it is seen that the overall agreement between the filter approach and the existing theory is very good. But because multiple frequency combinations induce bounded long waves on equal frequencies there will be some differences. From the figure it appears that these differences mainly are on the subharmonic components with relative high frequencies.

In Figure 7.2 the measured 1st and subharmonic 2nd order surface elevation, $\eta^{(1)}$ and $\eta^{(2)-}$, are shown for the paddle displacement calculated using the filter approach, the existing theory and without including the 2nd order terms. As for the paddle displacements in Figure 7.1 differences between the filter approach and the existing theory mainly are on the subharmonic components with relative high frequencies. But still the overall agreement is

very good. Furthermore the figure clearly indicates the problems when not including the bound long wave correction: The bounded long waves will be formed, but freely propagating long waves will be generated and the phase and amplitude of the observed long wave bounded to the wave group will vary along the flume.
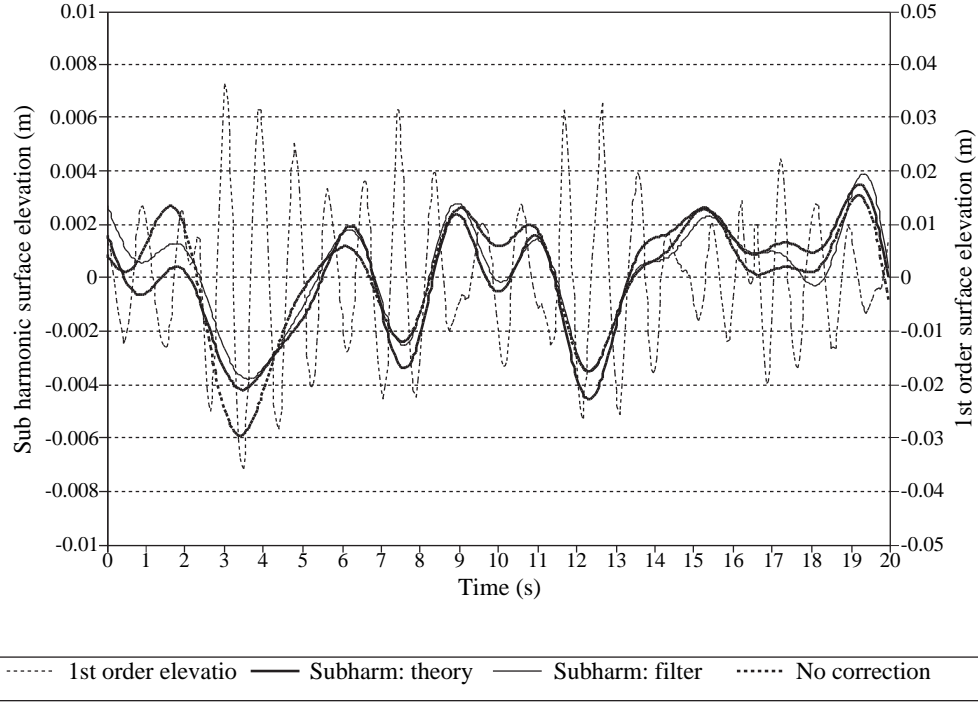
Figure 7.2: Measured 1st and 2nd order surface elevation, $\eta^{(1)}$ and $\eta^{(2)-}$. JONSWAP spectrum, peak frequency, $f_p = 1.0$ Hz, $\gamma = 10$ and $h = 0.5$ m. Wave generation not including (no correction) and including 2nd order subharmonic components, calculated using filter approach (filter) and existing theory (theory).

To change the internal correction method, described above, into an external correction method, $x^{(1)}$ is calculated from the sampled linear paddle control signal and filtered through an inverse Biesel filter, b^{-1}, defined by its Fourier transform $B^{-1}(f)$, to obtain $\eta^{(1)}$. For a piston type wave maker:

$$B^{-1}(f) = \frac{\sinh kh \cosh kh + kh}{2 \sinh^2 kh} \tag{7.20}$$

Equation 7.17 may then be rewritten

$$y'(t) = \frac{1}{2} h_2 * \left\{ (h_1 * b^{-1} * x^{(1)})^2 + (h * h_1 * b^{-1} * x^{(1)})^2 \right\} \tag{7.21}$$

The filters b^{-1}, h_1 and h_2 of course need to be calculated according to the actual wave parameters.
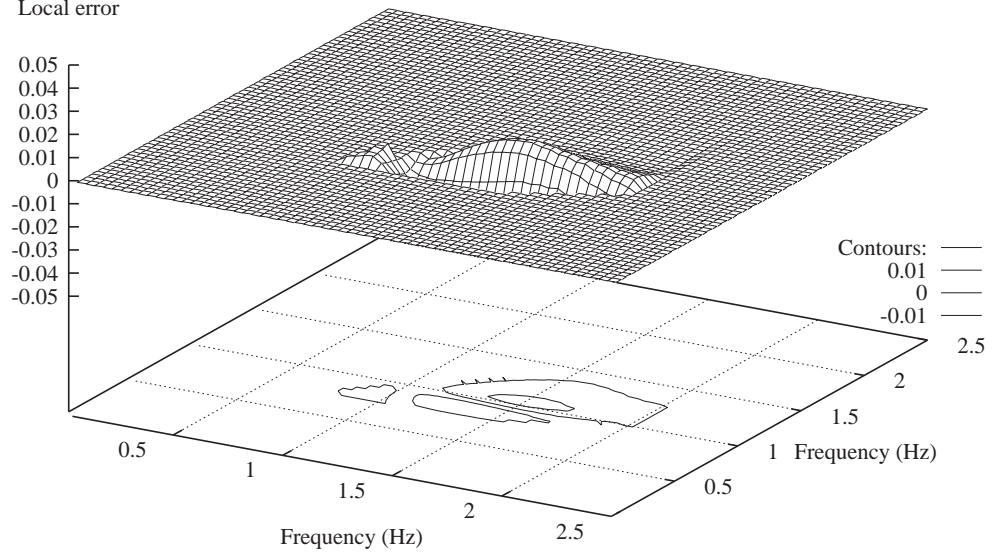
Figure 7.3: Induced relative long wave error ε when fitting $\mathcal{F}_1^-$ to F_1^-, $\varepsilon_{tot} = 2.3$ %. JONSWAP spectrum, peak frequency, $f_p = 1.0$ Hz, $\gamma = 10$ and $h = 0.5$ m.

7.8 Closure

A method has been presented for filtering a 1st order surface elevation to obtain the 2nd order bound subharmonic surface elevation or corresponding paddle displacement. The method has been compared in simulations and physical experiments to the existing theory. The filter approach gives exact 2nd order subharmonic components when only considering the interaction between two regular wavelets. For irregular wave spectra the filter approach gives estimates which differs slightly from the existing theory especially for relative high subharmonic frequencies. For the low subharmonic frequencies, which generally are the most important as far as long wave phenomena are concerned, only insignificant differences are observed. Hence, the method is suitable for applications were bounded subharmonics otherwise cannot be included using existing theory.

In addition a real-time scheme for manipulating the 1st order paddle control signal to include the 2nd order subharmonic components has been outlined.

Chapter 8

Generation of Oblique Waves

8.1   3-D Biésel Transfer Function

In chapter 1 the Biésel transfer function for uni-directional linear waves, F_2, was calculated for various types of generator systems. To generate oblique linear waves travelling in a direction different from the x-axis direction perpendicular to the front of the generator, a different transfer function, F_3, must be applied.

Consider a wave generating system where the generator front consists of a number of very small paddles. A oblique regular wave can then be generated using Huygens' principle, by introducing a suitable delay between the wave paddles as illustrated in Figure 8.1. Each wave paddle moves harmonically in the x-axis direction with the amplitude x_a. It is evident that the required delay of the individual wave paddles will lead to a sinusoidal shape of the front of the wave generator. If the front of the actual wave generating system fails to reproduce this shape correctly, as always will be the case due to the finite width of the wave paddles, undesired waves will be generated. In
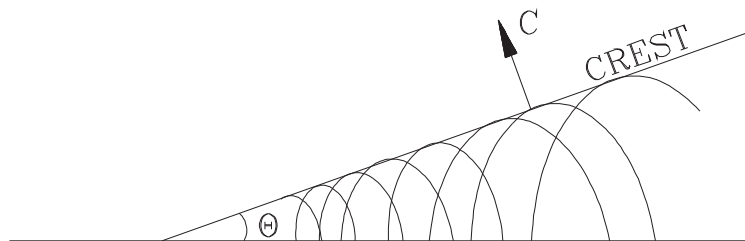

Figure 8.1: Huygens' principle in generating oblique waves. Regular wave travelling in the θ-direction.
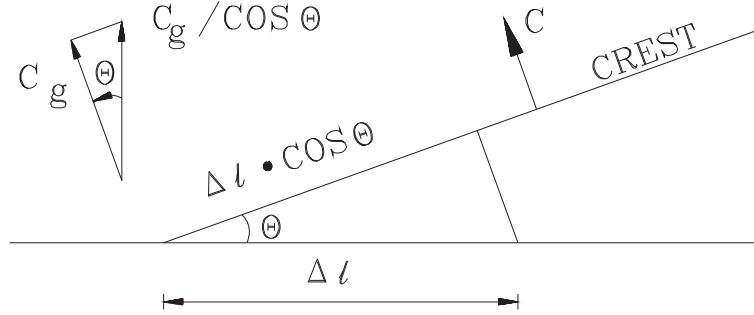
Figure 8.2: Small part of wave generator, generating a oblique regular wave.

chapter 9 these so-called spurious waves are discussed. If the wave length of the generated wave is L the wave length from maximum to maximum of the sinusoidal front of the wave generator, $l = L/\sin\theta$. The delay, φ_p, between neighbouring wave paddles of width l_p is $l_p \cdot 2\pi/l$, or more convenient

$$\varphi_p = l_p \cdot \frac{2\pi\sin\theta}{L} \tag{8.1}$$

Consider a small part of the wave generator, say of the length Δl, and let the generated regular wave travel in the θ direction with the group celerity, c_g, see Figure 8.2.

The energy flux, E_f, in the generated oblique wave over the length $\Delta l \cdot \cos\theta$ in Figure 8.2 is

$$E_f \sim a^2 \cdot c_g \cdot \Delta l \cos\theta \tag{8.2}$$

where a is the wave amplitude and θ the direction of travel. Assuming that no energy is transported along the crest of the generated wave, this energy flux must be balanced by the energy flux over the length Δl just in front of the wave paddle. As the wave amplitude in front of the paddle is $x_a \cdot F_2$, and the corresponding group velocity is $c_g/\cos\theta$, this energy flux can be written

$$E_f \sim (x_a \cdot F_2)^2 \frac{c_g}{\cos\theta}\Delta l \tag{8.3}$$

Combining Equation 8.2 and 8.3 the amplitude in the generated oblique wave,

a, equals $x_a \cdot F_2/\cos\theta$ and consequently the 3-D Biésel transfer function

$$F_3 \quad = \quad F_2/\cos\theta \tag{8.4}$$

Hence, by decomposing a specified directional wave spectrum into a number of wavelets of the form given in Equation 9.4, the wave paddle displacement necessary for generating the individual wavelets can be calculated using the transfer function given in Equation 8.4 and the delay between the wave paddles can be calculated using Equation 8.1. By superposition the total paddle displacement can then be obtained.

8.2 Phase Correction for Oblique Waves

The methods for generating 2-D waves perpendicular to the wave generators that have already been described in chapter 2, namely the

- Random Phase Method

- Random Complex Spectrum Method

- White Noise Filtering Method

are applicable when generating oblique 2-D waves as well. Basically the paddle displacement for one paddle, say the 0th, is calculated using one of the methods from Chapter 2 and the displacement for the ith paddle is calculated by introducing an appropriate delay, φ_{pi}, relative to the displacement of the 0th paddle.

Consider a wave generator system consisting of n segmented wave paddles with the width l_p. A coordinate system is introduced as illustrated in Figure 8.3.

If the wave paddle displacement is calculated for a regular wave with the wave length L travelling in the x-axis direction, the delay between the ith and the 0th wave paddle when generating the same regular wave travelling in the θ-direction, see Equation 8.1, is

$$\varphi_{pi}(f) \quad = \quad i \cdot l_p \frac{2\pi \sin\theta}{L(h,f)} \tag{8.5}$$
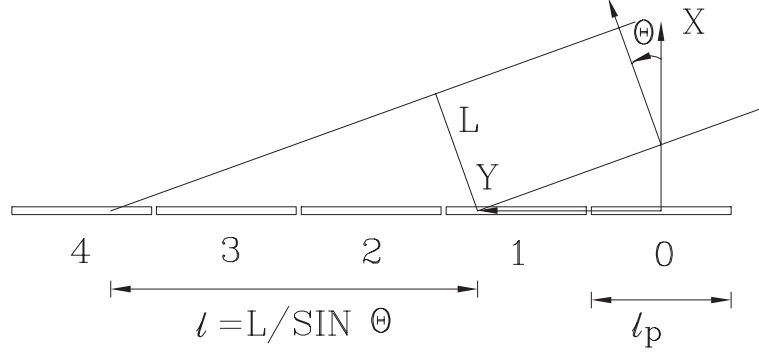
Figure 8.3: Wave generating system with segmented wave paddles. Definition sketch

As the paddle displacement must be calculated using the 3-D Biésel transfer function from Equation 8.4 the calculated 2-D displacement must be multiplied by $\cos\theta$.

8.3 Generation of Long Crested Irregular Oblique Waves

Random Phase and Random Complex Spectrum Methods

Both methods involve an inverse Fourier transform of calculated Fourier coefficients for the discrete paddle-displacement energy spectrum, $\sigma_x^2(f_j)$:

$$
\begin{aligned}
A_j &= a_j \cdot \cos\varphi(f_j) \\
B_j &= a_j \cdot \sin\varphi(f_j)
\end{aligned}
\tag{8.6}
$$

where $a_j = \sqrt{\sigma_x^2(f_j)/2}$ to produce the displacement of the wave paddle.

In the Random Complex Spectrum Method $\cos\varphi(f_j)$ and $\sin\varphi(f_j)$ are replaced by two random Gaussian variables with zero mean and $\sigma = 1$. This, however, does not affect the general principle in the following.

For each pair of frequency components the delay is introduced by substituting $\varphi(f_j)$ in 8.6 by $\varphi(f_j) - \varphi_{pi}(f_j)$. Using the trigonometric addition formulas, and assuming that a_j is calculated using the 2-D Biésel transfer function derived in chapter 1, the modified Fourier coefficients for the discrete paddle-

displacement energy spectrum are:

$$
\begin{aligned}
A_{ij} &= a_j \cdot \cos\theta(\cos\varphi(f_j)\cos\varphi_{pi}(f_j) + \sin\varphi(f_j)\sin\varphi_{pi}(f_j)) \\
B_{ij} &= a_j \cdot \cos\theta(\sin\varphi(f_j)\cos\varphi_{pi}(f_j) - \cos\varphi(f_j)\sin\varphi_{pi}(f_j)) \tag{8.7}
\end{aligned}
$$

Performing inverse Fourier transform on the n sets of Fourier coefficients in Equation 8.7 leads to the appropriate displacement time series for each of the n wave paddles.

White Noise Filtering Method

The White Noise Filtering Method involves the use of two filter operators:

The first filter operator, the Surface Elevation filter, is calculated by performing inverse Fourier transform on a discrete frequency response function corresponding to the target wave energy spectrum. Convolved with a white noise signal the Surface Elevation filter produces the appropriate surface elevation time series.

The second filter operator, the Biésel filter, is calculated by performing inverse Fourier transform on a discrete frequency response function corresponding to the inverse of the far field Biésel transfer function from chapter 1. Convolved with the surface elevation the Biésel filter produces the corresponding wave paddle displacement time series.

To generate oblique 2-D waves using the White Noise Filtering Method the approach described in the previous section can be used to calculate appropriate Biésel filter coefficients for each of the n wave paddles. Consequently, to generate oblique 2-D waves the 2-D discrete frequency response function for the Biésel filter:

$$
\begin{aligned}
H(f_j).re &= \cos(\Phi)\frac{1}{K_f(f_j)} \\
H(f_j).im &= \sin(\Phi)\frac{1}{K_f(f_j)} \tag{8.8}
\end{aligned}
$$

where K_f is the far field Biésel transfer function, must be modified to apply to the ith wave paddle:

$$
\begin{aligned}
H(f_j).re &= \frac{\cos\theta}{K_f(f_j)}(\cos\Phi\cos\varphi_{pi}(f_j) + \sin\Phi\sin\varphi_{pi}(f_j)) \\
H(f_j).im &= \frac{\cos\theta}{K_f(f_j)}(\sin\Phi\cos\varphi_{pi}(f_j) - \cos\Phi\sin\varphi_{pi}(f_j)) \tag{8.9}
\end{aligned}
$$

Performing inverse Fourier transform on the n frequency response functions in Equation 8.9, the Biésel filters for each of the n wave paddles are obtained. Convolved with the surface elevation time series, calculated by convolving the Surface Elevation filter with a white noise signal, these filter operators produce the appropriate displacement time series for each of the wave paddles.

Chapter 9

Short Crested Waves

In this chapter an introduction to short crested waves is given and the methods for generation of short-crested waves are presented.

From an engineering point of view the knowledge of the three-dimensional structure of ocean waves is essential for: design of off-shore structures, estimating transport of marine sediment, ship motion and so forth. Hence, the generation of 3-D waves in laboratory facilities will be of interest when conducting scaled experiments concerning such topics.

9.1   Description of Short Crested Waves

Measurements in the ocean environment have founded the basis for several theoretical descriptions of the 3-D wave field. The directional wave spectrum, $S_\eta(f, \theta)$, is often considered a product of the uni-directional wave spectrum, $S_\eta(f)$, and a spreading function, $D(f, \theta)$. That is

$$S_\eta(f, \theta) \quad = \quad D(f, \theta) \cdot S_\eta(f) \tag{9.1}$$

where f is the wave frequency, θ the wave propagation angle and $D(f, \theta)$ must satisfy

$$\int_{-\pi}^{\pi} D(f, \theta) d\theta \quad = \quad 1 \tag{9.2}$$

to assure identical wave energy in $S_\eta(f, \theta)$ and $S_\eta(f)$.

Several semi-empirical proposals to the formulation of $D(f, \theta)$ have been
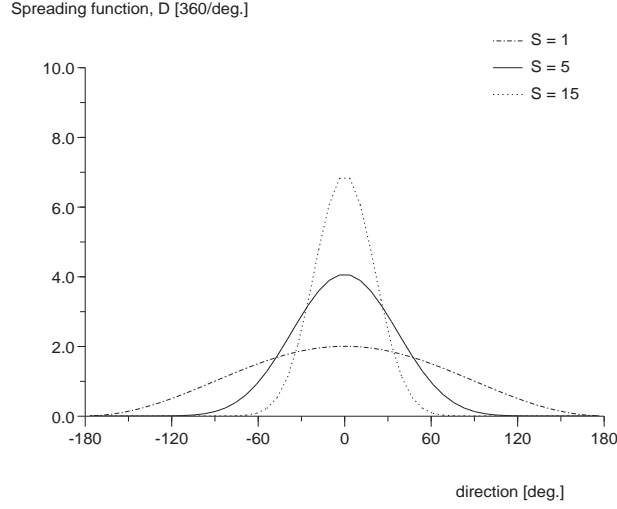
Figure 9.1: The spreading function, $D(f, \theta)$, for various constant values of the spreading parameter, s.

reported and most suggestions consider D to be independent of the frequency. The *Cosine-power* or $\cos^{2s}$ spreading function, see Mitsuyasu (1975):

$$D(f, \theta) \quad = \quad \frac{s^{2s-1}}{\pi} \frac{\Gamma^2 (s+1)}{\Gamma (2s+1)} \, cos^{2s} \left(\frac{\theta - \theta_0}{2} \right) \tag{9.3}$$

where s is a spreading parameter and Γ the Gamma function, was found to provide a reasonable fit to measured ocean wave spectra by Longuet-Higgins, Cartwright and Smith (1961) who used a frequency independent value of s.

In Figure 9.1 D is plotted as function of θ for various values of s.

Mitsuyasu et al. (1975) have reported on extensive measurements of directional spectra and proposed the *Cosine power* spreading function to be applied with a frequency dependent s parameter. In their suggestion the variation of D exhibits the smallest degree of directional spreading, maximum s value, at frequencies near the peak frequency.

If the directional wave field is considered the sum of a number of wavelets with the elevation $\eta(x, y, t)$:

$$\eta(x, y, t) \quad = \quad a \cdot \cos(2\pi f t - kx \cos \theta - ky \sin \theta + \varphi) \tag{9.4}$$

where
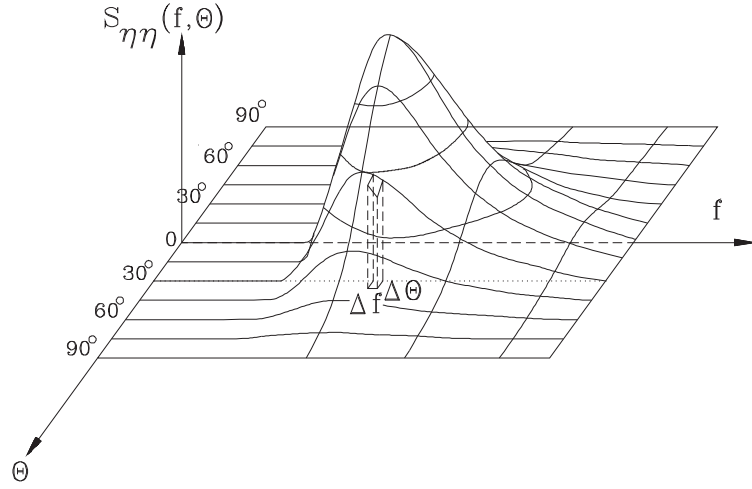
Figure 9.2: Energy 'packet' selection from a directional energy wave spectrum.

a	:	the wave amplitude,
t	:	the time,
k	:	the wave number, $2\pi/L$,
(x, y)	:	the spatial coordinates and
φ	:	an arbitrary phase, uniformly distributed in $[-\pi; \pi[$.

Introducing the total wave energy of the wavelet, E_t, the amplitude can be rewritten:

$$a = \sqrt{\frac{2}{\rho g} E_t} \qquad (9.5)$$

where ρ and g is the water density and gravitational acceleration ,respectively.

If the surface elevation is considered a Gaussian stochastic process characterized by a specified energy wave spectrum, S_η, sufficiently small $\Delta\theta$ and $\Delta\varphi$ can be chosen and the wave spectrum can be decomposed into a number of energy 'packets' each containing the approximate energy:

$$E_t \approx \rho g S_\eta(f, \theta) \Delta\theta \Delta f \qquad (9.6)$$

Figure 9.2 illustrates the choice of such an energy 'packet'.

Combining the Equations 9.4 - 9.6 and letting $\Delta\theta$ and Δf decrease towards

$d\theta$ and df, respectively, the total surface elevation can be written as

$$\eta(x,y,t) = \int_0^\infty \int_{-\pi}^\pi \sqrt{2S_\eta(f,\theta)d\theta\ df}\ \cos(2\pi ft - kx\cos\theta - ky\sin\theta + \varphi) \quad (9.7)$$

The integral in Equation 9.7 is often referred to as a pseudo-integral, referring to its lack of mathematical stringency. In any way it is a descriptive way to symbolize the limiting processes, $\Delta\theta \to d\theta$ and $\Delta f \to df$.

9.2 Generating Irregular Short Crested Waves

Directional irregular waves can be expressed as a linear superposition of a large number of wavelets of the type shown in Equation 5, with frequency f, propagation direction θ, wave length L, and phase φ. Thus, a simultaneous generation of a number of oblique linear waves enables a reproduction of a directional wave field in a laboratory wave basin.

Two in principle different models are available when generating input signals for 3-D wave systems:

- Single summation model:
  In this model a single direction is assigned to each frequency component. Consequently the double pseudo-integral, Equation 9.7, is represented by a single summation leading to a paddle displacement for the ith wave paddle, x_i:

$$x_i(t) \quad = \quad \sum_{j=1}^{N\cdot M} \frac{b_j}{F_3(f_j,\theta_j)}\cos(2\pi f_j t - \varphi_{pi}(f_j,\theta_j) + \varphi(f_j)) \quad (9.8)$$

  where

$$b_j = \sqrt{2S_eta(f_j)\Delta f}\quad,$$
$$F_3(f_j,\theta_j) = \frac{F_2(f_j)}{\cos\theta_j}\quad\text{and}$$
$$\varphi_{pi}(f_j,\theta_j) = il_p\frac{2\pi\sin\theta_j}{L(h,f_j)}$$

  in which $F_2(f_j)$ is the 2-D Biésel transfer function given in chapter 1. For the method to be successful the choise of θ_j must represent the adopted directional spreading function, $D(f,\theta)$. This is often achieved by picking θ_j as a random number with a propability density function equal to $D(f,\theta)$.

- Double summation model:
  In this model multiple directions are assigned to each frequency component. The paddle displacement of the ith paddle can then be written:

$$x_i(t) = \sum_{j=1}^{N} \sum_{k=1}^{M} \frac{b_{jk}}{F_3(f_j, \theta_k)} \cos(2\pi f_j t - \varphi_{pi}(f_j, \theta_k) + \varphi(f_j, \theta_k)) \quad (9.9)$$

where

$$b_j = \sqrt{2 S_e ta(f_j, \theta_k) \Delta f \Delta \theta} \quad ,$$
$$F_3(f_j, \theta_k) = \frac{F_2(f_j)}{\cos \theta_k} \quad \text{and}$$
$$\varphi_{pi}(f_j, \theta_k) = i l_p \frac{2\pi \sin \theta_k}{L(h, f_j)}$$

in which θ_k often simply is chosen equally distributed from $-\frac{\pi}{2}$ to $\frac{\pi}{2}$.

A specific problem relates to the double summation model. The phase difference between two wavelets with equal frequencies but different propagation directions does not vanish in the cross spectra. The phenomenon, known as phase locking, results in different spectral properties of the generated irregular wave field dependent on the spatial coordinates. Consequently, the irregular surface is non-ergodic. To reduce this effect the number of wave components in the double summation model, $N \cdot M$, must be increased significantly relative to the number of components in the single summation model, $N \cdot M$. Takayama et al. (1989) conclude that the required number of wave components in the double summation model must be 20 times larger than in the single summation model to obtain the same quality of the generated wave field. Therefore several authors generally advocate the single summation model for laboratory use, simply to reduce computation time. In some generation methods, however, the double summation model can be attractive in order to avoid, for example, inverse Fourier transform of very long arrays.

In the following generation methods only the single summation model will be discussed, but the applicability to a double summation model is straight forward and will briefly be described.

Consider a wave generation system with n segmented wave paddles and coordinate system as outlined in chapter 8.

Inverse Fourier Transform methods

The two Inverse Fourier Transform methods for generating irregular 2-D waves described in chapter 2:

- Random Phase Method

- Random Complex Spectrum Method

The single summation model is applied using a technique very similar to the method for generating oblique 2-D waves, as described previously.

Calculating the discrete wave energy spectrum, $\sigma_\eta^2(f_j) = S_\eta(j \cdot \Delta f)\Delta f$, the $N \cdot M$ frequency components for the ith wave paddle can be calculated by picking appropriate propagation directions, θ_j, using the techniques described in the previous section, and random phases, $\varphi(f_j)$ equally distributed from 0 to 2π:

$$
\begin{aligned}
A_{ij} &= \frac{b_j}{F_3(f_j, \theta_j)}(\cos\varphi(f_j)\cos\varphi_{pi}(f_j, \theta_j) + \sin\varphi(f_j)\sin\varphi_{pi}(f_j, \theta_j)) \\
B_{ij} &= \frac{b_j}{F_3(f_j, \theta_j)}(\sin\varphi(f_j)\cos\varphi_{pi}(f_j, \theta_j) - \cos\varphi(f_j)\sin\varphi_{pi}(f_j, \theta_j)) \quad (9.10)
\end{aligned}
$$

where $b_j = \sqrt{\sigma_\eta^2(f_j)/2}$.

Using the Random Complex method $\cos\varphi(f_j)$ and $\sin\varphi(f_j)$ are replaced by two random Gaussian variables as described in chapter 2.

Performing inverse Fourier Transform on the n set of $N \cdot M$ Fourier coefficients in Equation 9.10 will lead to the appropriate displacement time series for each of the n wave paddles.

A double summation model could be applied by calculating M discrete wave energy spectra, $\sigma_{eta}^2(f_j, \theta_k) = S_\eta(j \cdot \Delta f, k \cdot \Delta\theta - \frac{\pi}{2})\Delta f\Delta\theta$, and creating M set of N frequency components for each of the n wave paddles, performing inverse Fourier Transform and superpositioning the M displacement time series for each of the wave paddles.

White Noise Filtering methods

The method described below is strictly following the equivalent method described in chapter 2:

- White Noise Filtering Method

Consequently, the Biésel filter and the Surface Elevation filter could be combined when generating 3-D irregular waves, in case the surface elevation time series are required. The surface elevation time series could for example be used for calculating bounded sub or super harmonic waves, as discussed in

chapters 6 and 7. If the two filters not are combined only the Biésel filter needs to be modified for generating irregular 3-D waves.

In a single summation model a Biésel filter for each of the n wave paddles must be designed. In alignment with chapters 1, 2 and 8 it is easily recognized that the frequency response function for the 3-D Biésel filter assigned to the ith wave paddle can be calculated as:

$$
\begin{aligned}
H(f_j).re &= \frac{1}{F_3(f_j, \theta_j)}(\cos\Phi\cos\varphi_{pi}(f_j, \theta_j) + \sin\Phi\sin\varphi_{pi}(f_j, \theta_j)) \\
H(f_j).im &= \frac{1}{F_3(f_j, \theta_j)}(\sin\Phi\cos\varphi_{pi}(f_j, \theta_j) - \cos\Phi\sin\varphi_{pi}(f_j, \theta_j))
\end{aligned}
\tag{9.11}
$$

where $\varphi_{pi}(f_j, \theta_j)$ and $F_3(f_j, \theta_j)$ are defined in the previous section and $\Phi = -\frac{\pi}{2}$.

Performing inverse Fourier Transform on the n frequency response functions in Equation 9.11 the Biésel filters for each of the wave paddles are obtained. Convolved with the surface elevation time series these filter operators produce the appropriate displacement time series for each of the wave paddles.

If the two filters, the Surface Elevation filter and the Biésel filter, are to be combined, this is achieved by creating a frequency response function consisting of the components from the Biésel frequency responce function multiplied by the complex conjugate of the corresponding components in the Surface Elevation frequency response function, that is $H(f_j, \theta_j) = H_B(f_j, \theta_j) \cdot H_S^*(f_j, \theta_j)$, and performing inverse Fourier Transform to obtain the filter operators. A double summation model can be applied by creating M filters for M different directions for each of the n wave paddles. By convolving M white noise arrays with each of the directional filters and sum up for all directions the n paddle displacements are calculated.

9.3 Spurious Waves and Other Laboratory Difficulties

Generating laboratory waves using a truncated segmented paddle system will generally affect the quality of the generated wave field. Due to the incapability of the segmented front of the wave maker to form a perfect sinusoid the principles outlined in the previous pages are not completely valid.

The error in the wave generation is dependent on the wave length L, the

propagation direction θ and the paddle width l_p, for example expressed as the ratio $l/l_p = L/(l_p \sin \theta)$, and two fold:

Incorrect energy is feed into the generated waves because the integrated variance of the actual displacement of the wave paddle front is different from that of an ideal sinusoidal displacement.

Incorrect directed energy is feed into the generated waves causing spurious waves, travelling in directions different from the main waves, to be generated. Both effects cause the actual transfer function between the stroke of the wave paddle and the wave height to be different from the theoretical 3-D Biésel transfer function F_3. Reference can be made to Sand (1979) for a detailed description of the phenomena and useful implementations into a specified wave generating system.

Other effects are

- The truncation of the wave maker causes diffraction, that is wave energy travelling along the wave crest and, consequently, reducing the height of the generated wave.

- The truncation of the wave basin causes reflection from the side walls which, consequently, affects the directional spreading of the wave field.

These effects significantly reduce the horizontal area inside which the specified wave field is generated. It will not be discussed here but it is possible to take into account these effects. References are made to Funke and Miles 1987, who developed *The Corner Reflection Method* taking into account reflections from side walls. Futhermore several different methods for taking into account diffraction of the individual wavelets exists.

Chapter 10

References

Biésel, F., 1951.
Les Apparails Generateurs de Houle en Laboratorie. La Houille Blanche, Vol. 6, nos. 2,4 et 5.

Bose, N.K., (1985), *Digital Filters; Theory and Applications.* Elsevier Science Publishing B.V., The NetherLands, 1985.

Brorsen, M. and Frigaard, P., 1992.
Active Absorption of Irregular Gravity Waves in BEM-models. Boundary Elements XIV, Vol.1 Editors: Brebbia, Dominiquez and Paris. Computational Mechanics Publications, Southampton.

Bullock, G.N., Murton, G.J., 1989,
Performance of a Wedge Type Absorbing Wave Maker. Journal of Waterway, Port, Coastal and Ocean Engineering, Vol. 115, No. 1.

Burcharth, H.F. (1979).
The Effect of Wave Grouping on On-Shore Structures. Coastal Engineering, No. 2, pp. 189-199.

Fredsø, J., 1990.
Hydrodynamik. (in danish). Den private Ingeni>rfond, DtH.

Frigaard, P., 1993,
AWASYS - Active Wave Absorption System - Users Guide. Hydraulics & Coastal Engineering Laboratory, Department of Civil Engineering, Aalborg

University.

Frigaard, P., Brorsen, M., 1995,
A Time-Domain Method for Separating Incident and Reflected Irregular Waves.
Coastal Engineering, Vol. 24, Nos. 3 and 4.

Frigaard, F., Christensen, M., 1994,
An Absorbing Wave-Maker Based on Digital Filters. Proceedings of Int.
Symp.: Waves - Physical and Numerical Modelling, Vol. 1, Vancouver.

Frigaard, P., Helm–Petersen, J., Klopman, G., Stansberg, C.T., Benoit, M.,
Briggs, M.J., Miles, M., Santas, J., Schäffer, H.A. and Hawkes, P.J., 1997
IAHR list of sea state parameters – an update for multidirectional waves.
Proc. IAHR Seminar Multidirectional Waves and their Interaction with
Structures. 27th IAHR Congress, San Francisco, Aug 10–15, 1997

Funke, E.R., Mansard, E.P.D. (1979).
*On The Synthesis of Realistic Sea States in a Laboratory Flume, Technical
Report, LTR-HY-66.* National Research Council of Canada, Hydraulics Lab-
oratory, Ottawa, 1979.

Funke, E., and Miles, M. D. 1987.
Multi–directional wave generation with corner reflectors. Technical report
TR–HY–021, NRC.

Gilbert, G., 1978,
Absorbing Wave Generators. Hydr. Res. Station notes, Hydr. Res. Station,
Wallingford, Oxon, United Kingdom, Vol. 20, Nos. 3-4.

Goda, Y. and Suzuki, Y., 1976.
Estimation of Incident and Reflected Waves in Random Wave Experiments.
Proceedings, 15th International Conference on Coastal Engineering, Vol. 1,
pp. 828-845, Honolulu, Hawaii.

Hald, Tue (1994).
Wave Group Analysis by means of the Hilbert Transform Technique. Aalborg
University.

Hirakuchi, H., Kajima, R., Kawaguchi, T., 1990,
Application of a Piston-Type Absorbing Wavemaker to Irregular Wave Experiments. Coastal Eng. Japan, Vol. 33, No. 1.

Hudspeth, R.T., Medina, J.R. (1988).
Wave Group Analysis by the Hilbert Transform. Proceedings, 21st ICCE, 1988, Torremolinos, pp. 884-898.

Høgedal, M., Frigaard, P. and Christensen, M. (1994).
Generation of Long Waves using Non–linear Digital Filters. Proc. Int. Symp. Waves – Physical and Numerical Modelling, University of British Columbia, Vancouver, Canada.

Johnson, R.R., Mansard, E.P.D., Ploeg, J. (1978).
Effects of Wave Grouping on Breakwater Stability. Proceedings, 16th ICCE, 1978, Hamburg, pp. 2228-2243.

Karl, J. H., 1989.
An Introduction to Digital Signal Processing. Academic Press, San Diego.

Longuet-Higgins, M.S., Cartwright, D.E. and Smith, N.D., 1961.
Observations of the directional spectrum of sea waves using the motions of a floating buoy. Ocean Wave Spectra, Prentice-Hall, pp. 111-132.

Mansard, E. and Funke, E., 1980.
The Measurement of Incident and Reflected Spectra Using a Least Squares Method. Proceedings, 17th International Conference on Coastal Engineering, Vol. 1, pp 154-172, Sydney, Australia.

Milgram, J.S., 1970,
Active Water-Wave Absorbers. J. Fluid Mech., Vol. 43, No. 4.

Mitsuyasu, H, et al., 1975.
Observations of the directional spectrum of ocean waves using a cloverleaf buoy. Journal of Physical Oceanography, Vol. I, pp. 750-760.

Nunes, D., 1981.
Random Wave Generation by Linear Digital Filtering of Gaussian White

Noise. 2nd Congress of I.M.A.E.M., Trieste.

Oppenheim, A.V., Schafer, R.W. (1989).
Discrete-Time Signal Processing. Prentice-Hall International, Inc., 1989.

Ottesen-Hansen, N. E., 1978.
Long Period Waves in Natural Wave Trains. Prog. Rep. 46, Aug. 1978, Inst. Hydrodyn. and Hydraulic Eng., DTH.

Rye, H. (1982).
Ocean Wave Groups, Report UR-82-18. Department of Marine Technology, Norwegian Institute of Technology, 1982.

Sand, S.E., 1979
Three-Dimensional Deterministic Structure of Ocean Waves. PhD thesis from The Technical University of Denmark.

Sand, S.E., 1982.
Long Wave Problems in Laboratory Models. Journal of Waterway, Port, Coastal and Ocean Division, ASCE, 108 (WW4):492-503

Sand, S.E. and Mansard, E.P.D., 1986.
Reproduction of higher harmonics in irregular waves. Ocean Engineering, 13(1):57-83.

Schäffer, H.A., 1993 *Laboratory wave generation correct to second order.* In Volume 29: Wave Kinematics and Environmental Forces, pp 115-139. Society for Underwater Technology.

Schäffer, H.A., Stolborg, T., Hyllested, P., 1994.
Simultaneous Generation and Active Absorption of Waves in Flumes. Proceedings of Int. Symp.: Waves - Physical and Numerical Modelling, Vol. 1, Vancouver.

Spangenberg, S. (1980).
The Effect of Wave Grouping on Slow Drift Oscillations of an Offshore Structure. Bulletin No. 46, Danish Ship Research Laboratory, 1980.

Takayama, T., T. Hiraishi, and Y. Goda, 1989.
Comparison of single and double summation models for multi-directional wave generation. Proc. International Association for Hydraulic Research XXIII Congress, Ottawa, Canada, August 21-25.

Tuah, H. and Hudspeth, R. T., 1982.
Comparison of Numerical Random Sea Simulations. Jour. of the Waterway, Port, Coastal and Ocean Div., Vol. 108, no. WW4.